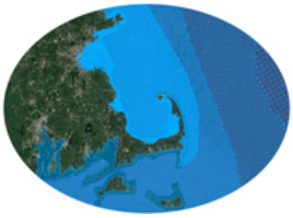

Simulations of 2020 Hydrodynamics and Water Quality in the Massachusetts Bay System using the Bays Eutrophication Model

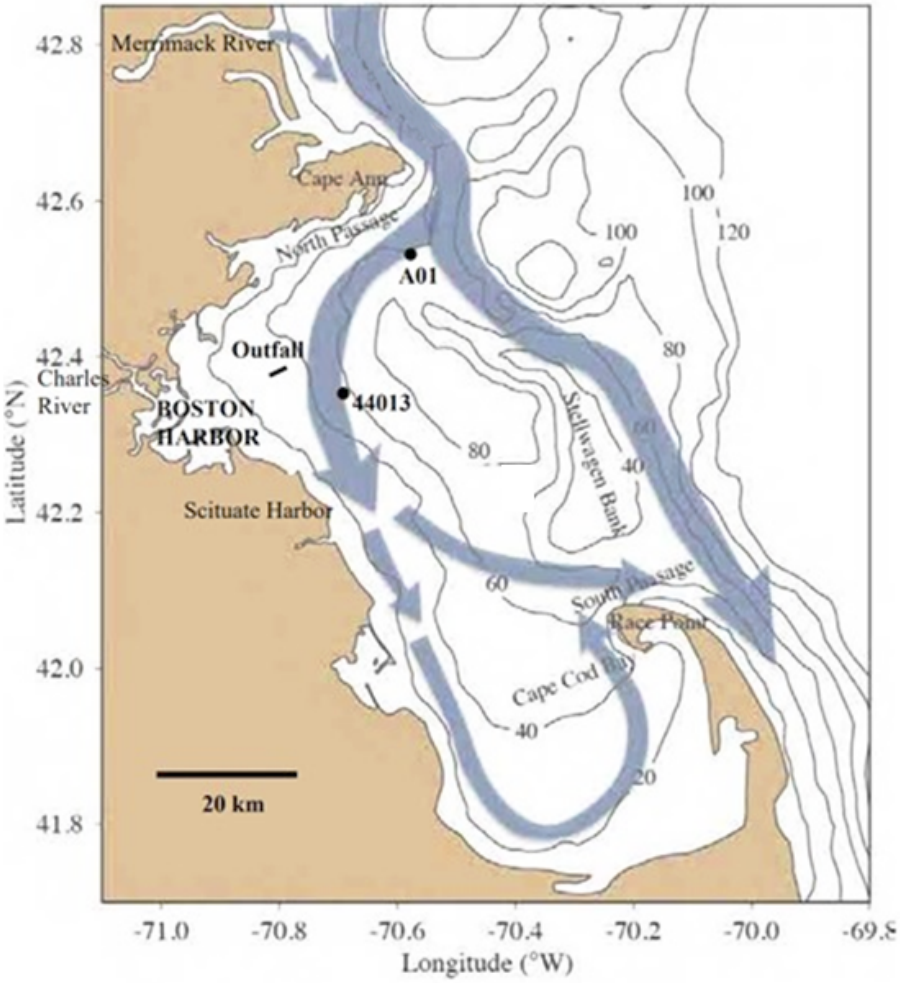

Massachusetts Water Resources Authority
Environmental Quality Department

Report 2022-08

Citation:

Deltares, 2022**. Simulations of 2020 Hydrodynamics and Water Quality in the Massachusetts Bay System using the Bays Eutrophication Model.** Boston: Massachusetts Water Resources Authority. Report 2022-08. 90 p.

MWRA Environmental Quality Department reports can be downloaded from http://www.mwra.com/harbor/enquad/trlist.html.

Summary

Background. This report presents hydrodynamic and water quality model results for the Massachusetts Bays system (Massachusetts Bay, Cape Cod Bay, and Boston Harbor) during 2020. Treated effluent sent from the Massachusetts Water Resources Authority (MWRA) treatment plant through a 15 km (9.5 mi) long tunnel and released at an outfall offshore in Massachusetts Bay contains nutrients. Nutrients are necessary and important to support healthy and diverse marine ecosystems. However, excess nutrients can cause eutrophication, the overgrowth of phytoplankton (microscopic marine algae) which degrades water quality and can harm marine life by depleting oxygen when it decays. To address potential eutrophication and other concerns, MWRA maintains an extensive bay and harbor field monitoring program, which this modelling complements. The hydrodynamic model simulates temperature, salinity, and currents, and is the foundation for the water quality model, which simulates key eutrophication parameters including nutrients, chlorophyll (a measure of phytoplankton), and oxygen.

Results for 2020. Consistent with field observations, the model did not show effects of effluent on chlorophyll or oxygen, nor indications that eutrophication was occurring. Hydrodynamic results for 2020 agree well with available observations and capture the geographic and vertical structure, and temporal variability, of temperature and salinity distributions and density stratification, as well as tidal and non-tidal currents. The 2020 water quality simulation captured general patterns in observed seasonal variations, geographic distributions, and vertical structure for many variables. This included the late spring reduction in near-surface dissolved inorganic nitrogen (DIN) due to phytoplankton uptake, and its replenishment after mixing in fall due to cooling and storms. It also included seasonal dissolved oxygen variations, with peak values in spring at shallow depths due to colder water and phytoplankton growth, and late summer minima at depth where stratification inhibits reaeration by air-sea exchange. In addition to those more bay-wide patterns, in the model as in observations, DIN was elevated persistently within about 10 km (6 mi) of the outfall and intermittently as far as about 20 km (12 mi) away, mainly due to nitrogen from ammonium in the treated effluent. The model captured the observed vertical structure of this effluent influence, which reached the surface in winter months and remained at depth from about May through October when the bay was stratified.

As in observations, model temperature stratification reached a record-high maximum in July, probably due to weak wind-driven upwelling. Due to weak river flow, particularly in summer, observed and modeled salinity stratification was very weak. Observations suggested there was a spring *Phaeocystis* bloom and *Phaeocystis* appeared in the model during this period but at low abundance; the model underestimated a large observed summer dinoflagellate bloom; and the model did not capture historic minima in measured seafloor oxygen at many stations in May and June. Despite this, model results were mostly within ranges of past years, and did capture observed summer and fall oxygen levels.

Overall, the 2020 simulation supports the conclusions from field monitoring, that eutrophication was not a concern and bay-wide ecological function was not appreciably influenced by the outfall.

Special study. A hypothetical scenario run, to explore further the potential for eutrophication, was identical but with 1.5 times higher effluent nutrient concentrations. This increased the nitrogen load to the bays, from all sources, by about 4-5% and system-wide productivity increased similarly. DIN increased notably near the outfall as expected, but effects on chlorophyll and oxygen were minor. The total nitrogen load was about 24% higher than the Contingency Plan warning level threshold.

Contents

List of Figures

List of Tables

1 Introduction

The Massachusetts Water Resources Authority (MWRA) has established a long-term monitoring program to evaluate the impact of its sewage treatment plant effluent on the water quality and ecosystem function of Massachusetts Bay, Cape Cod Bay, and Boston Harbor. The monitoring program primarily consists of a series of ongoing field observation surveys and includes complementary water quality modeling as required by the discharge permit. The water quality simulations are carried out using the Bays Eutrophication Model (BEM, Deltares, 2021). This report presents simulation results for the 2020 calendar year. The content of this report is derived from internal Deltares document 11203379-005-ZKS-0005, dated 10 June 2022.

1.1 Background on oceanographic processes influencing water quality

Massachusetts Bay and Cape Cod Bay (Figure 1-1) comprise a temperate coastal embayment system. Readers unfamiliar with the geography and/or the current understanding of the physical and biological oceanographic processes characterizing the system are referred to the introductory summaries found in sections 1.2 and 1.3 of MWRA Technical Report 2011-13 (Zhao et al., 2012), in the annual MWRA water column monitoring reports (e.g., for calendar year 2020, Libby et al., 2021), and in references cited by them. (All MWRA Technical Reports, including those just cited, are available online at http://www.mwra.state.ma.us/harbor/enquad/trlist.html.) A brief summary follows here. In this subsection the focus is on processes and influences other than effluent from the MWRA outfall, which has been shown in past studies to have a minor system-wide effect.

System hydrodynamics are characterized by a persistent general circulation pattern driving the flow of offshore Gulf of Maine waters into Massachusetts Bay via the Western Maine Coastal Current off Cape Ann, then southward before returning offshore just to the north of Cape Cod, with a portion of the flow first passing through Cape Cod Bay to the south (Figure 1-1). Rough estimates of the water residence time are about a month based on the surface currents, somewhat longer at mid-depth or deeper, where currents are weaker, and also longer in Cape Cod Bay than in Massachusetts Bay. While this slow general circulation is important in determining long-term average transport pathways, superposed on it are stronger and more variable wind-driven currents, and oscillatory tidal motions. Temperatures follow the characteristic temperate seasonal pattern of minima in late winter and peaks in late summer. Salinities are freshest inshore and in the upper several meters; in addition to the influence of offshore oceanographic conditions, they vary mainly in response to riverine inputs including primarily those brought by the Western Maine Coastal Current and the Merrimack River outflow to the north, and to a lesser extent the smaller amounts delivered via Boston Harbor. There is a seasonal cycle in vertical structure that includes transitions between well-mixed conditions, present from fall through early spring due to higher winds and atmospheric cooling, and strong density stratification during the late spring and summer due mainly to increased surface temperatures resulting from atmospheric heating.

The biology of the system is plankton-based and exhibits clear seasonal cycles that are tied closely to those hydrodynamic features, but with more pronounced spatial and inter-annual variability. Phytoplankton abundance typically peaks most strongly during bloom-favorable conditions in the late winter and early spring, as temperatures rise, light increases, and nutrients remain plentiful near the surface due to the active vertical mixing. Following the transition from spring to summer, near-surface nutrient concentrations become depleted as density stratification impedes the vertical mixing that

replenishes them. Zooplankton abundance and biomass generally peak in late summer, following the spring increase in phytoplankton prey levels. Primary productivity is commonly sustained at modest levels through summer and typically there is a second increase in phytoplankton during fall, when vertical mixing increases again and delivers nutrients to the surface while temperature and light conditions are still favorable before winter. Dissolved oxygen concentrations are influenced by a combination of biological and physical processes; the net result is a seasonal peak in late spring, due to phytoplankton production increasing winter levels already high due to strong reaeration, then steady decreases to a late summer minimum due to respiration and reduced reaeration. The summer oxygen minimum is lower at depth, where stratification limits reaeration.

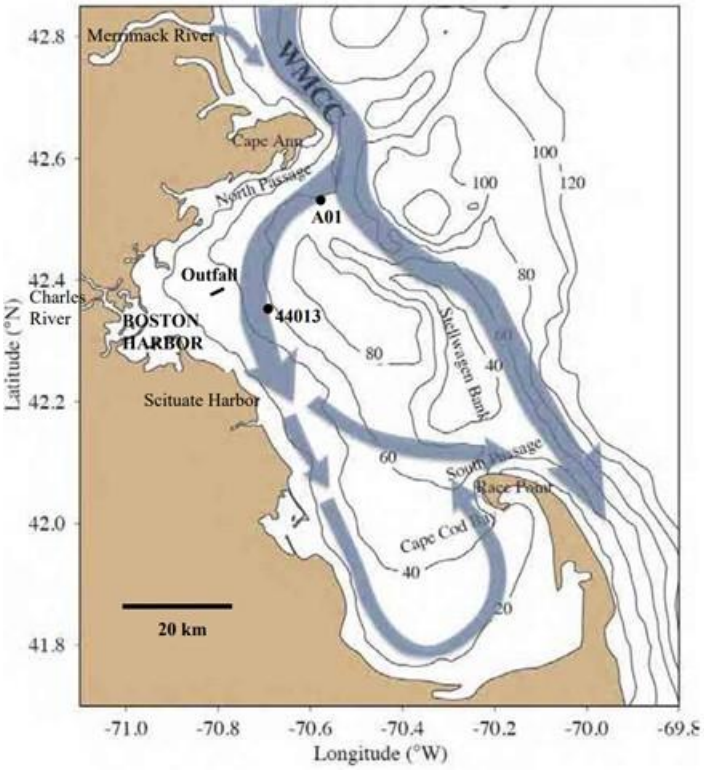

Figure 1-1 Geography, bathymetry, schematic long-term mean circulation.

WMCC = Western Maine Coastal Current. A01 = Oceanographic mooring (Northeastern Regional Association of Coastal and Ocean Observing Systems). 44013 = Weather buoy (National Data Buoy Center). Contours = water depth in meters. Figure from Zhao et al. (2017), adapted from Xue et al. (2014).

1.2 Summary of observed 2020 conditions

To provide context for descriptions of model simulations of 2020 throughout this report, a brief summary is given here of observed 2020 conditions based on monitoring results (Libby et al., 2021). Due to the COVID pandemic, monitoring was disrupted and fewer measurements were collected. River flow was lower than typical, there was no large spring freshet, and for the Merrimack River discharge the summertime period was indicative of moderate drought conditions. High chlorophyll levels were observed during surveys in February in Cape Cod Bay, in early May in Massachusetts Bay, and in August and September across much of both bays due to a large dinoflagellate bloom. During the May survey *Phaeocystis* was abundant and there was a sharp increase in the nitrate to silicate ratio suggesting that the high chlorophyll, which ocean color satellite images showed was

present from mid-April to mid-May, was due to a *Phaeocystis* bloom. Nutrient concentrations, including the influence of MWRA effluent near the outfall, followed the typical annual cycle. Summer average water temperature was the warmest over the 29-year period of observations, which contributed to record-high stratification strength in July. Summer upwelling due to wind forcing, which generally causes cooling, was weaker than typical and likely contributed to the warm temperatures. Relative to the typical annual cycle, bottom water dissolved oxygen was low from February to June, with historic minima at many stations in May and June; from June to July it increased, presumably as a result of some physical process such as mixing due to a wind or circulation event, such that the annual minima in late summer were at typical levels over most of Massachusetts Bay. In Cape Cod Bay, there was a similar increase in oxygen during July, but then it declined to very low levels in August, and for the second year in a row hypoxia (oxygen < 2 mg L^{-1}) occurred there in the shallow southwestern nearshore area. A combination of factors is thought to have contributed to the hypoxia (Scully et al., 2022): the large dinoflagellate bloom, including *Karenia mikimotoi,* in August/September as a source of biomass; the strong stratification; and the relatively small pool of deep oxygen, due to the depth of the pycnocline being near the seafloor.

2 Methods

A complete model description is documented in MWRA's technical report 2021-02 and its appendices (Deltares, 2021). The model is set up in the Delft3D Flexible Mesh Suite, developed by Deltares. Technical details on the model set-up, its grid and forcing is presented in Appendix A of Deltares (2021). A description of the software package and underlying hydrodynamic and water quality equations are available in Section A1 of Deltares (2021), and in Deltares (2019a, b). The model was calibrated using the years 2012-2016, as described in Appendix B of Deltares (2021). The results of the model validation are given in the main report body of Deltares (2021).

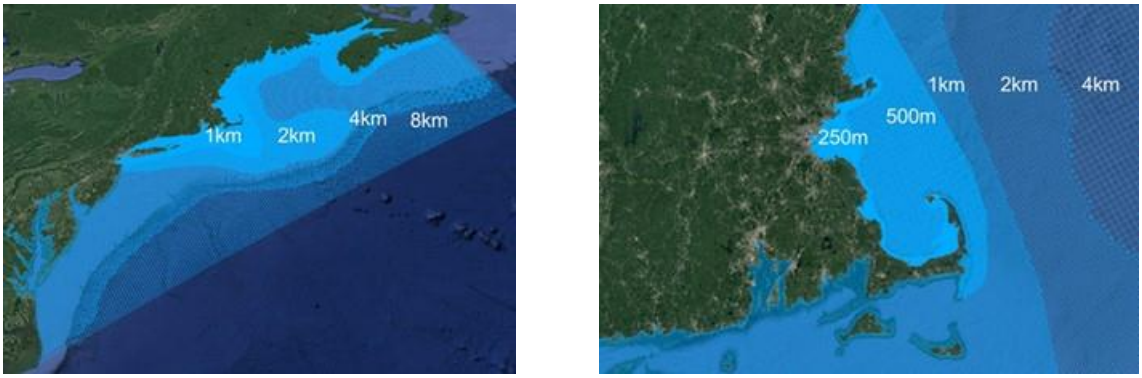

Figure 2-1 Model grid of the entire model domain (left) and zoomed-in for Massachusetts Bay (right)

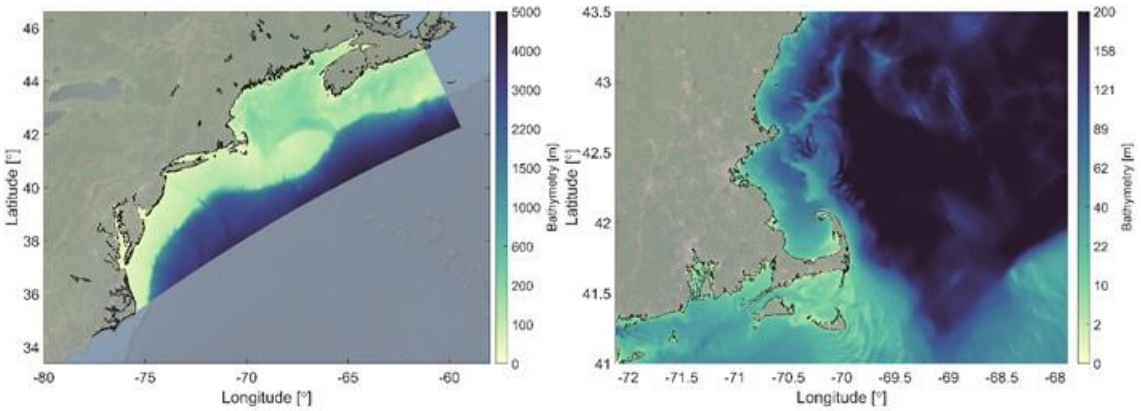

Figure 2-2 Model bathymetry of the entire model domain (left) and zoomed-in for Massachusetts Bay (right)

The model domain is large in order to best handle influences of offshore boundaries, as explained in Deltares (2021); it covers the entire Gulf of Maine region as well as the coastal region to the south, down to and including Chesapeake Bay (Figure 2-1 and Figure 2-2). Model performance in comparison to field measurements has been demonstrated most carefully in the area of Massachusetts Bay nearest the outfall, using MWRA observations (Deltares, 2021). The horizontal resolution is roughly 8 km at the open ocean and is gradually refined toward the coast, with a maximum resolution of 250 m in Boston Harbor and along the surrounding coastline, including at the outfall location.

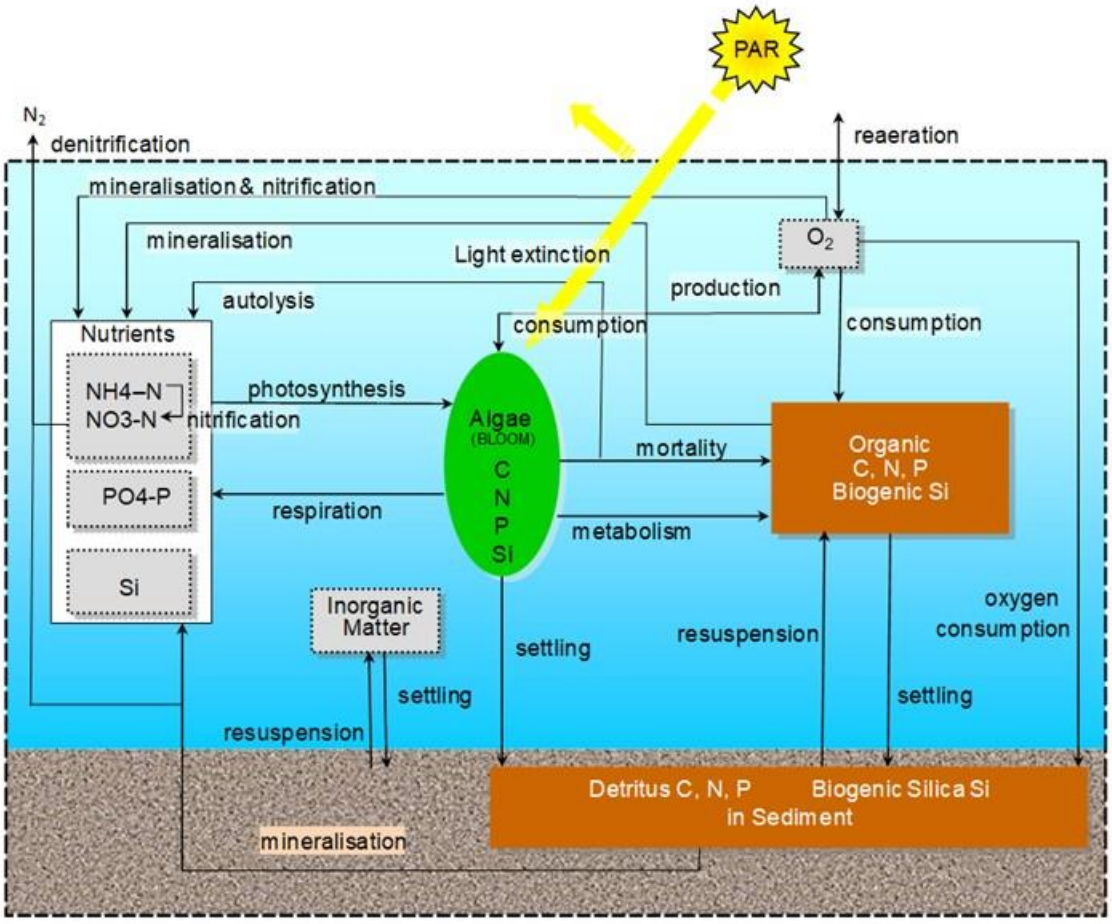

Figure 2-3 Schematic overview of all state variables and processes. Reproduced from Deltares (2021). Note that Inorganic Matter, Algae and Detritus affect light extinction in the water column.

Figure 2-3 provides an overview of the simulated state variables and processes for the water quality component. Four functional groups of pelagic phytoplankton are simulated (“Algae” in the figure): diatoms, dinoflagellates, other flagellates, and *Phaeocystis*.

The monitoring stations used to assess model performance and the transects along which water quality variables are examined are mapped in Figure 2-4. Model-observation comparison time-series are plotted for a representative selection of eight stations: N01 in the Northern Mass Bay, F22 with a greater oceanic influence, F23 near the outlet of Boston Harbor, N18 close to the MWRA outfall, N07 southeast of the outfall, F13 and F06 toward the south shore, and F02 in Cape Cod Bay.

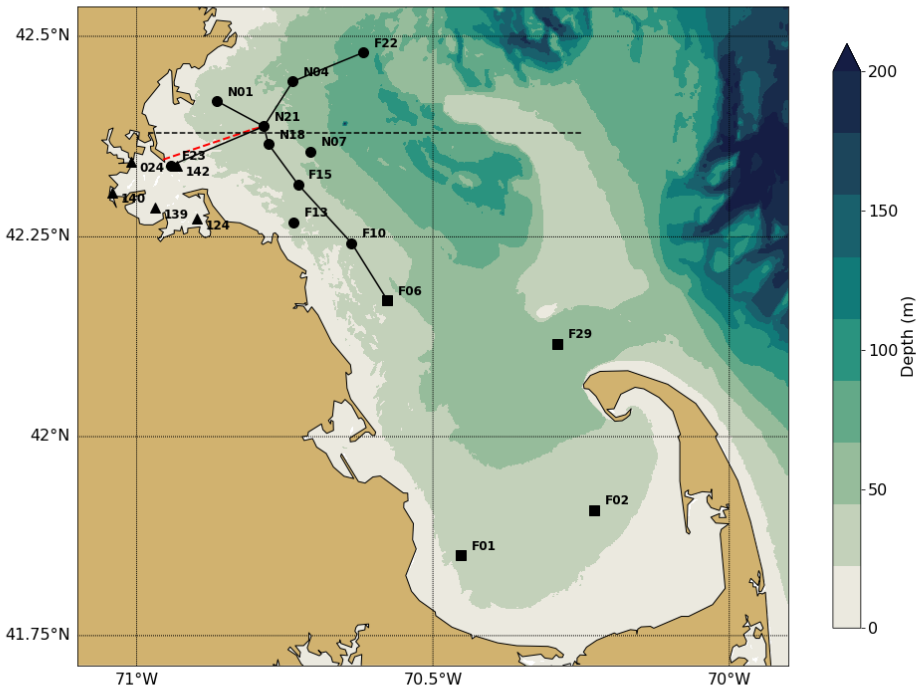

Figure 2-4 Location of MWRA monitoring locations (circles=Northern stations, squares=Southern stations, triangles=Harbor stations). The red dashed line indicates the tunnel to the outfall diffusers. The black lines are the West-East and North-South transects used for model-observation comparisons. The horizontal black dashed line represents the transect through the outfall on which model results are presented in later figures.

2.1 Updated methods

In the 2020 BEM run, no changes to the methods as used for the 2019 BEM run (Deltares, 2022b) were implemented.

3 Forcing

3.1 Wind, heat flux, solar radiation and rivers

3.1.1 Wind

In Figure 3-1, the main characteristics of the monthly-mean wind forcing for the simulated year 2020 are compared to the means of the previous 20 years (1999-2019) for the A01 mooring location off Cape Ann (Figure 1-1). Ranges of the standard deviation and of the minimum and maximum values are also shown.

The seasonal pattern of the vector-averaged velocities (top frame) largely followed the long-term mean. Notable differences were visible in the months of February, November and December, when the usual southward component was not present, and winds were directed to the east. In April and May, the northward component was smaller than average.

Wind speeds (second frame) were lower than the long-term mean in January, February, July, October and November. In April and May, the wind speeds were higher than the long-term mean. Monthly-mean wind stress magnitudes (third frame) show a similar pattern. The mean wind stresses were weak in the first three months, and in July and October. North-south wind stresses (bottom frame) are an indicator for upwelling. North-south wind stress was weaker than normal in the period April to June, which is in agreement with 2020 observations of weaker upwelling than typical.

3.1.2 Heat flux

A comparison between time series of the calculated net air-sea heat flux (including solar radiation) for 2020 and for the previous years is given in Figure 3-2. A moving average with a window of 3 days is applied to visualize the instantaneous values. The time series of the net flux includes ranges of the standard deviation from the mean and of the minimum and maximum values. The cumulative flux (middle frame) is presented without any filtering.

The seasonal pattern in 2020 (top frame) showed an overall negative heat flux in winter (loss of heat from the surface, cooling of the ocean) and an overall positive heat flux in summer (heating of the ocean). In the first months of the year the net flux was above the long-term mean. The rest of the year, it was close to average. It was slightly above average during the last months of the year.

The effect of January and February stayed visible in the cumulative flux (middle frame) throughout the year. It remained at about 0.5 GJ/m² above the long-term mean until the end of the year. The same pattern was visible in the cumulative anomaly of the heat flux (bottom frame).

3.1.3 Solar radiation

The solar radiation from the meteorological forcing product is given in Figure 3-3. The solar radiation was similar to the long-term mean in most months. However, in April it fell below average, causing a decrease in the cumulative flux, which remained at about -0.1 GJ m^{-2} until the end of the year. So, on an annual-mean basis, 2020 had slightly less incident surface solar radiation than a typical year.

The higher than average net surface heat flux in 2020 occurred despite the lower than average incident radiation in 2020. Every year there is a net influx of solar radiation of about 5.5 GJ m^{-2}. Since the net air-surface heat flux was about 1.0 GJ m^{-2} in 2020, around 4.5 GJ m^{-2} was lost through other air-sea heat fluxes. These fluxes consist of evaporative and convective turbulent fluxes or long wave radiation.

3.1.4 Rivers

In Figure 3-4 the volume transport for Merrimack River is presented. The figures include the daily-averaged discharges (top frame) for the simulated year 2020 and for the previous twenty years (1999-2019). Ranges of the standard deviation and of the minimum and maximum values are also given.

The discharge in the Merrimack River was similar to the long-term mean in the first five months of the year. After that, it remained below average with only two events above average in December. This was visible in the total discharged volume (middle frame), which deviated from the long-term mean after May. The end-of-the-year anomaly of the discharged volume (bottom frame) was negative with a value of about -1.8 km^3.

The combined volume transport for the rivers discharging directly to Massachusetts Bay and Cape Cod Bay is presented in Figure 3-5. These rivers are Saugus, Mystic, Charles, Neponset, North and Jones. The pattern of the combined discharge was similar to the pattern of discharge of the Merrimack River. The discharged volume was lower than the long-term mean from June onward. This resulted in a negative anomaly of the discharged volume (bottom frame) of -0.14 km^3 at the end of the year.

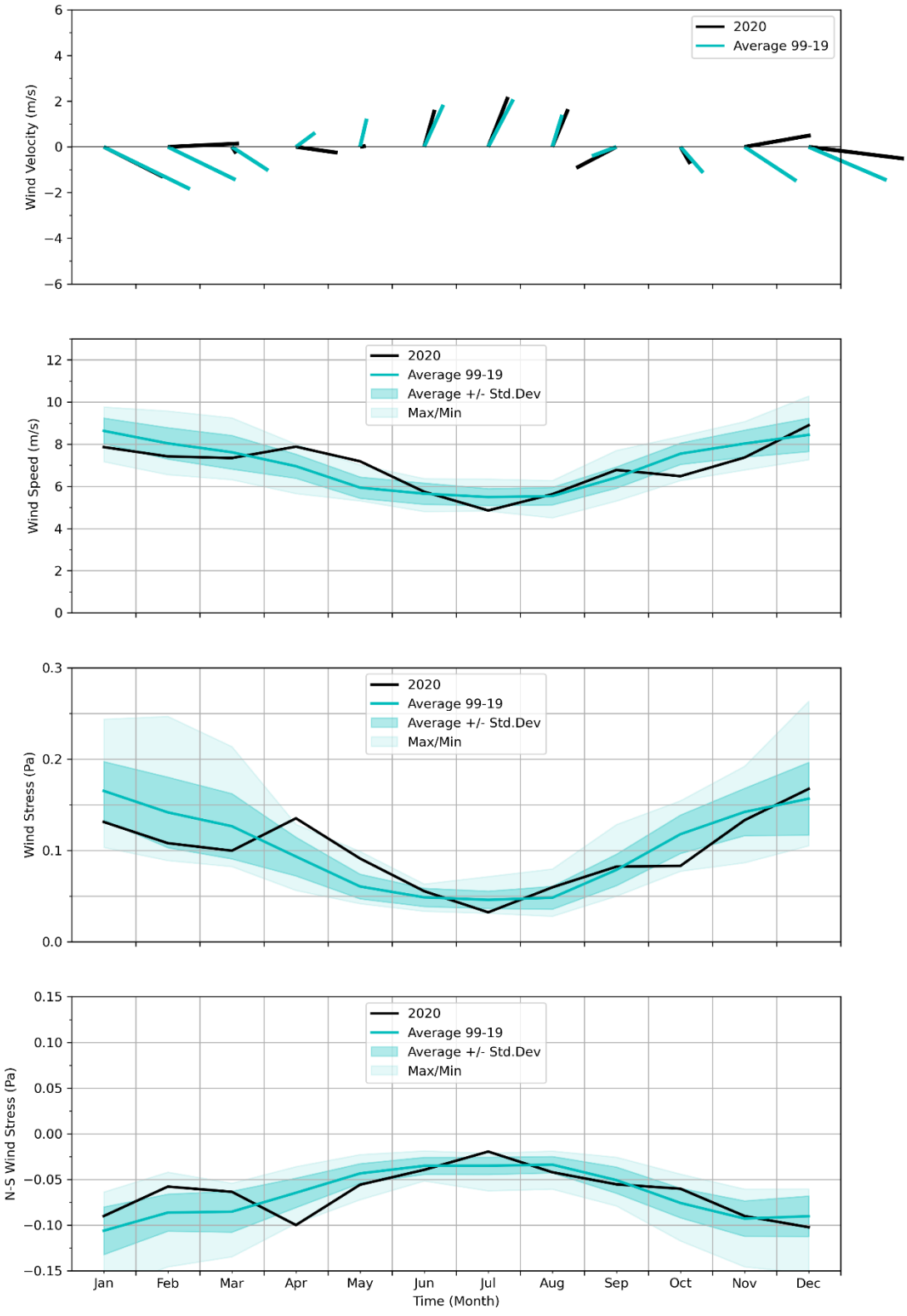

Figure 3-1 Surface wind forcing, monthly averages, compared to prior 20-year period.

Top frame: Vector-averaged wind velocities. Second frame: Wind speed. Third frame: Wind stress magnitude. Bottom frame: North-south component of wind stress, an indicator for wind-driven upwelling.

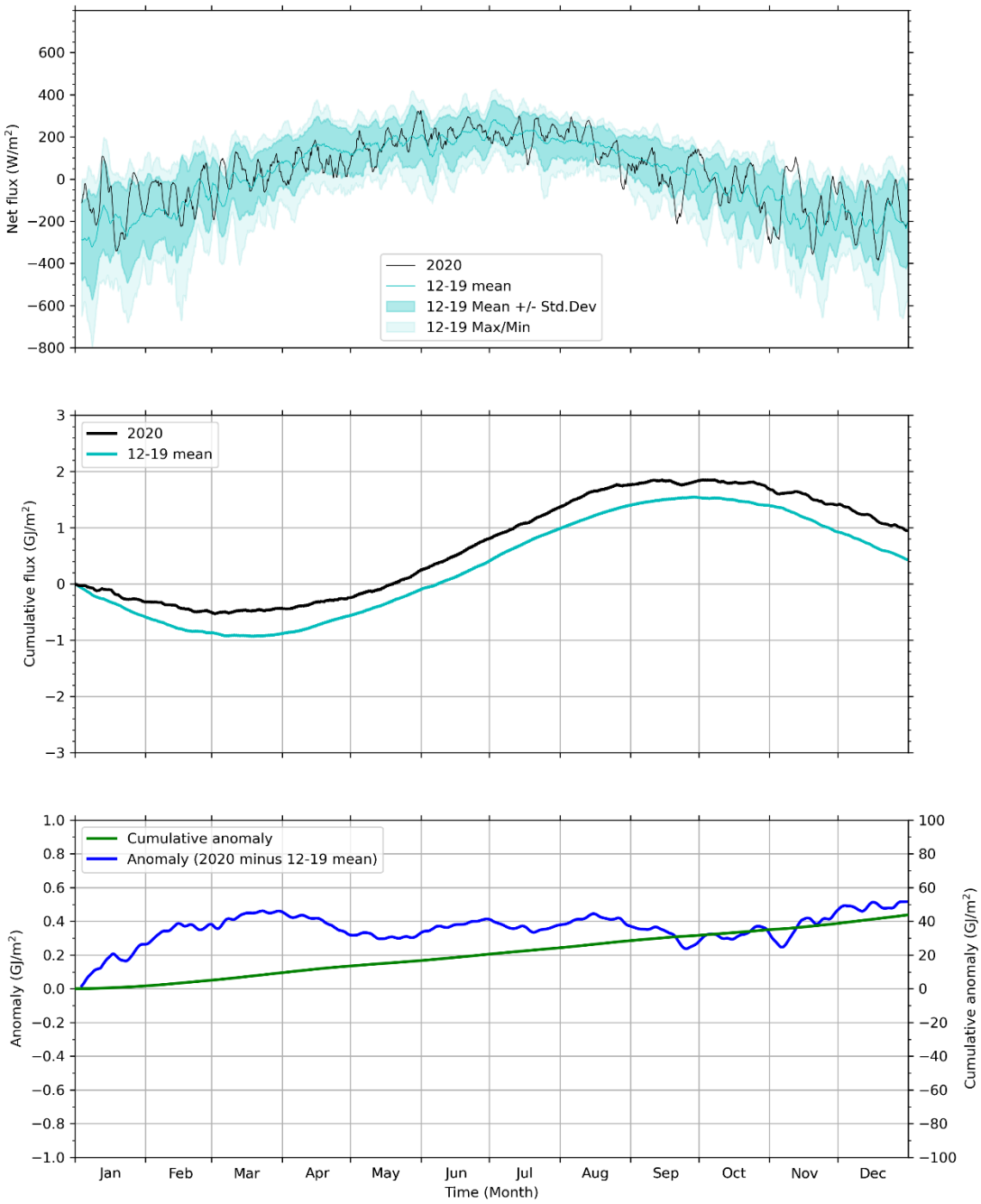

Figure 3-2 Surface heat flux, compared to prior 8-year period.

Top frame: Net heat flux into ocean. Middle frame: Cumulative net heat flux starting from January 1. Bottom frame: Anomaly (blue, left axis) and cumulative anomaly (cumulative sum of daily mean anomaly; green, right axis) of 2020 net cumulative heat flux relative to 2012-2019 average. The 2012-2019 reference period has been used because direct simulation output is available; it is shorter than the 20 years used for the long-term mean.

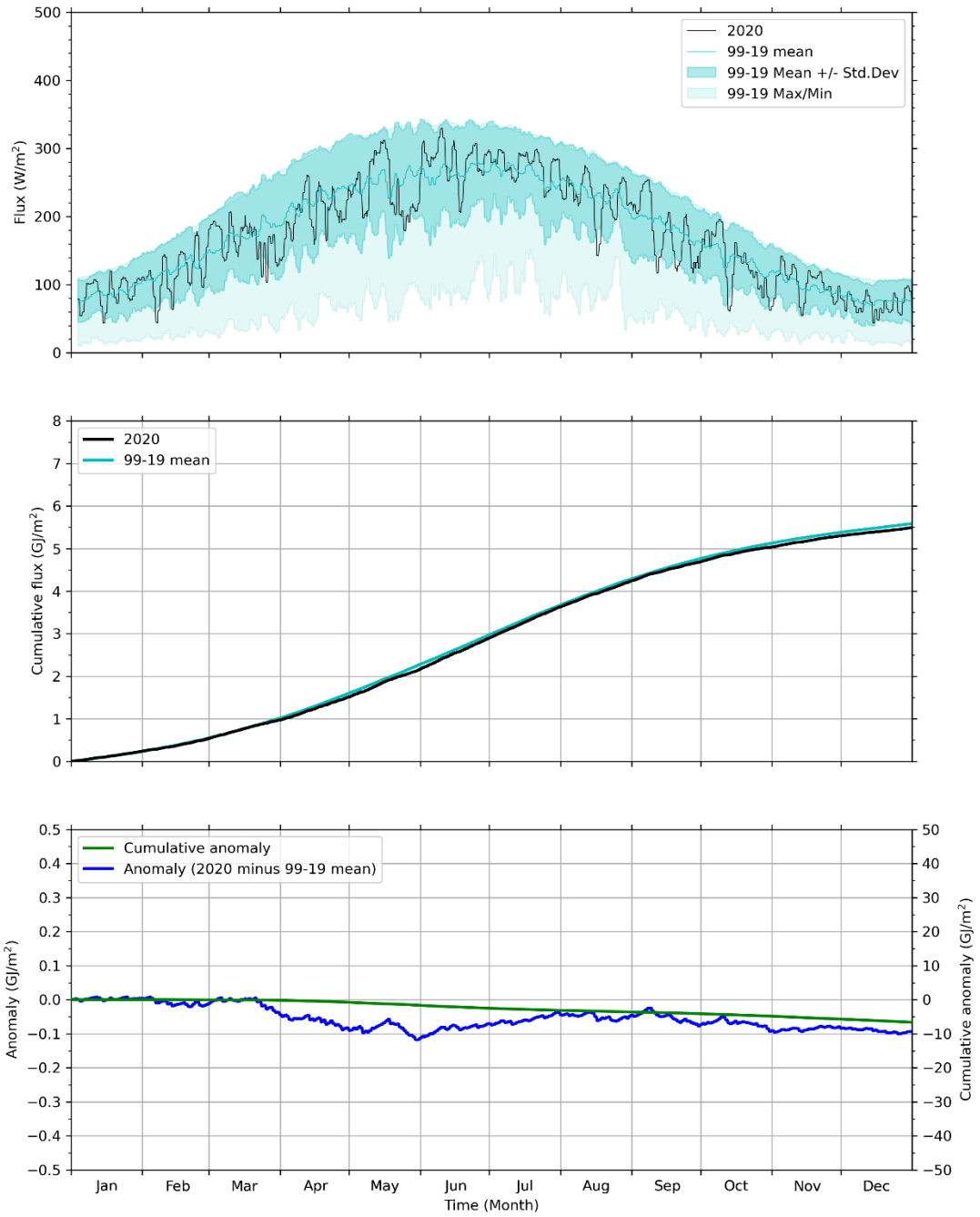

Figure 3-3 Solar radiation, compared to prior 20-year period.

Top frame: Solar radiation into ocean. Middle frame: Cumulative solar radiation starting from January 1. Bottom frame: Anomaly and cumulative anomaly (cumulative sum of daily mean anomaly) of 2020 cumulative solar radiation relative to 1999-2019 average.

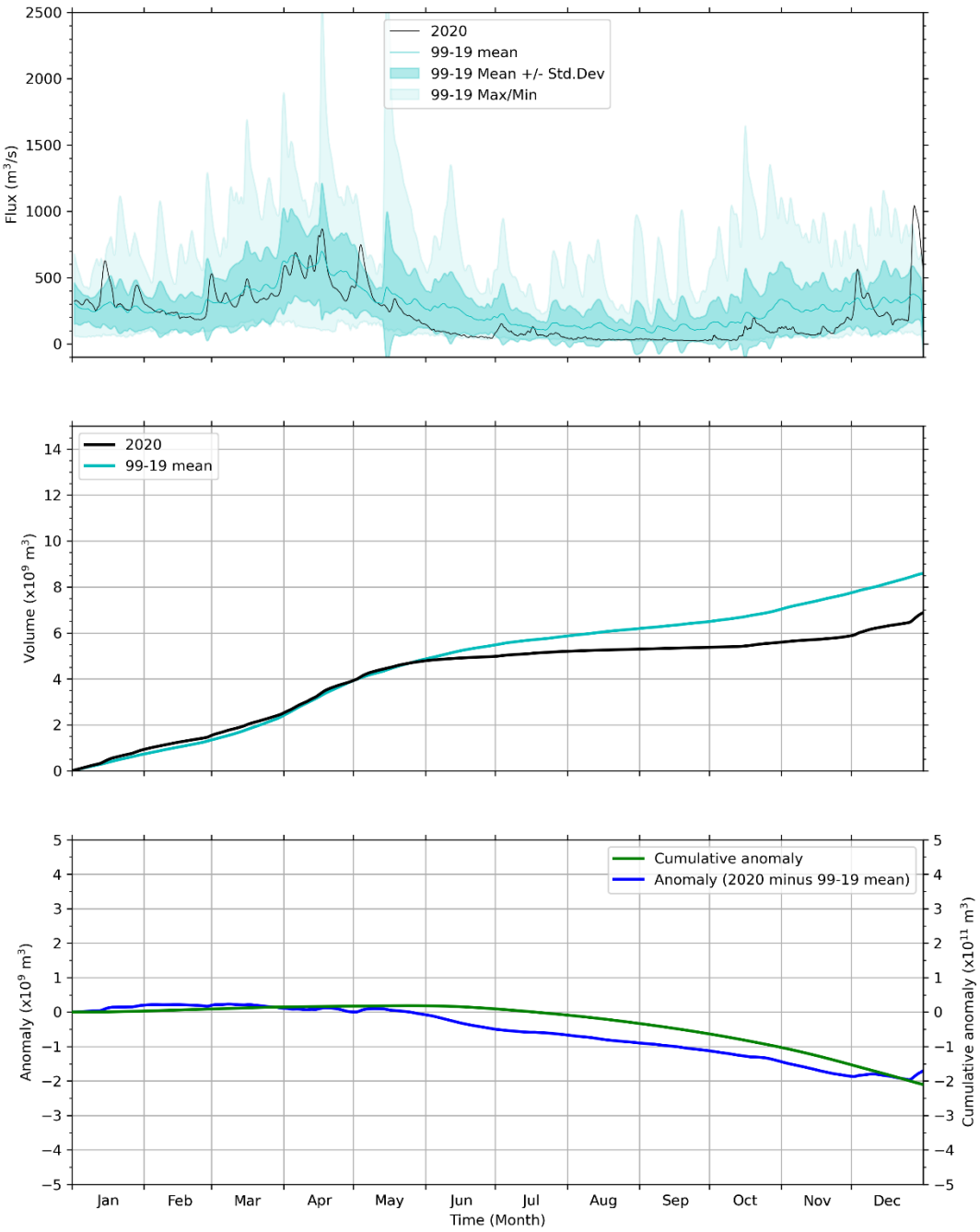

Figure 3-4 Merrimack River daily/cumulative flux and anomaly relative to previous 20 years.

Top frame: Merrimack River volume flux. Middle frame: Cumulative flux relative to January 1. Bottom frame: Anomaly and cumulative anomaly (cumulative sum of daily mean anomaly) of flux in 2020 relative to 1999-2019 average.

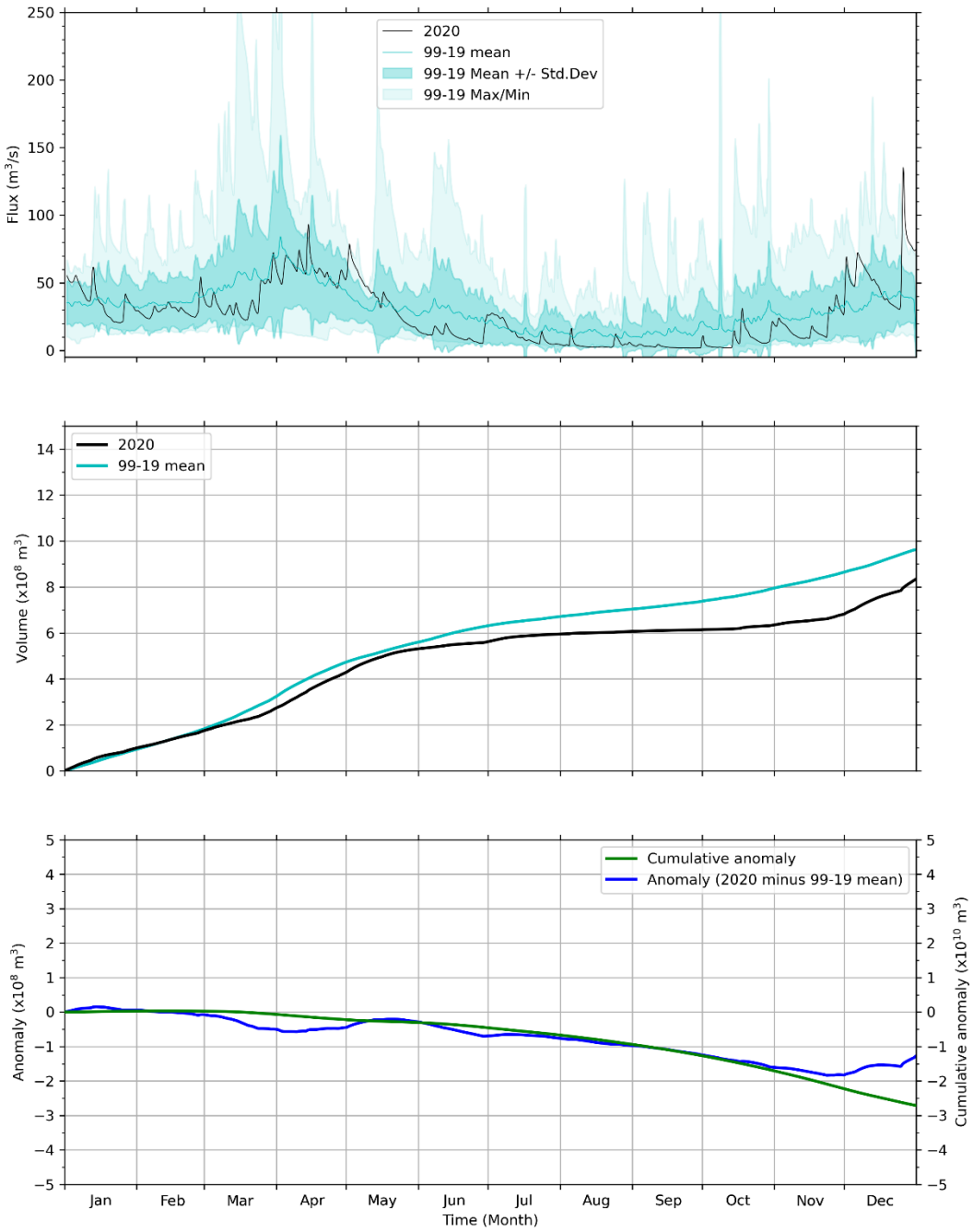

Figure 3-5 Summed discharge of all modeled rivers (Saugus, Mystic, Charles, Neponset, North, and Jones) flowing directly in to Massachusetts and Cape Cod Bays.

Presented as in Figure 3-4.

3.2 Loading of organic carbon, nitrogen, and phosphorous

Loads directly entering Massachusetts and Cape Cod Bays from rivers, the Deer Island treatment plant, and the atmosphere are shown in Figure 3-6. Loads entering the system through its offshore boundary are marked “oceanic input”, for example originating from rivers to the north including the Merrimack.

Model results show that oceanic input was the dominant source of organic carbon (OC), nitrogen and phosphorus (both in organic and inorganic forms), accounting for 99%, 89% and 95% of their total inputs, respectively (Figure 3-6). The simulated oceanic inputs of total nitrogen (TN) and total phosphorus (TP) were slightly lower than for previous years (by ~2 percentage points). TN input was comparable to the estimates based on the simulation of 1992 conditions from Hunt et al. (1999), reported by Zhao et al. (2017), though slightly lower. Hunt et al. (1999) indicated that 93% of the TN entering the Mass Bay originated from the Gulf of Maine.

Rivers were the second largest source of OC, accounting for 79% of the non-oceanic input. MWRA loads constitute the main non-oceanic source of TN and total phosphorus (TP). These occur mainly in the inorganic form. Atmospheric deposition accounted for approximately 11% of the non-oceanic TN inputs. Finally, rivers are the smallest source of TN and TP to Massachusetts and Cape Cod Bays, representing 6% and 4% of their non-oceanic inputs, respectively. The contributions of river inputs to total OC, TN and TP loads were lower in 2020 than in previous years.

The 2020 OC loads from the MWRA effluent were in the middle of the range of loads from the preceding years 2015-2019. The 2020 TN and TP effluent loads were on the low side compared to 2015-2019. The organic fraction of TN effluent loads was relatively high compared to the years 2015-2018.

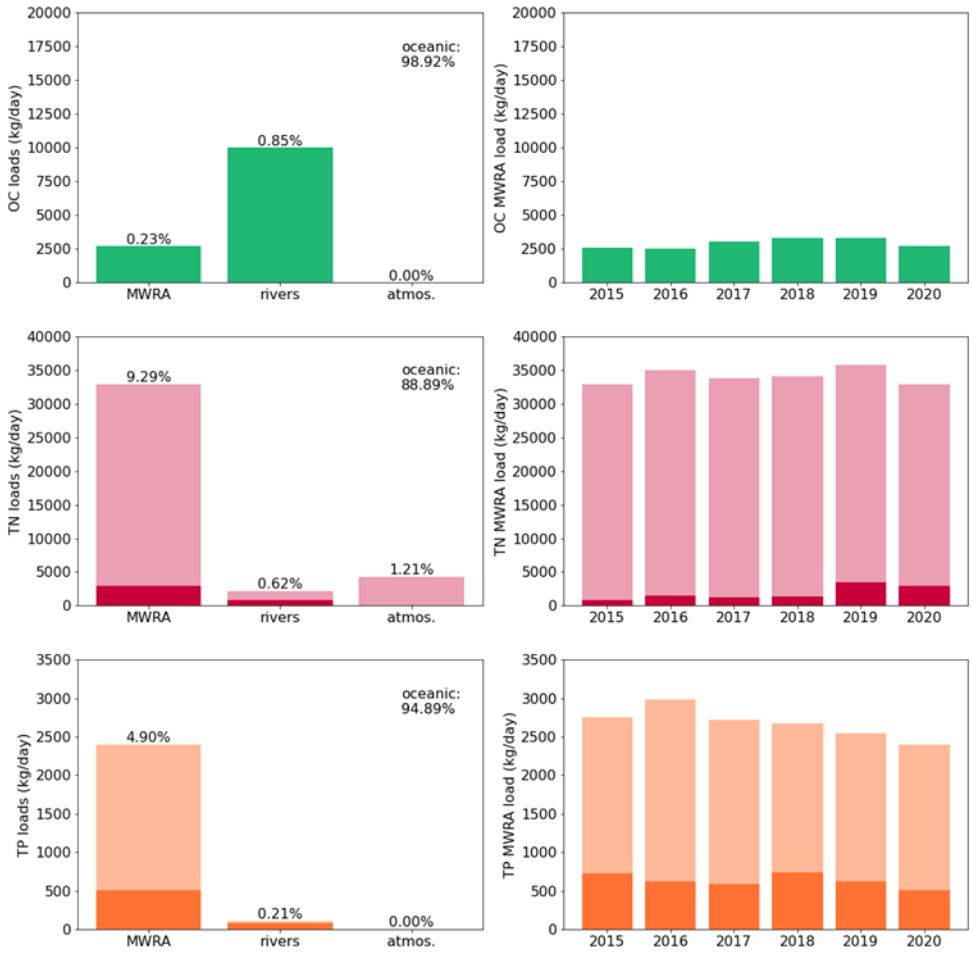

Figure 3-6: Organic Carbon (OC), Total Nitrogen (TN) and Total Phosphorus (TP) loads to Massachusetts and Cape Cod Bays in 2020. In the TN and TP plots, the darker sections of the bars represent the organic fractions. Left: loads from non-oceanic sources; percent of total is shown at top of each bar, and percent oceanic input (offshore boundary) shown at upper right. (Percentages correspond to summed organic and inorganic fractions.) Right: Deer Island Treatment Plant loads since 2015. OC=organic carbon; TN=total nitrogen; TP=total phosphorus.

4 Hydrodynamic Model

In this section the performance of the hydrodynamic model is discussed, and model results are compared to measurements.

4.1 Verification of model performance

The model skill was assessed for surface and bottom temperature and salinity by means of a statistical analysis. Three quantitative skill measures (correlation, normalized standard deviation Std*, and normalized unbiased root mean square error uRMSE*) were determined, based on simulation results and vessel-based observations by MWRA surveys. The result is presented in four sets of Taylor diagrams in Figure 4-1. The left column shows the 2012-2016 validation period (Deltares, 2021) and the right column shows the 2020 simulation. See also the box below for further details and an explanation of the statistics in the diagrams.

Temperatures had correlation of over 0.96 and 0.90, Std* of 0.90-1.10 and 0.80-1.25, and uRMSE* of under 0.30 and 0.45, at the surface and bottom respectively. The performance at the surface was slightly improved compared to the validation result, while at the bottom the larger spread of points indicates slightly worse performance.

The skill of simulated salinity varied more per observation station, compared to temperature. The performance at the surface and at the bottom is mostly similar to the validation result. At the surface, lower correlations are noted for stations F02 and F23, and at the bottom the skill is poorer at stations F02 and F29. These can be explained by the smaller salinity variation throughout the year due to weaker stratification associated with the lower than typical Merrimack River flow.

Overall, the figures presented here serve to verify that the performance of the hydrodynamic model in the simulations of 2020 did not deviate substantially from its performance during the 5-year validation period. For completeness, Taylor diagrams broken out for individual years 2012-2016, are presented in Appendix A of the Annual BEM Report on 2017 (Deltares, 2022a).

How to read a Taylor diagram

A Taylor diagram consists of a combination of three quantitative skill measures:

- Correlation Coefficient, represented in the plot by the azimuthal angle or blue lines.
- Normalized Standard Deviation (Std*), the Standard Deviation of the model results, normalized (*) by the standard deviation of the corresponding measurements. This ratio represents the relative amplitude of the modeled and observed variations, with a value of less than one indicating less modeled variability. It is represented in the plot by the radial distance from the origin (0,0).
- Unbiased Root-Mean-Square Error or standard deviation of the error, normalized with the standard deviation of the corresponding measurements (uRMSE*). It is represented in the plot by the grey contours, whose values are proportional to the radial distance from the target (black star).

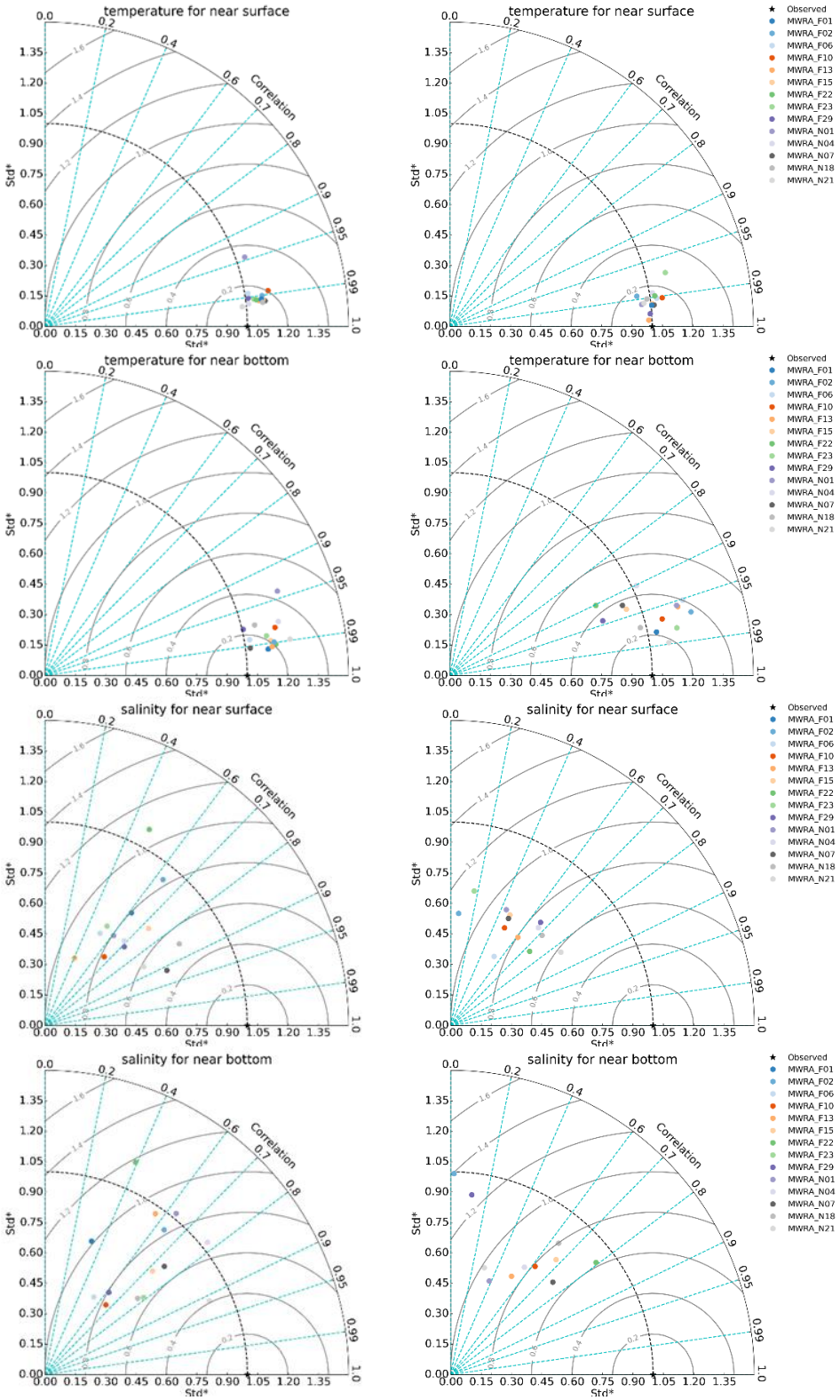

Figure 4-1 Taylor diagrams of model quality for MWRA vessel-based survey observations.

Temperature (upper frames), salinity (lower frames); 2012-2016 validation period (left column) and 2020 simulation (right column)

4.2 Model-observation comparisons

The simulation for 2020 was compared to observations to assess the level of agreement between them for temperature and salinity, both in time and space.

4.2.1 Time series of temperature and salinity

For eight observation stations in the Massachusetts Bay and Cape Cod Bay, simulation timeseries of the surface (less than 5 m deep) and bottom (within 5 m of seafloor) temperature and salinity are presented in Figure 4-2 and Figure 4-4, respectively. Additionally, a comparison at three levels within the water column, between the surface and seafloor, is given for temperature and salinity in Figure 4-3 and Figure 4-5 (described below), respectively.

In these figures, vessel-based observations by MWRA surveys are included as individual symbols. The locations of the observation stations are given on a bathymetric map in the upper left frame. They include four stations generally surrounding the outfall (N01, N07, N18, and F13), one to the south (F06), one farther offshore (F22), one at the mouth of Boston Harbor (F23), and one in central Cape Cod Bay (F02).

In Figure 4-3 and Figure 4-5. showing results from within the water column, the depths vary from station to station and survey to survey but are nominally at 25%, 50%, and 75% of the water depth. The model output between surveys is not shown on these figures because the depths used, set by the observations, differ from survey to survey.

Overall, the seasonal cycle and most events were well captured by the model. Simulated stratification was in line with observations. At most stations, the onset of temperature stratification was in early May with a maximum in July. The water column started to become mixed again over the course of October. The seasonal variations in salinity and salinity stratification in 2020 were less pronounced than in previous years. Both sea surface as seafloor salinities were rather constant at about 32.0 PSU. In the last days of September, stations in the shallower parts of Massachusetts Bay and Cape Cod Bay (N01, N18, F02, F06 and F13) were suddenly mixed after which the temperature stratification partially returned. This can be attributed to a storm event, visible in the timeseries of wind velocities in Figure 4-12. A sudden drop of bottom temperature mid-July was observed in the observations (N01, F02, F13 and F23), which was also reproduced by the model. In most cases model-observation differences for temperature were less than 1°C at the surface and seafloor and slightly larger within the water column. An exception is the 2°C underestimation at N01 in the first half of July. Simulated salinity showed a bias of about 0.50-0.75 PSU throughout the water column, as discussed in Deltares (2021). In general, the model-observation differences were larger in the upper part of the water column and during the summer, when stratification occurred.

4.2.2 Spatial representation of temperature and salinity

To assess the simulation spatially, maps have been plotted for surface and seafloor conditions, with the mean of the modeled results averaged over a period of 5 days centered on the observation dates (Figure 4-6 and Figure 4-7 for temperature; Figure 4-8 and Figure 4-9 for salinity). The five presented periods span the seasonal cycle of stratification. For the model-observation comparison, the available observations are plotted over the simulation fields as colored symbols. Note that the presented simulation fields are the average over 5 days, where the observations are instantaneous values, usually measured in the morning. This might introduce a bias.

These figures show a good agreement between the simulation and observations. The spatial variation at both the surface and bottom was comparable, with near-shore temperatures warmer in summer and

colder in winter. At both depths, salinities were generally fresher near the coast. In contrast with other years, no large freshwater plume was present in the spring or summer of 2020. This is probably due to the low discharge from the Merrimack River in the summer months (Figure 3-4), which was indicative of moderate drought conditions, and the absence of a large spring freshet. Model-observation differences for temperature and salinity were largest in June. The salinity in the simulated plume was overestimated by about 1.0 PSU. At the seafloor, the maximum overestimation of the salinity of the simulated plume was 0.5 PSU. Model-observation differences for surface temperatures in June show an underestimation of up to 2°C. Throughout the rest of the year, and at the seafloor, model-observation differences were at most 1°C.

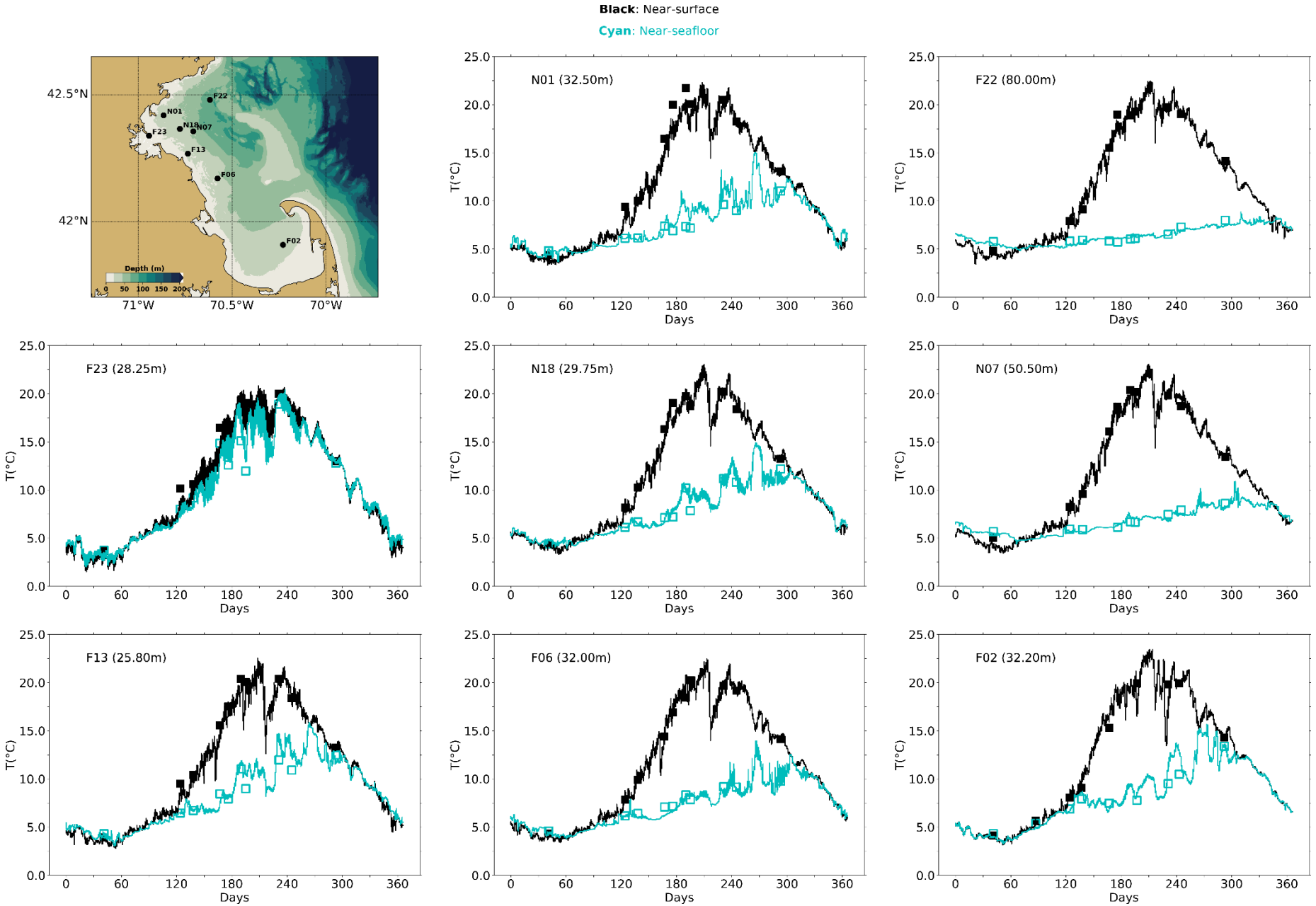

Figure 4-2 Temperature time series, model-observation comparison near surface (black) and seafloor (cyan).

Model results: lines. MWRA vessel-based survey observations: symbols.

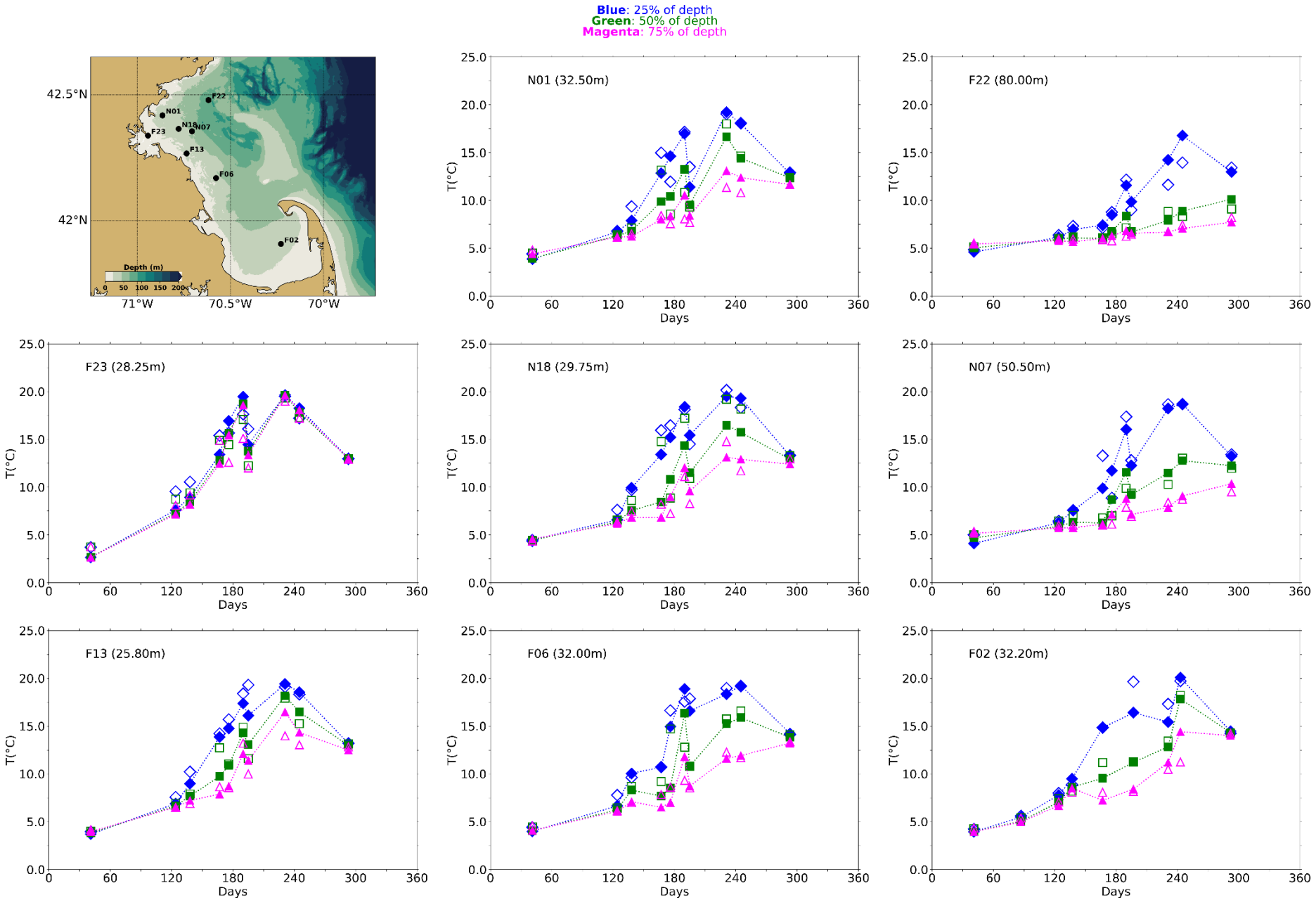

Figure 4-3 Temperature time series, model-observation comparison in water column (between surface and seafloor).

Model results: lines with filled symbols. MWRA vessel-based survey observations: open symbols.

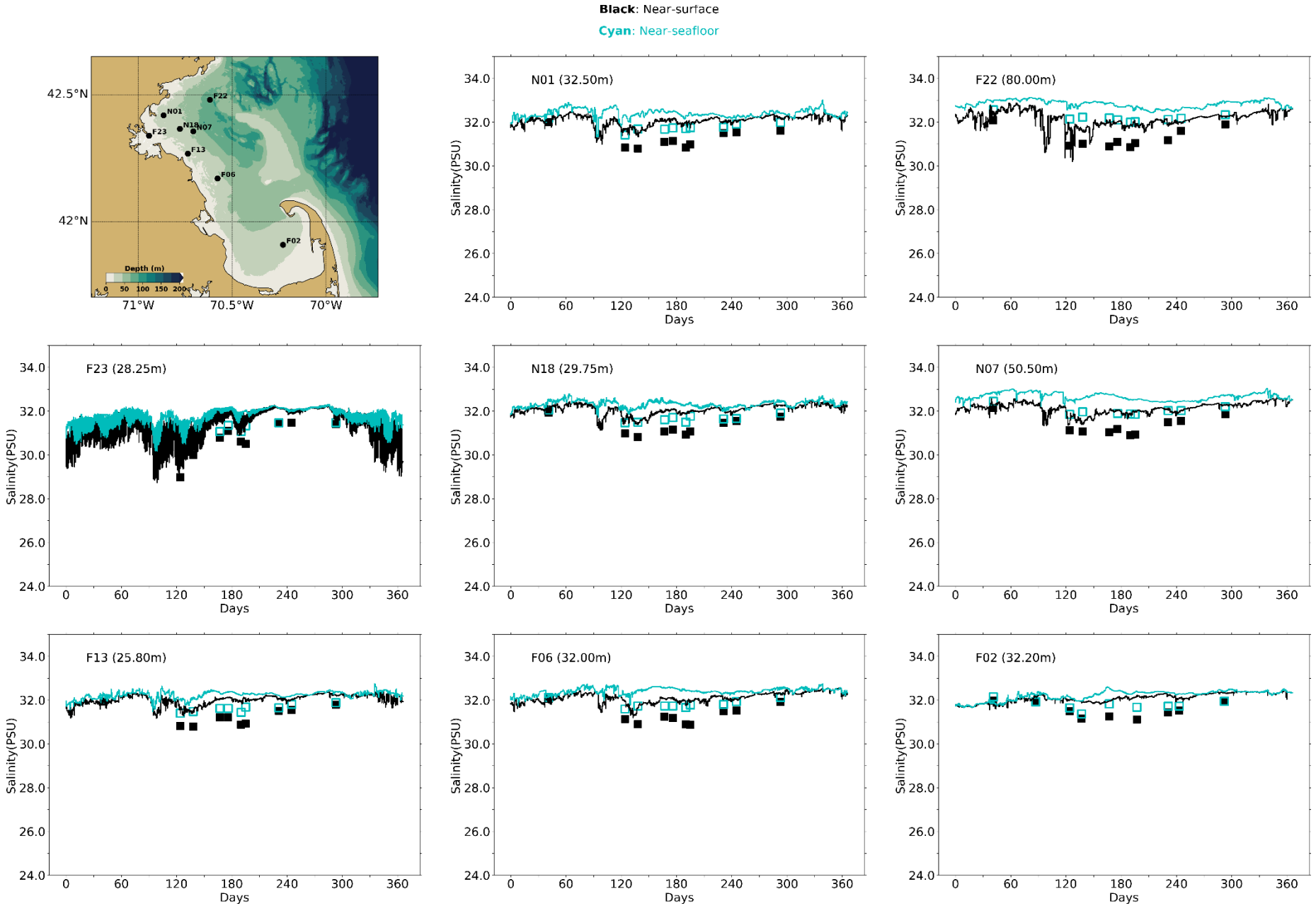

Figure 4-4 Salinity time series, model-observation comparison near surface (black) and seafloor (cyan).

Model results: lines. MWRA vessel-based survey observations: symbols.

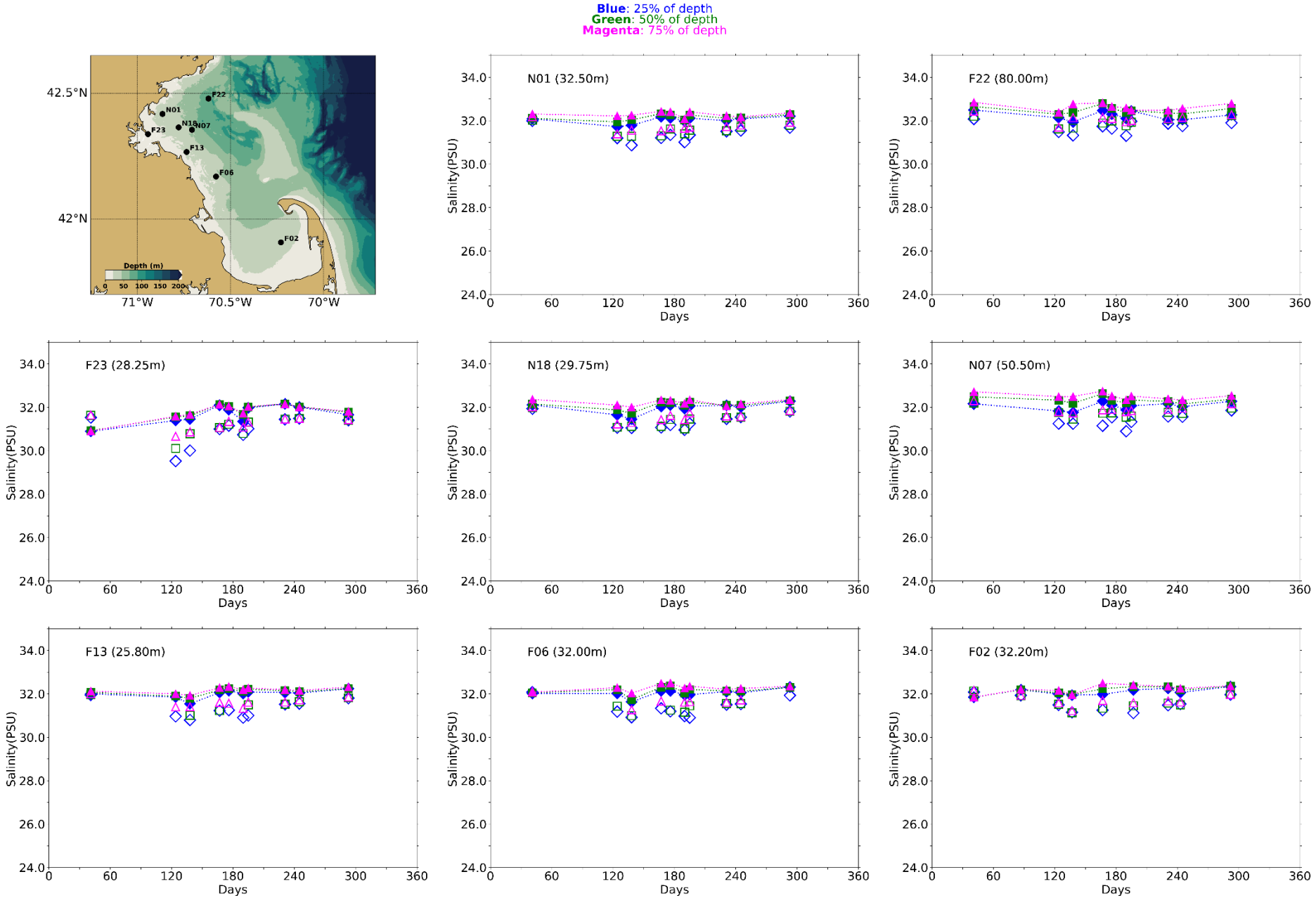

Figure 4-5 Salinity time series, model-observation comparison in water column (between surface and seafloor).

Model results: lines with filled symbols. MWRA vessel-based survey observations: open symbols.

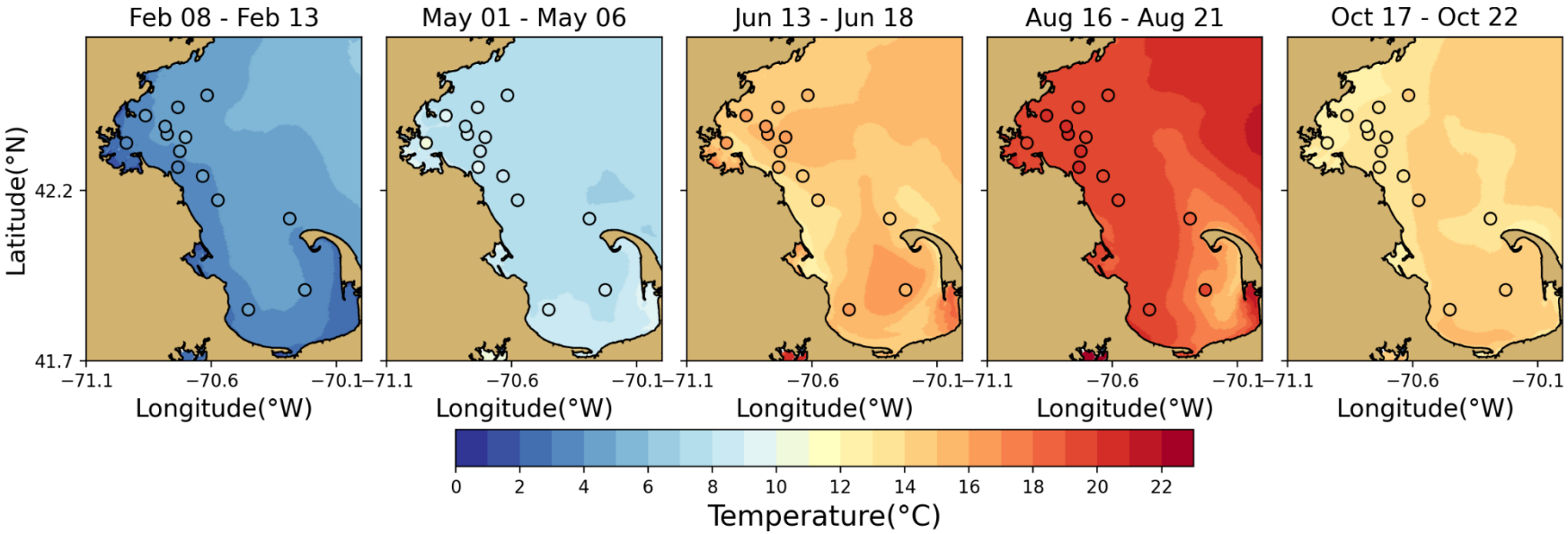

Figure 4-6 Temperature spatial structure, at/near sea surface, model-observation comparison.

Model results: background. MWRA vessel-based survey observations: symbols. Model results are averaged over the 5-day period centered on the measurement date.

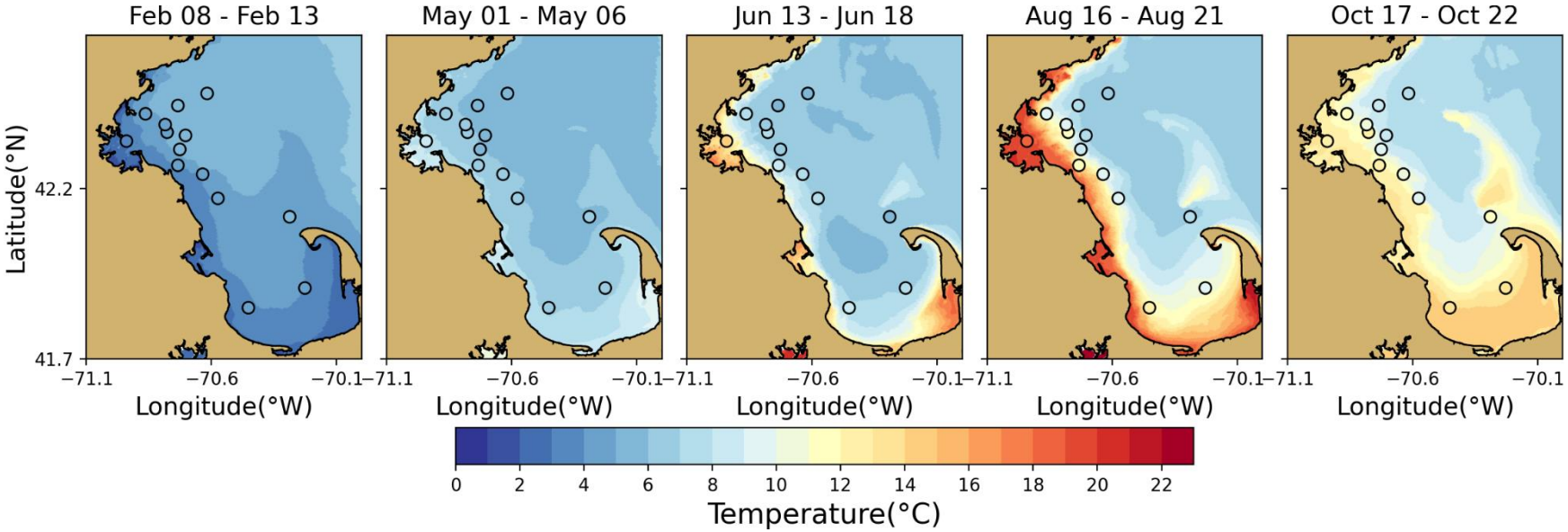

Figure 4-7 Temperature spatial structure, at/near seafloor, model-observation comparison.

Model results: background. MWRA vessel-based survey observations: symbols. Model results are averaged over the 5-day period centered on the measurement date.

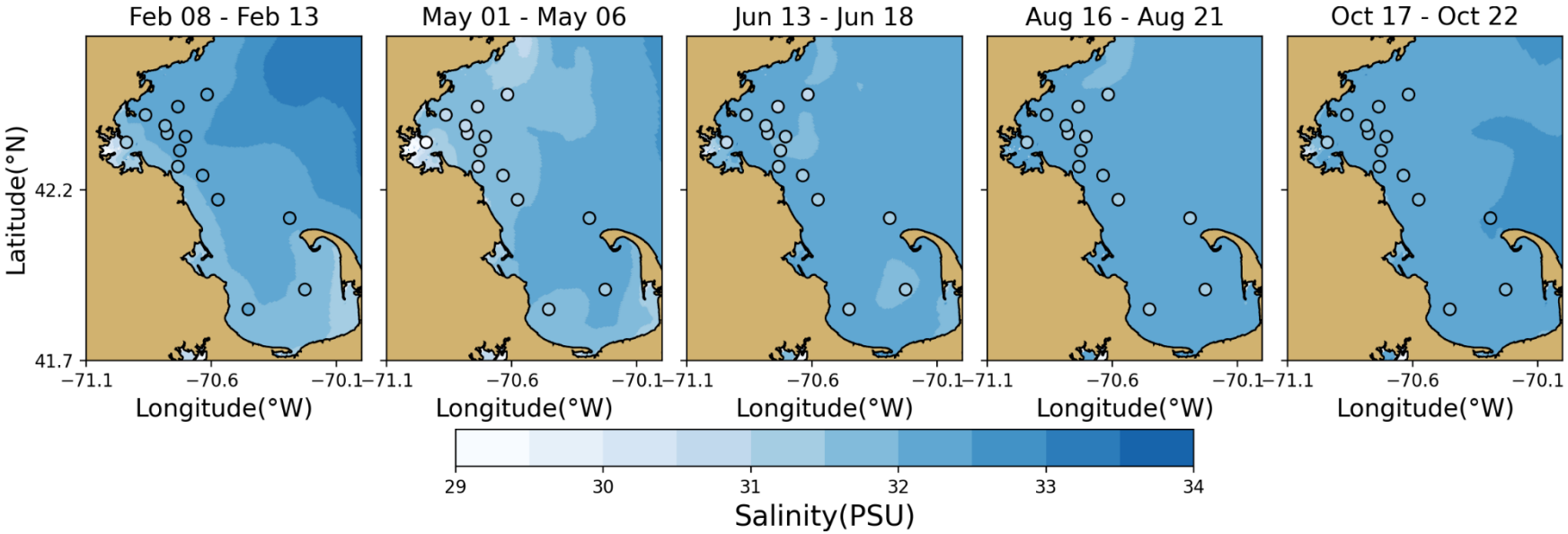

Figure 4-8 Salinity spatial structure, at/near sea surface, model-observation comparison.

Model results: background. MWRA vessel-based survey observations: symbols. Model results are averaged over the 5-day period centered on the measurement date.

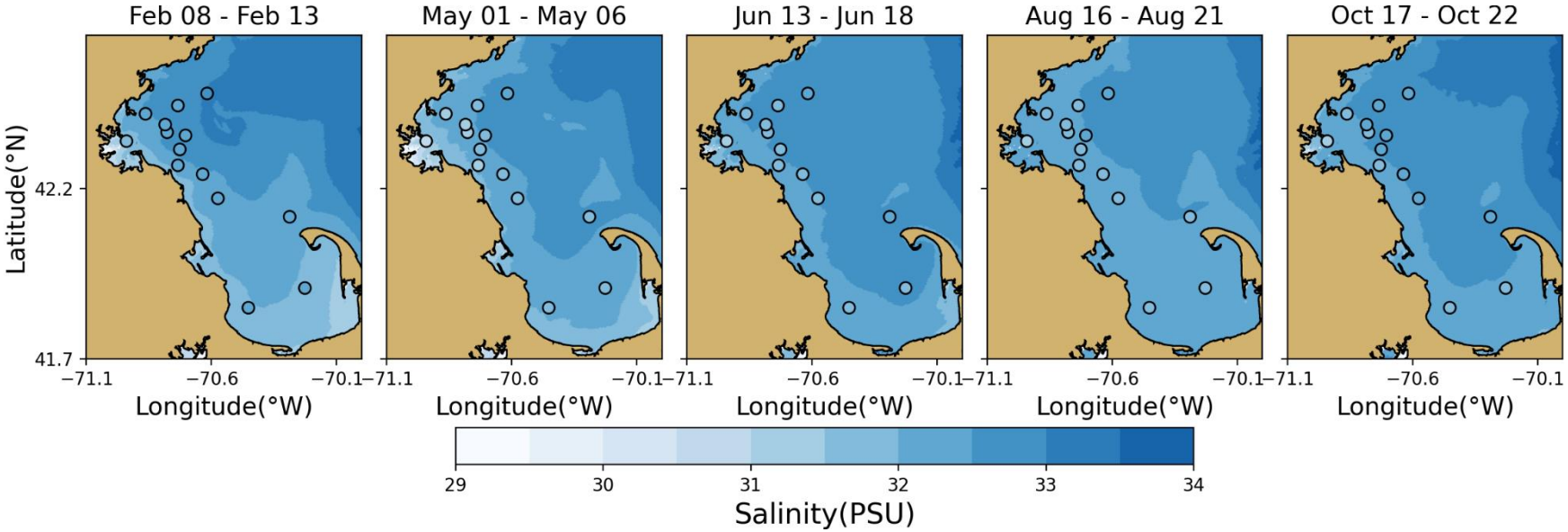

Figure 4-9 Salinity spatial structure, at/near seafloor, model-observation comparison.

Model results: background. MWRA vessel-based survey observations: symbols. Model results are averaged over the 5-day period centered on the measurement date.

4.2.3 Continuous measurements of temperature and salinity

Hourly measurements were available from Mooring A01 at multiple depths. This station is located south of Cape Ann, northeast from MWRA station F22. To provide a more complete assessment of the model-observation comparison in time, timeseries for this station are presented in Figure 4-10. For three depths (1m, 20m and 50m) the simulated and observed temperature and salinity are given. However, no observation data for temperature and salinity was available at the surface during the summer months. Consequently, large gaps were also present in the vertical salinity difference between 1m and 20m as well as 1m and 50m, as a measure of stratification. In contrast to other years, alternative surface temperature data at 2m deep was used. For salinity no alternative source was available.

The available data showed a good result of the model-observation comparison for temperature and salinity and different depths. The bias of about 0.50-0.75 PSU throughout the water column, as explained in Deltares (2021), is clear in the second frame of the figure. In 2020, there was an absence of the seasonal cycle of less saline water in summer. This can be explained by the low discharge from Merrimack River in 2020. In the summer months, surface temperature was slightly underestimated and temperature at 20m deep was slightly overestimated. In 2020, observed water temperature was the warmest over the 29-year period of measurements, so this represents an extreme situation for the model. Temperature stratification was well represented in the model. Individual events were captured, but in summer months, an underestimation of up to 2 degrees occurred. The salinity difference between the two deeper layers at 20m and 50m showed a good comparison between model and observations. Overall, the model captures features of observed stratification well, as is important for the water quality simulation because stratification is a main influence on vertical transport.

4.2.4 Continuous measurements of non-tidal currents

For Mooring A01 observed currents were available as well, although surface currents in the last three months of 2020 were missing. In Figure 4-11 and Figure 4-12 a model-observation comparison is presented for the first and second halves of the year, respectively. In the top frame, time series of wind from the meteorological product used to force the model is given for context. In the frames below, simulated and observed time series of non-tidal currents at four depths (2m, 10m, 22m and 50m) are given alternately. To remove the tidal variability, timeseries have been filtered using a low-pass filter with a 33h filter half amplitude (Alessi, 1985). The resulting signal consists mainly of weather-related and seasonal changes. For plotting this has been subsampled to a 6h resolution.

The time series of the filtered wind showed wind in all directions. Winds were generally changing on timescales of multiple days. In general, the wind speeds were lower during the calmer summer months. Winds included a dominantly eastward component year-round, with a dominant southward component in winter and a dominant northward component in summer.

Simulated and observed non-tidal currents showed a similar pattern with a prevailing direction to the south and west. The simulated currents showed less variability in direction than observed, but similar amplitudes. Strong currents occurred at the end of March due to a south-westward wind event. Throughout the year, smaller current events were well represented in the model. Winter was generally a calm, with some strong winds at the end of December causing increased observed current strengths at 10m depth that were not captured by the model. This model-observation comparison at a specific location is a challenging test of the hydrodynamic simulation performance. The agreement between the two was sufficient to conclude that the representation of processes in the hydrodynamic model was adequate to support water quality modelling.

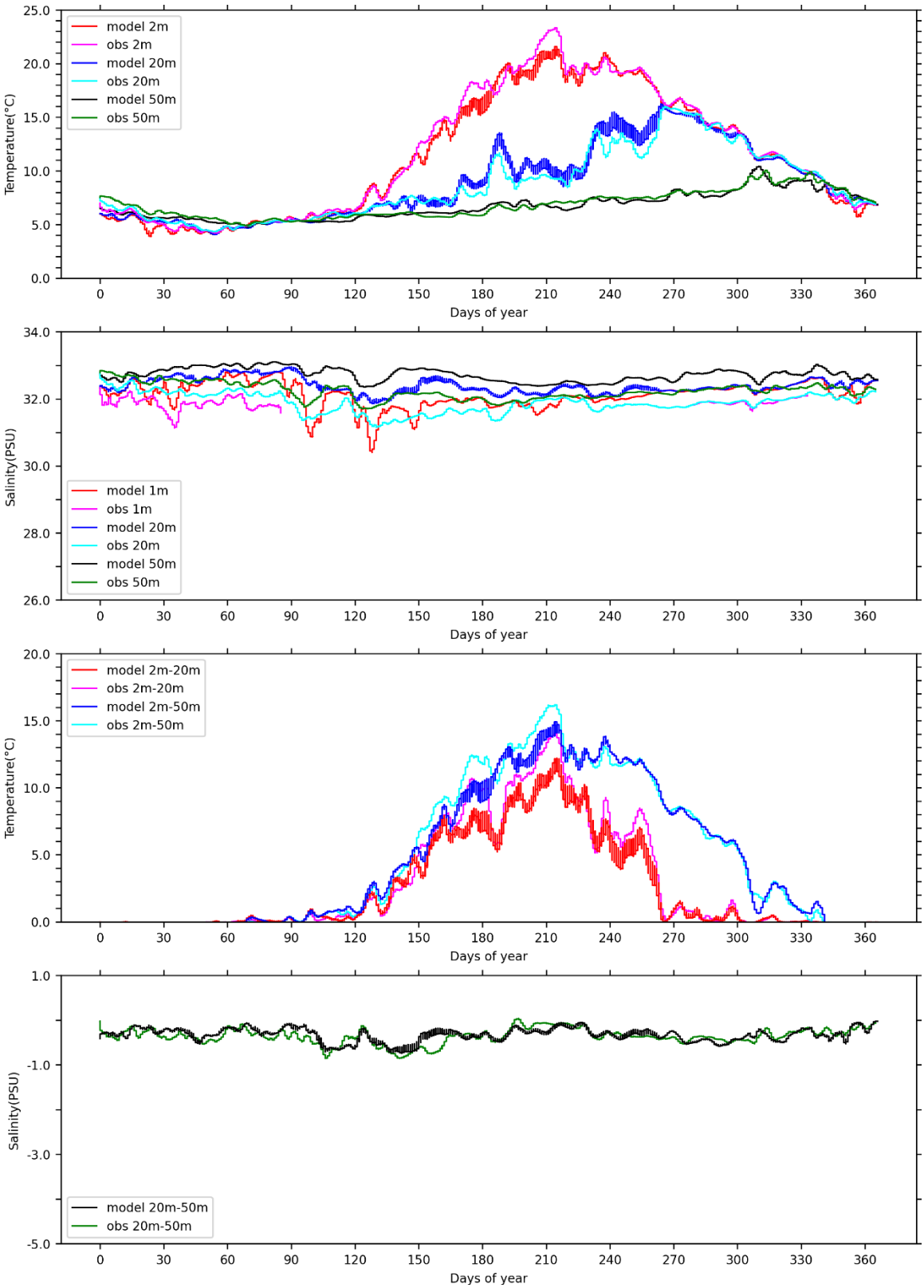

Figure 4-10 Time series Mooring A01 temperature/salinity model-observation comparison (3-day means), three depths and two stratification levels.

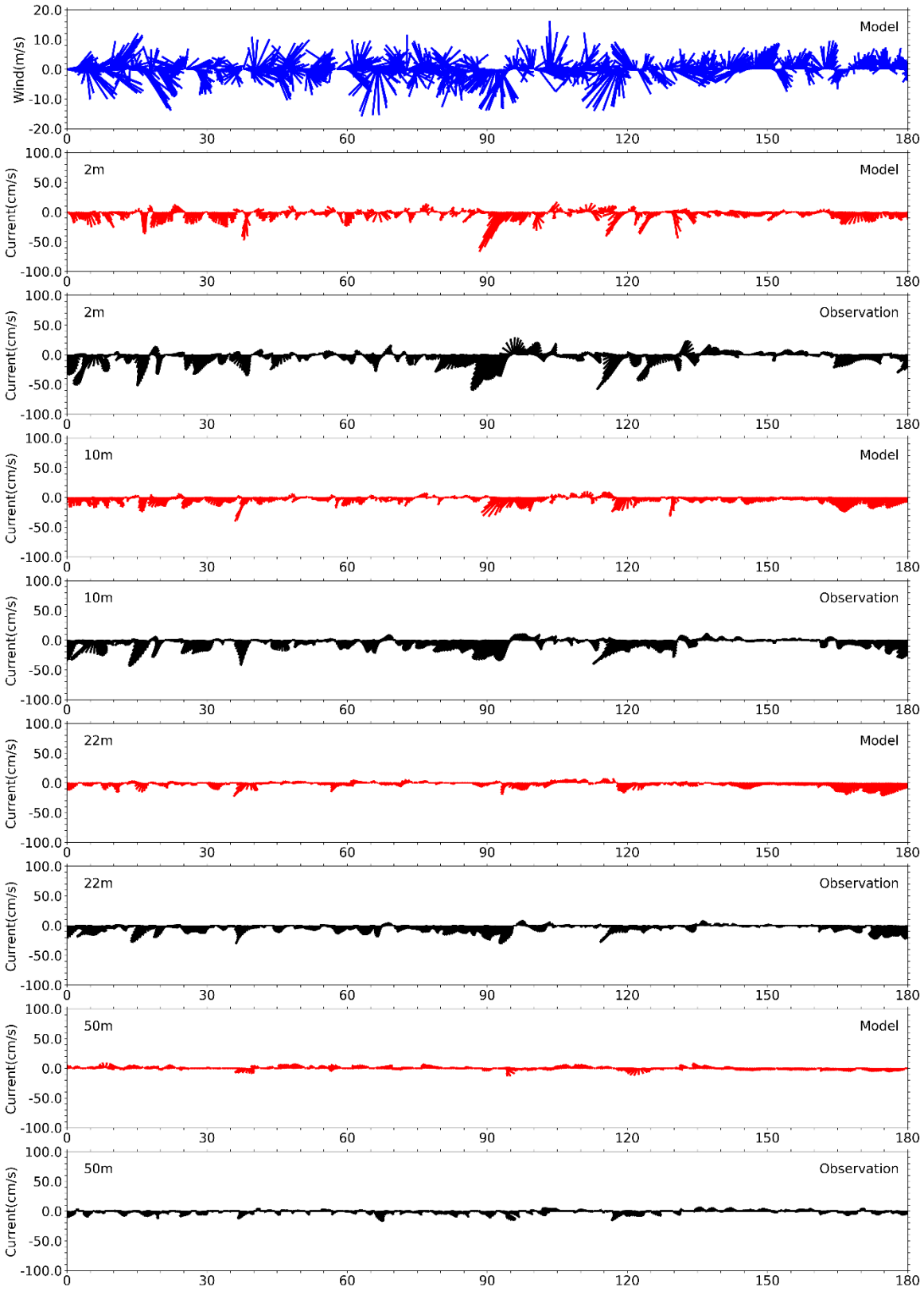

Figure 4-11 Currents time series model-observation comparison, Jan – Jun.

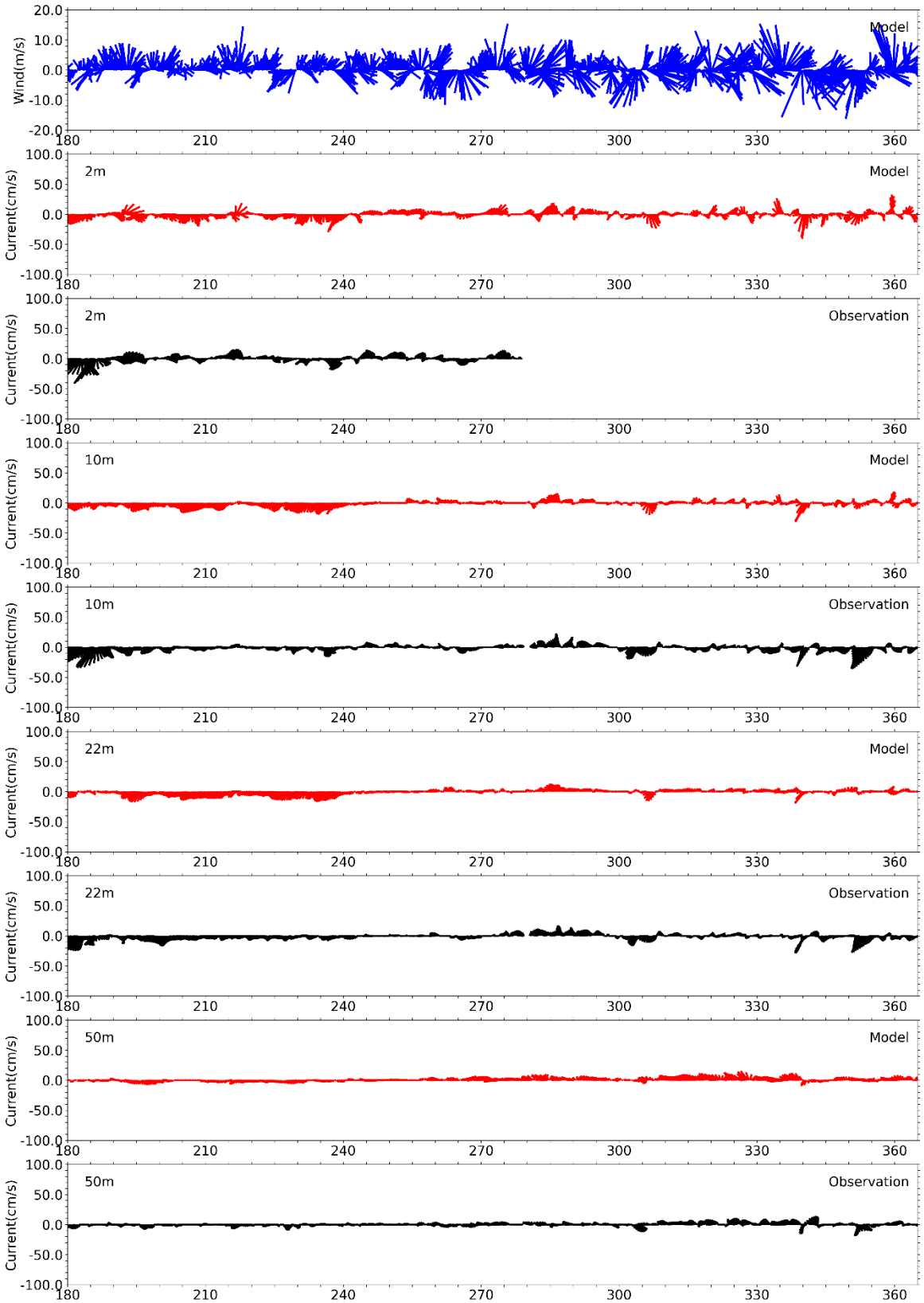

Figure 4-12 Currents time series model-observation comparison, Jul – Dec.

4.3 Model monthly-mean circulation

Figure 4-13 and Figure 4-14 present the simulated monthly-mean currents at the surface and at a depth of 15 m. Flow was largely consistent with the general circulation pattern recognized to hold (Figure 1-1).

This schematic pattern was most apparent in the residual surface currents between January and August. In December the direction of the currents was the same, but the magnitude was very low. From September to November the circulation was partially reversed. Surface currents were strongest off Cape Ann and Cape Cod with the largest magnitudes in May, reaching up to 0.20-0.30 m s^{-1}. This was lower than the maximum in other years. Residual currents within Massachusetts Bay were strongest in February with magnitudes up to 0.15 m s^{-1} near North Passage (see Figure 4-13). During the rest of the year surface currents were calmer and did not exceed 0.10 m s^{-1}. The strongest north-eastward currents off Cape Ann occurred in November, reaching up to 0.15 m s^{-1}.

In general, the circulation pattern at 15 m depth (Figure 4-14) was somewhat similar to the general circulation pattern of Figure 1-1, including a flow directed into northern Massachusetts Bay from offshore, and changed little from month to month. Current magnitudes were lower than at the surface, with maxima in May of up to 0.25 m s^{-1} at Cape Cod. Within Massachusetts Bay, residual currents were smaller than at the surface, reaching up to 0.15 m s^{-1} at North Passage in July. In Cape Cod Bay, residual current magnitudes at this level were weaker, due to its limited depth and sheltered geometry.

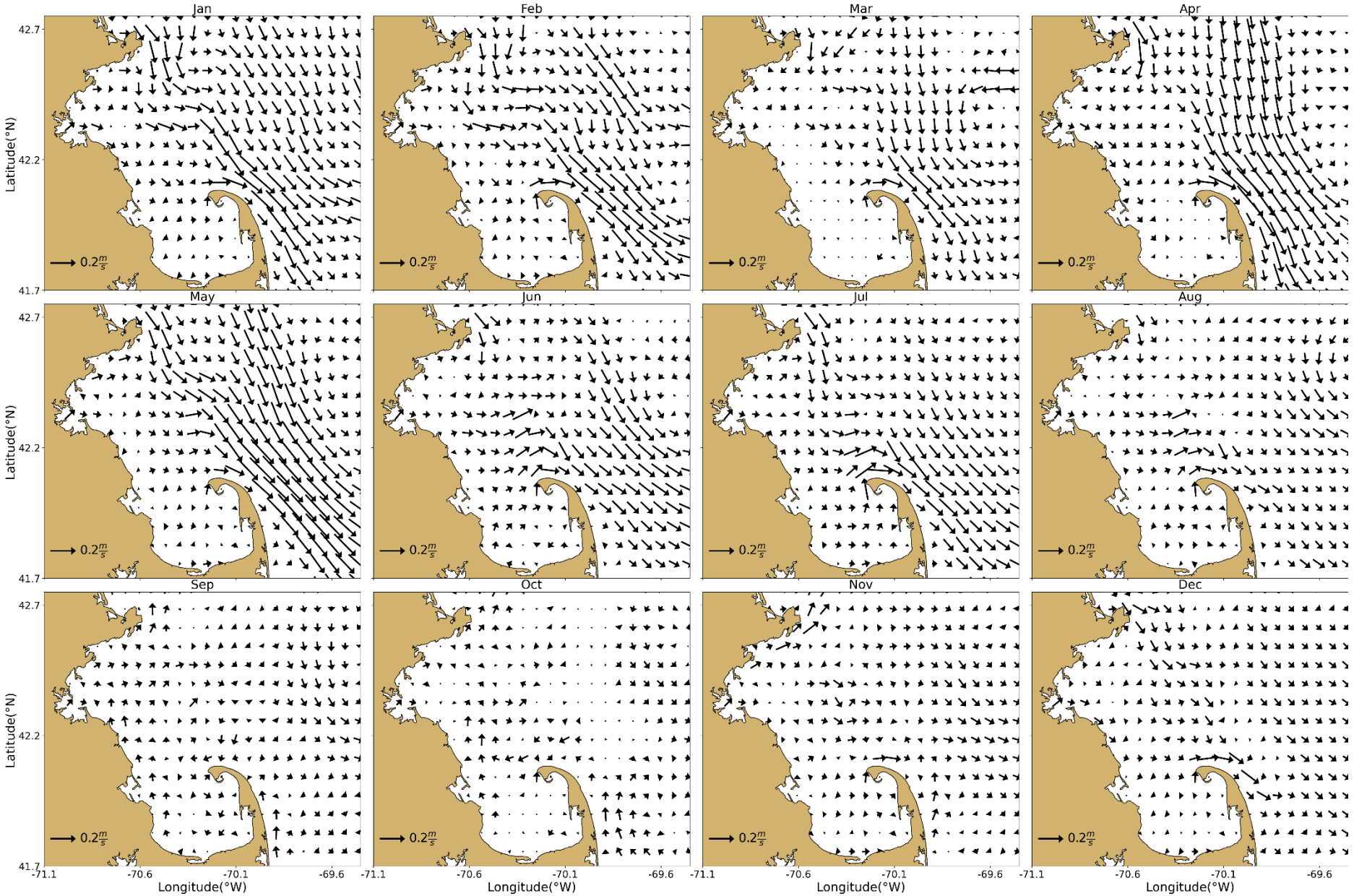

Figure 4-13 Model currents, monthly-mean spatial structure, at sea surface.

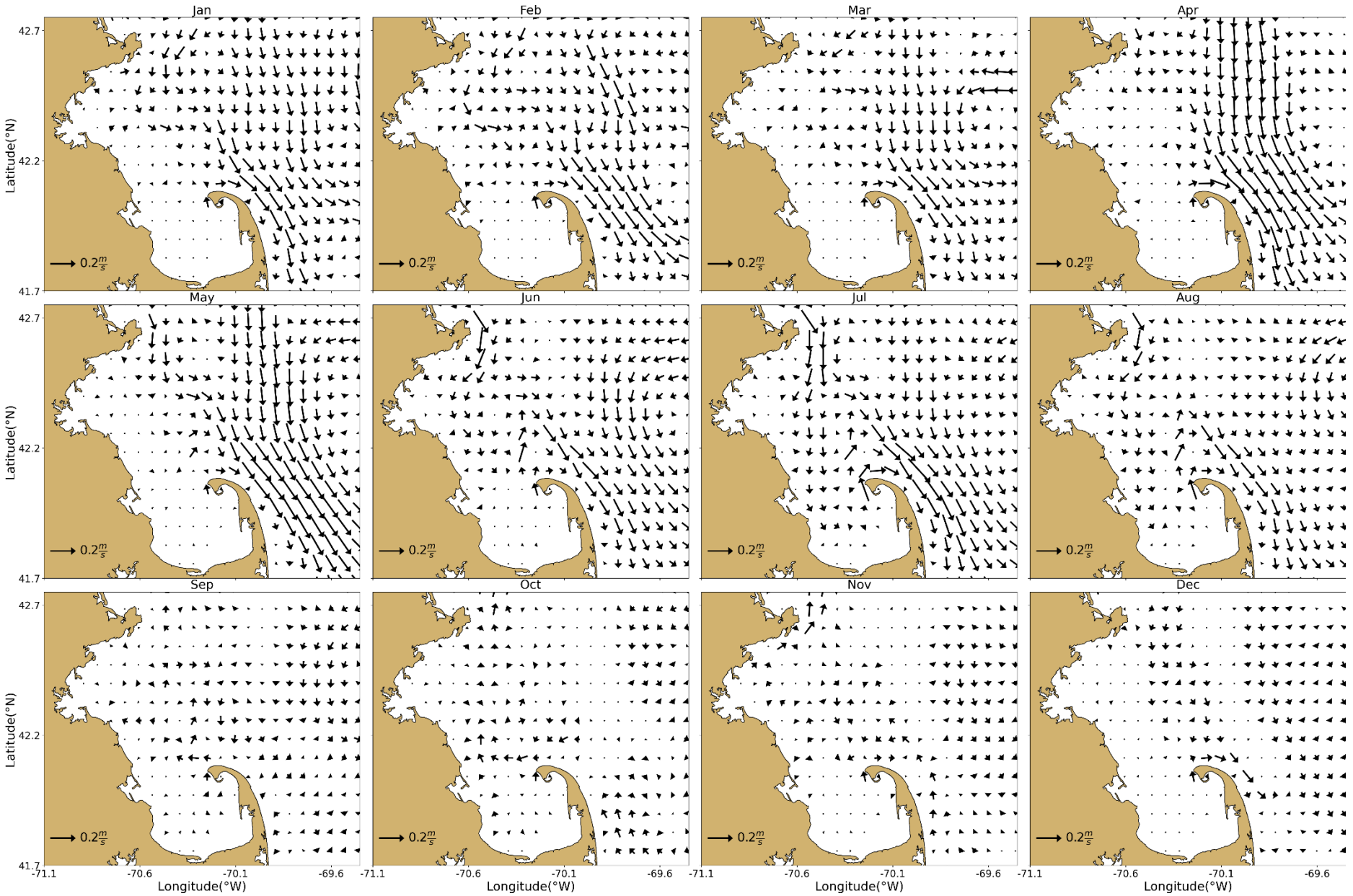

Figure 4-14 Model currents, monthly-mean spatial structure, 15 m deep.

5 Water Quality Model

5.1 Verification of model performance

To demonstrate that the model performance during 2020 was comparable to the performance for the calibration and validation period 2012-2016, skill metrics were calculated and plotted on Taylor diagrams as in Section 4. Station N21 directly on top of the outfall was excluded, as a comparison to field data is of limited value for this station, as discussed by Deltares (2021). Information on how to interpret Taylor diagrams can be found in section 4.1 (box “How to read a Taylor diagram”).

Taylor diagrams are plotted for the light extinction coefficient and dissolved inorganic nitrogen (DIN) in Figure 5-1, and for chlorophyll a and dissolved oxygen (DO) in Figure 5-2. These parameters were selected because they are key drivers of ecosystem functioning. Statistics for the period 2012-2016 are plotted on the left side and statistics for 2020 on the right side. For reference, the 2017 simulation report (Deltares, 2022a) provides, in its Appendix A, similar diagrams for the individual years 2012 to 2016. The plots show statistics for three clusters of monitoring stations: Northern Bay stations (F22, N01, N04, N07, F10, N18, F15, F13 and F23), Southern Bay and Cape Cod stations (F06, F29, F01 and F02) and harbor stations (024, 140, 142, 139 and 124) (see Figure 2-4 for station locations).

Extinction skill metrics (Figure 5-1) for 2020 show somewhat smaller unbiased RMSE errors than for the calibration period 2012-2016. Even though correlations are weak, they are better overall than in 2012-2016. Extinction variability was underestimated at all monitoring stations in the 2020 simulation (except for station N07). This is in contrast to the calibration period 2012-2016 in which the extinction variability was overestimated at some monitoring locations and underestimated at others. Examination of the time-series of light climate in section 5.2.1 indicates that this is not an issue of concern regarding the skill of the model.

Skill metrics for DIN (Figure 5-1) include smaller dimensionless unbiased RMSE errors than 2012-2016 for most stations. Correlations for surface concentrations are better than 2012-2016. Variability of surface concentrations tended to be underestimated for 2020. This is likely due to the low sampling frequency during non-depleted periods. There was only one sampling date at most stations, and at the moment of measurement, the model predicted a lower value (see also section 5.2.2).

Skill metrics for chlorophyll a (Figure 5-2) in 2020 are more scattered than for other years. Correlations are weak or negative, and near-surface chlorophyll a variability is underestimated at all stations except for F06 and F22. This is due to the fact that the model does not reproduce the observed phytoplankton bloom in late summer/fall. The latter was not captured by measurements at F06 and F22.

DO skill metrics (Figure 5-2) are more scattered than for other years as well. The model performs very well for surface concentrations at Northern and Southern stations, even though correlation is weaker than for other years at a few stations. Skill metrics at harbor stations cannot be compared to other years, since only a few winter measurements are available at these locations. Variability is overall underestimated by the model near the seabed.

Although there was less measurement data available in 2020 due to the pandemic, the figures presented here serve to verify that the performance of the water quality model in the simulations of 2020 does not deviate substantially from the validation period 2012-2016.

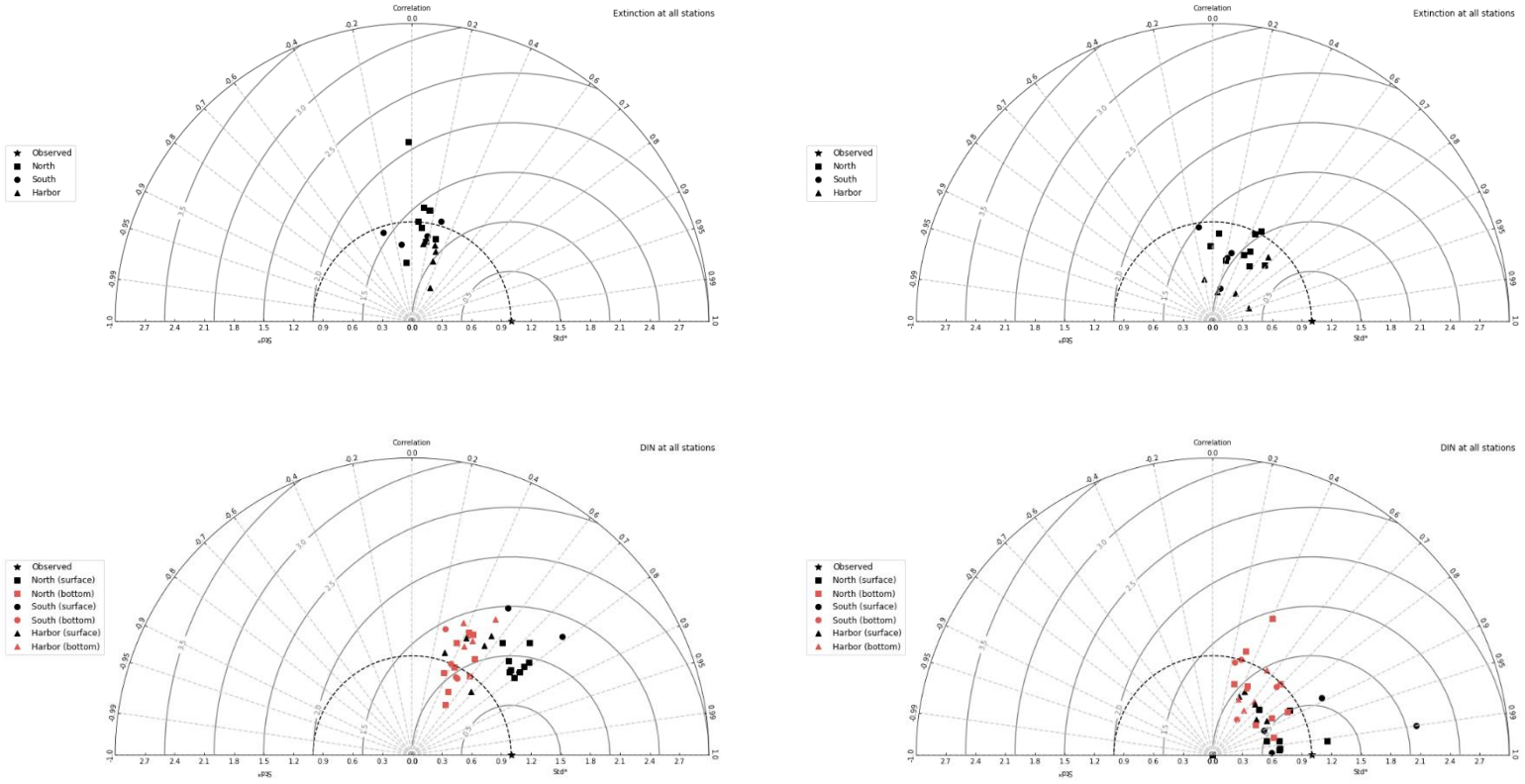

Figure 5-1: Taylor diagrams for MWRA vessel-based survey observations. Top panels show the parameter Extinction and bottom panels Dissolved Inorganic Nitrogen. Left panels show results for the simulation period 2012-2016 and right panels for the year 2020.

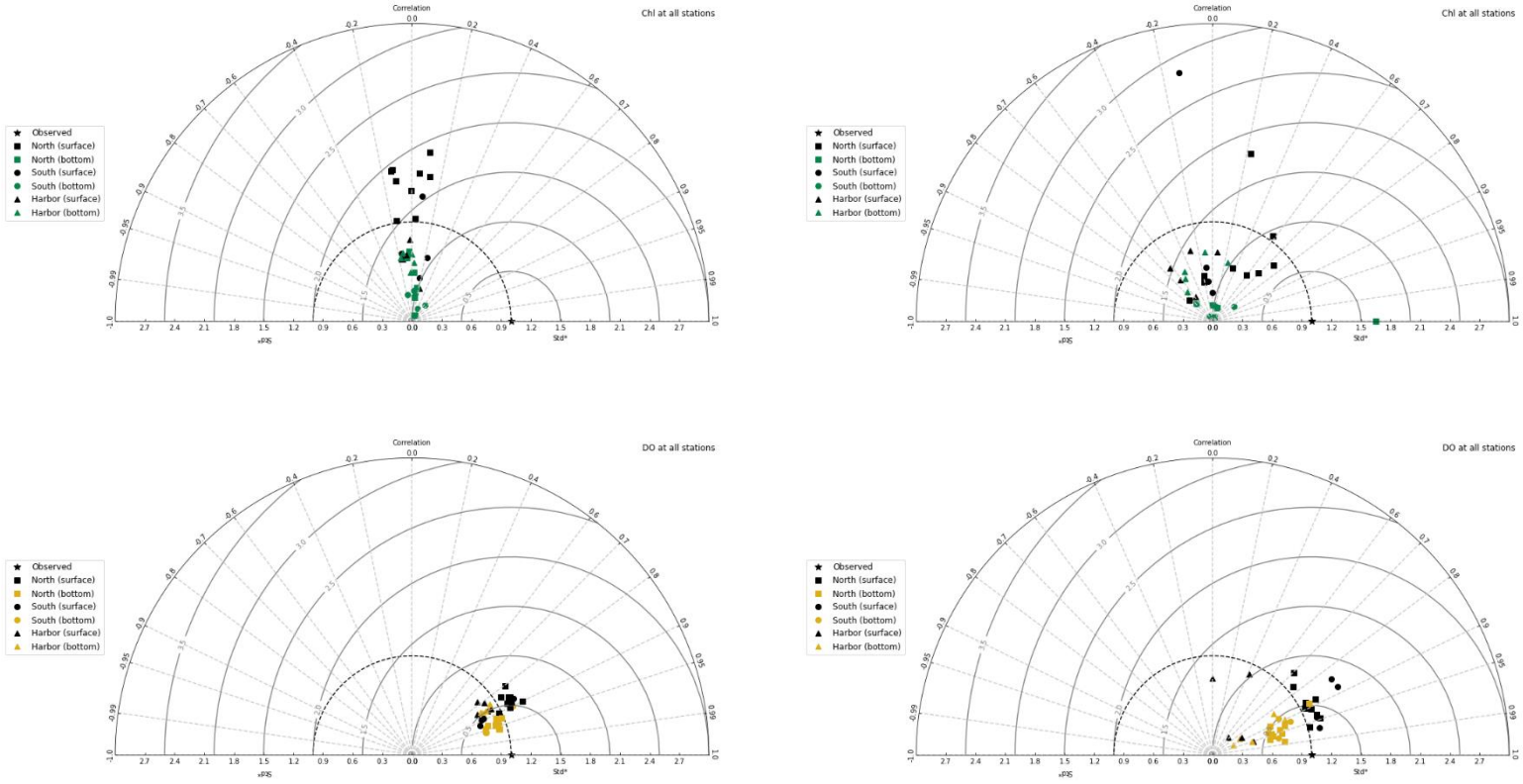

Figure 5-2: Taylor diagrams for MWRA vessel-based survey observations. Top panels show the parameter Chlorophyll-a and bottom panels Dissolved Oxygen. Left panels show results for the simulation period 2012-2016 and right panels for the year 2020.

5.2 Model-observation comparisons

In this section model-observation comparisons in the same format as for the hydrodynamic model (Section 4) are provided. For time series plots, a 3-day moving average is applied to the model outputs to smooth high-frequency variability.

To assess the simulation spatially, vertical transects have been plotted along North-South and West-East transects (Figure 2-4). Model results in these figures are 5-day averages centered on the sampling date indicated in each plot.

5.2.1 Light extinction

Measured extinction for the year 2020 (Figure 5-3) ranged from 0.1 to 0.4 at all stations, except at F23, near the harbor, where it ranged between 0.3 and 0.6. This was similar to previous years, for which higher and more variable extinction was observed at harbor stations (e.g. Zhao et al., 2017). The model reproduced the extinction range and variability well at most stations. As for previous years, extinction was generally underestimated at station F23.

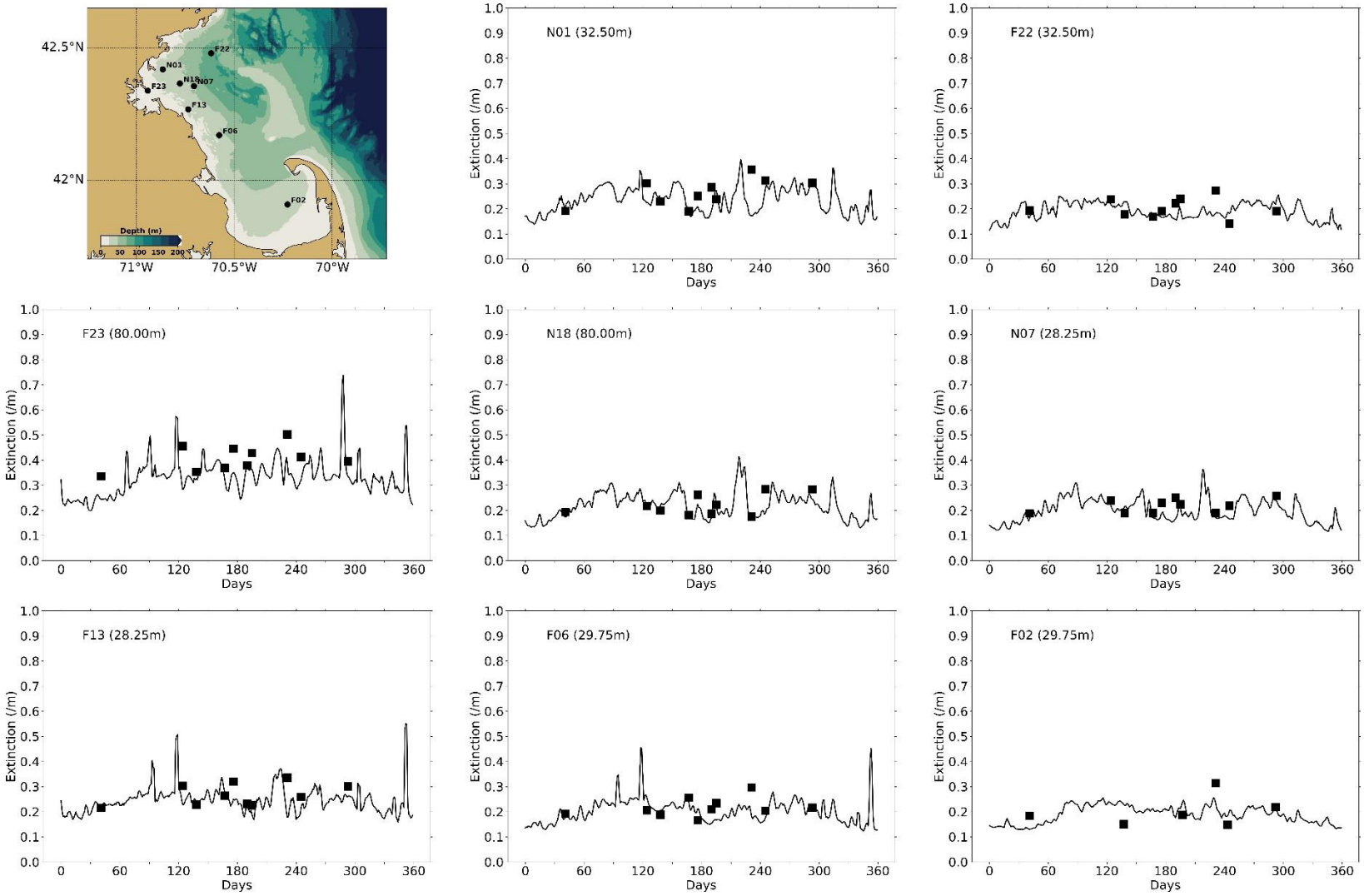

Figure 5-3: Extinction time series, model-observation comparison for 2020. Model: lines. MWRA vessel-based survey observations: symbols.

5.2.2 Dissolved inorganic nitrogen

Seasonal variations of surface and bottom DIN concentrations in 2020 were similar to those observed and simulated for previous years (Figure 5-4). Surface and bottom concentrations were comparable in winter, when the water column was well mixed. Surface DIN concentrations declined at the end of winter and were depleted from April to October, before increasing again mid-fall. Decreases in bottom concentrations were smaller in spring and summer. The model generally reproduced these observed seasonal variations and vertical differences. Due to the frequency of measurements in 2020, the onset of stratification was not observed in the measurements. Observed variations at intermediate depths in the water column were generally well reproduced by the model (Figure 5-5).

According to the model results, the signature of the outfall in terms of DIN concentrations was visible all year round, leading to increased concentrations up to a distance of about 10 km or more (Figure 5-6). The extra DIN load remained in the lower layers of the water column during the period of stratification (April-October). During the other months, the effluent led to an increase in DIN concentrations throughout the water column over the outfall (station N21). This was similar to simulations of previous years. In the model during stratified periods, the highest concentrations at N21 (directly over the outfall) were always simulated at the bottom of the water column, while the highest measured concentrations were sometimes higher up in the water column (e.g., July 14th, August 19th and October 20th). This aspect of the model directly over the outfall was discussed by Deltares (2021).

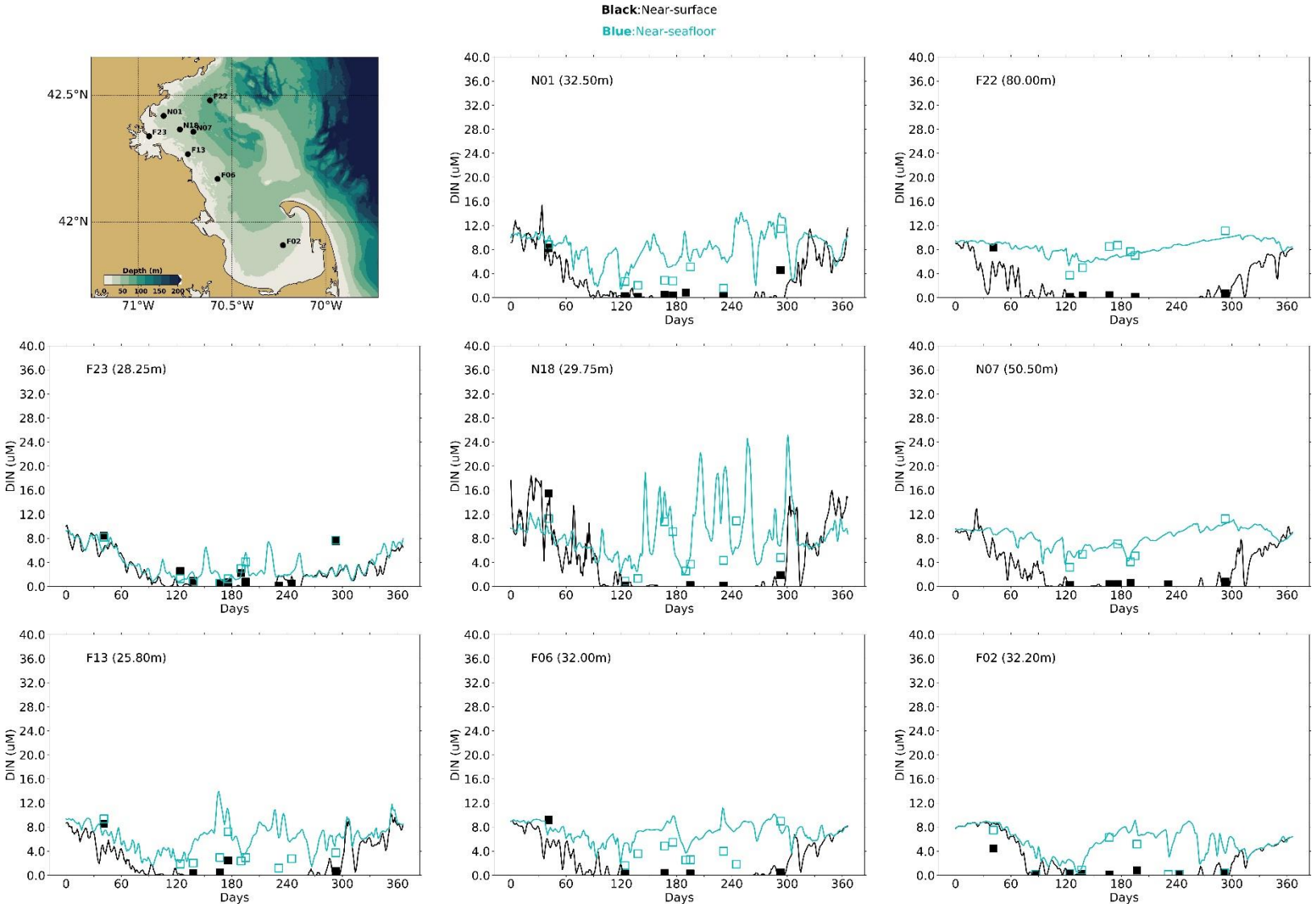

Figure 5-4: Dissolved Inorganic Nitrogen time series, model-observation comparison near surface (black) and seafloor (cyan). Model results: lines. MWRA vessel-based survey observations: symbols.

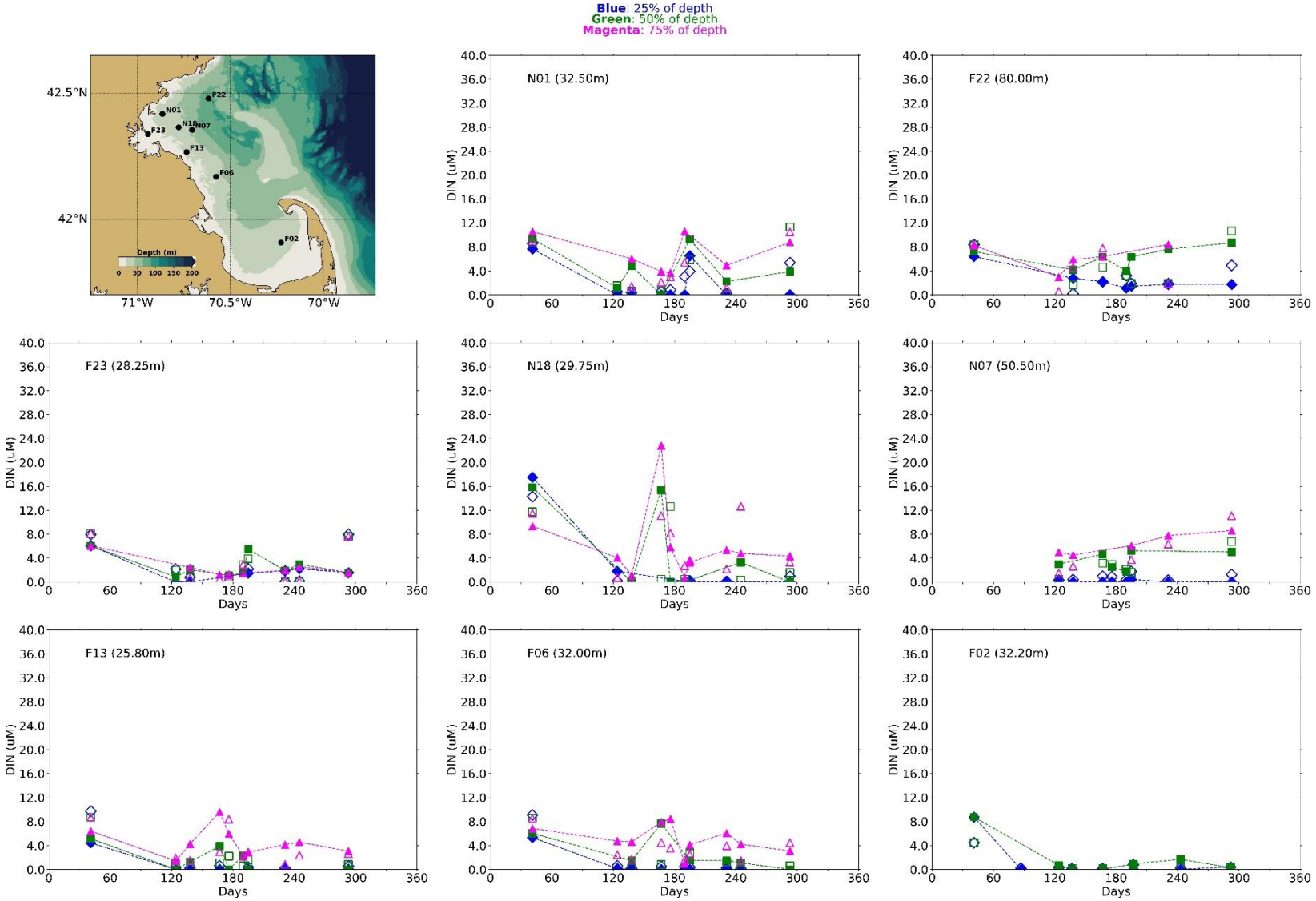

Figure 5-5: Dissolved Inorganic Nitrogen time series, model-observation comparison within water column (between surface and seafloor). Model results: lines and full symbols. MWRA vessel-based survey observations: open symbols.

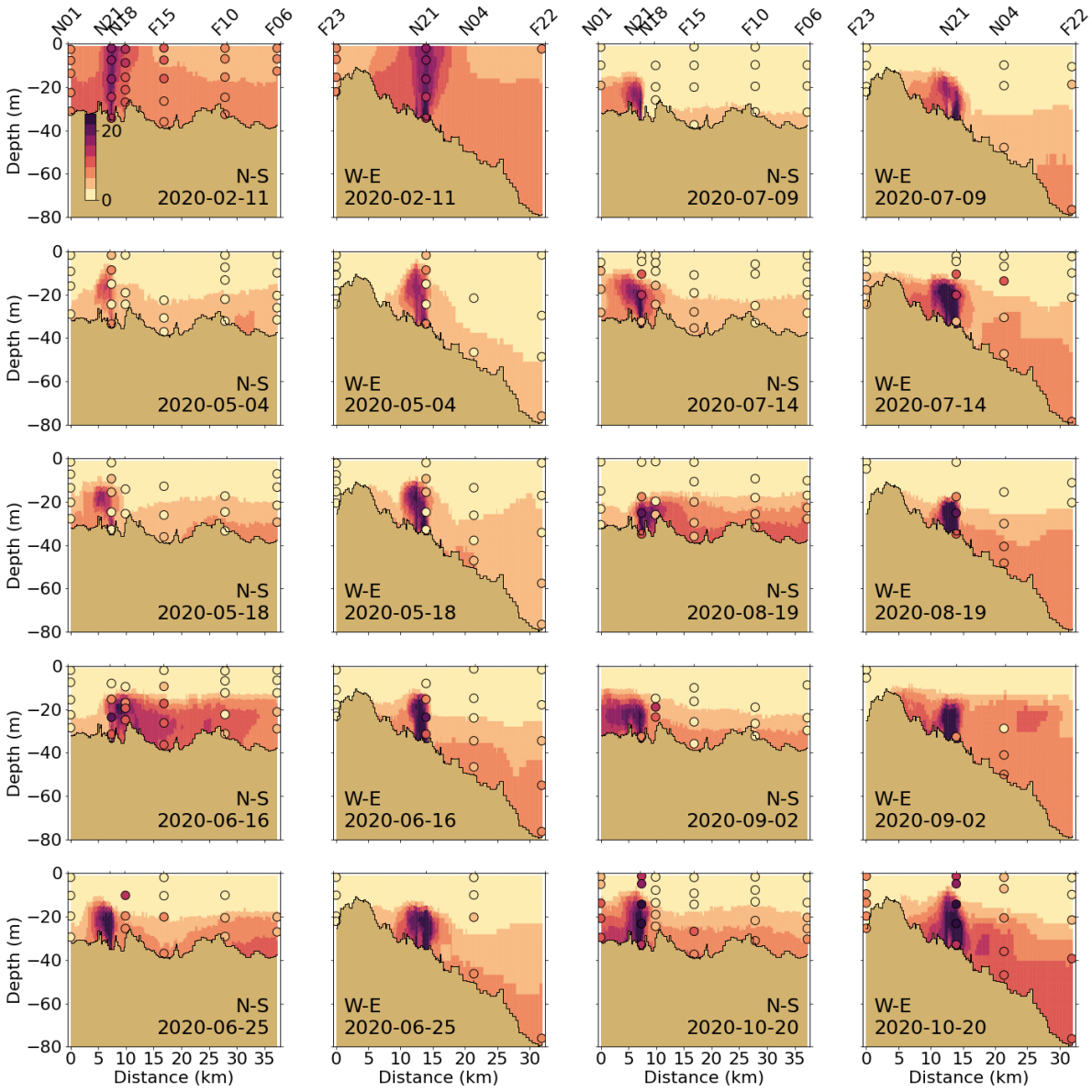

Figure 5-6: Dissolved Inorganic Nitrogen (µM) for 2020 along North-South (N-S) and West-East (W-E) transects (Figure 2-4). MWRA measurements are plotted with round symbols. Model results are 5-day averages around sampling date.

5.2.3 Chlorophyll a

Seasonal variations of chlorophyll a observations in 2020 showed high values mostly at the end of summer or beginning of fall (e.g. stations N01, F23, F13, see Figure 5-7); the sampling frequency of the MWRA observations makes it difficult to see a clear seasonal pattern. The model simulated the higher observed chlorophyll a peaks at the end of winter or in spring and at the end of fall, but did not capture the observed late-summer chlorophyll a peak (Figure 5-7). As observed in 2019, this end-of-summer-bloom is dominated by dinoflagellates. The model does simulate a peak of dinoflagellate biomass in the end of summer (Figure 5-20), but most likely underestimates it. The low chlorophyll-to-carbon ratio used to characterize nitrogen-limited dinoflagellates in the BEM (compared to e.g. diatoms) possibly leads to further underestimating chlorophyll a concentrations in that period. As for previous years, near surface simulated concentrations were usually in the same range as observations, although the temporal variability was less well reproduced. This was likely related to the relatively low sampling frequency and the high temporal variability. Bottom chlorophyll a measurements appear to be higher than for previous years. In Cape Cod Bay (station F02), the surface concentrations also exceeded the bottom concentrations for most of the year. As in the simulations for previous years, simulated bottom chlorophyll a was underestimated. Chlorophyll a concentrations in summer and fall were underestimated at the observation stations at intermediate depths as well (Figure 5-7 and Figure 5-8).

Simulated chlorophyll a concentrations decreased eastward from the coast (Figure 5-9). Early spring increases (May 4th) occurred throughout the water column as it was relatively well mixed. During the months in which stratification occurred, simulated bottom chlorophyll a remained low and highest values occurred in the subsurface. This is consistent with the depth of highest measured concentrations in this period (e.g. June 16th). Highest observed concentrations occurred in late summer, from the surface to depths of about 30 m, which was not captured by the model.

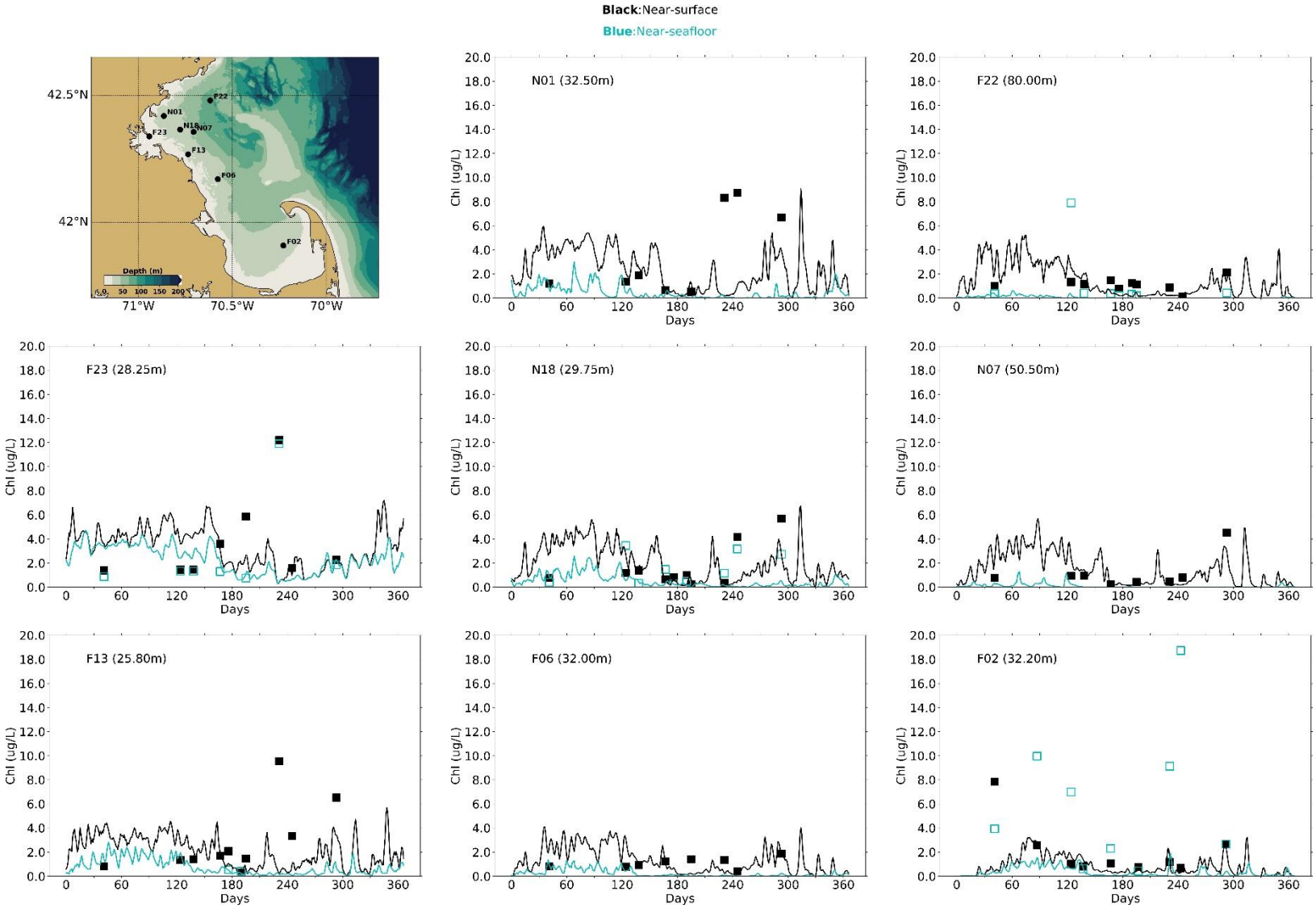

Figure 5-7: Chlorophyll a time series, model-observation comparison near surface and seafloor. Model results: lines. MWRA vessel-based survey observations: symbols.

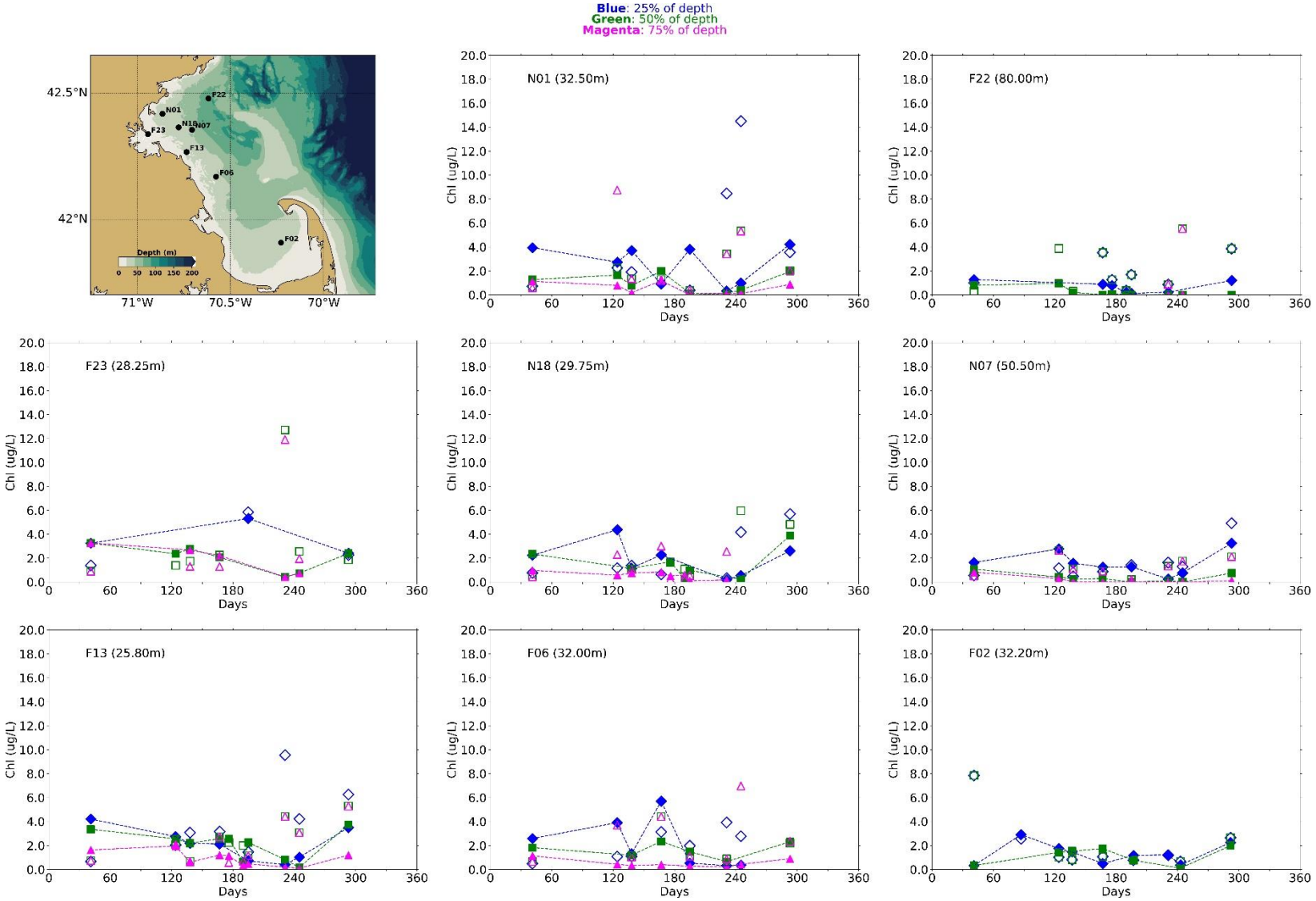

Figure 5-8: Chlorophyll a time series, model-observation comparison within water column (between surface and seafloor). Model results: lines and full symbols. MWRA vessel-based survey observations: empty symbols.

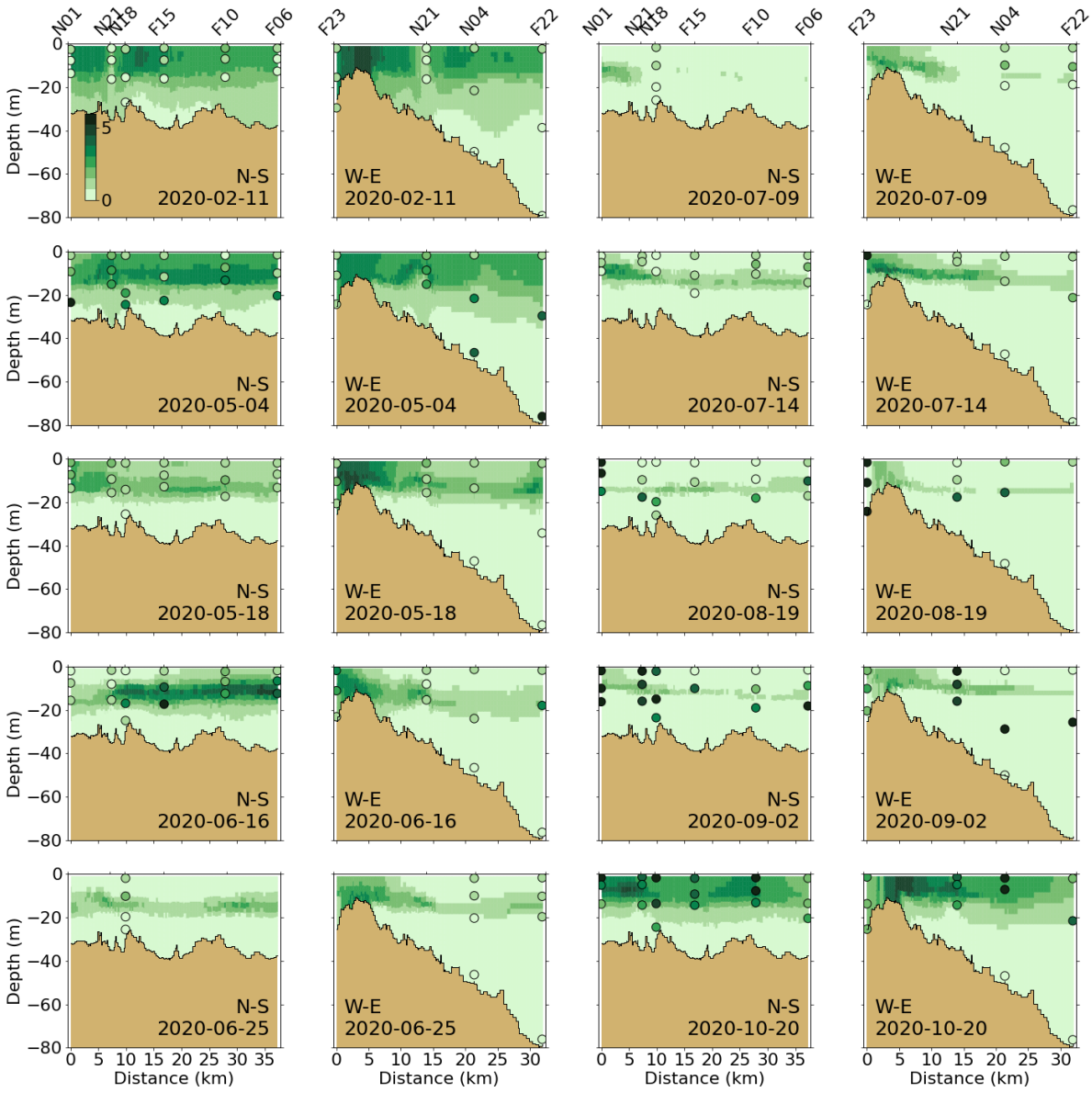

Figure 5-9: Chlorophyll a (µg/L) for 2020 along North-South (N-S) and West-East (W-E) transects (Figure 2-4). MWRA measurements are plotted with round symbols. Model results are 5-day averages around the sampling date.

5.2.4 Particulate organic carbon

POC measurements at plotted stations were very sparse in 2020, which makes it difficult to identify seasonal patterns and carry out an in-depth model-observations comparison (Figure 5-10). Concentrations were significantly lower near the bottom than at the surface, except at harbor station F23.

The model seemed to generally capture POC concentration ranges and vertical gradients at the locations presented (Figure 5-10 and Figure 5-11). As for previous years, POC concentrations were overestimated at F23, closer to the harbor.

According to the model results, POC concentrations decreased from the coast eastward (Figure 5-12). The signature of the outfall was not visible along either the North-South or the West-East transects. This was consistent with the fact that the MWRA outfall only represented a small part of the total non-oceanic OC inputs to the study area (Figure 3-6). Highest simulated concentrations occurred in July in the Northwest. In deeper areas, during periods of stratification, concentrations are higher in the subsurface, most likely due to higher phytoplankton biomass. High concentrations were measured at the beginning of September along both transects. This was not fully captured by the model and was most likely due to the underestimation of phytoplankton biomass (chlorophyll a) for that period.

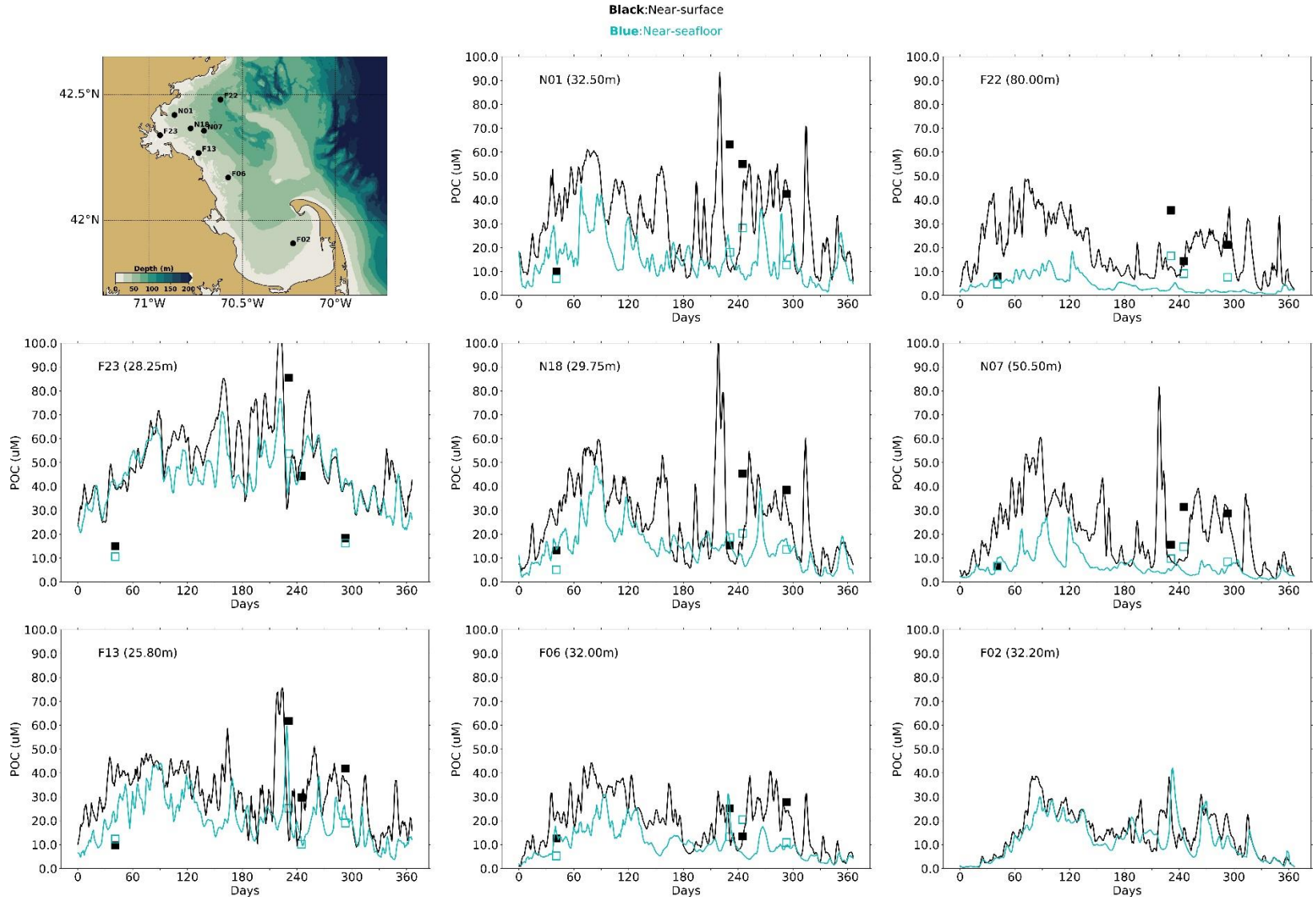

Figure 5-10: Particulate Organic Carbon time series, model-observation comparison near surface and seafloor. Model results: lines. MWRA vessel-based survey observations: symbols.

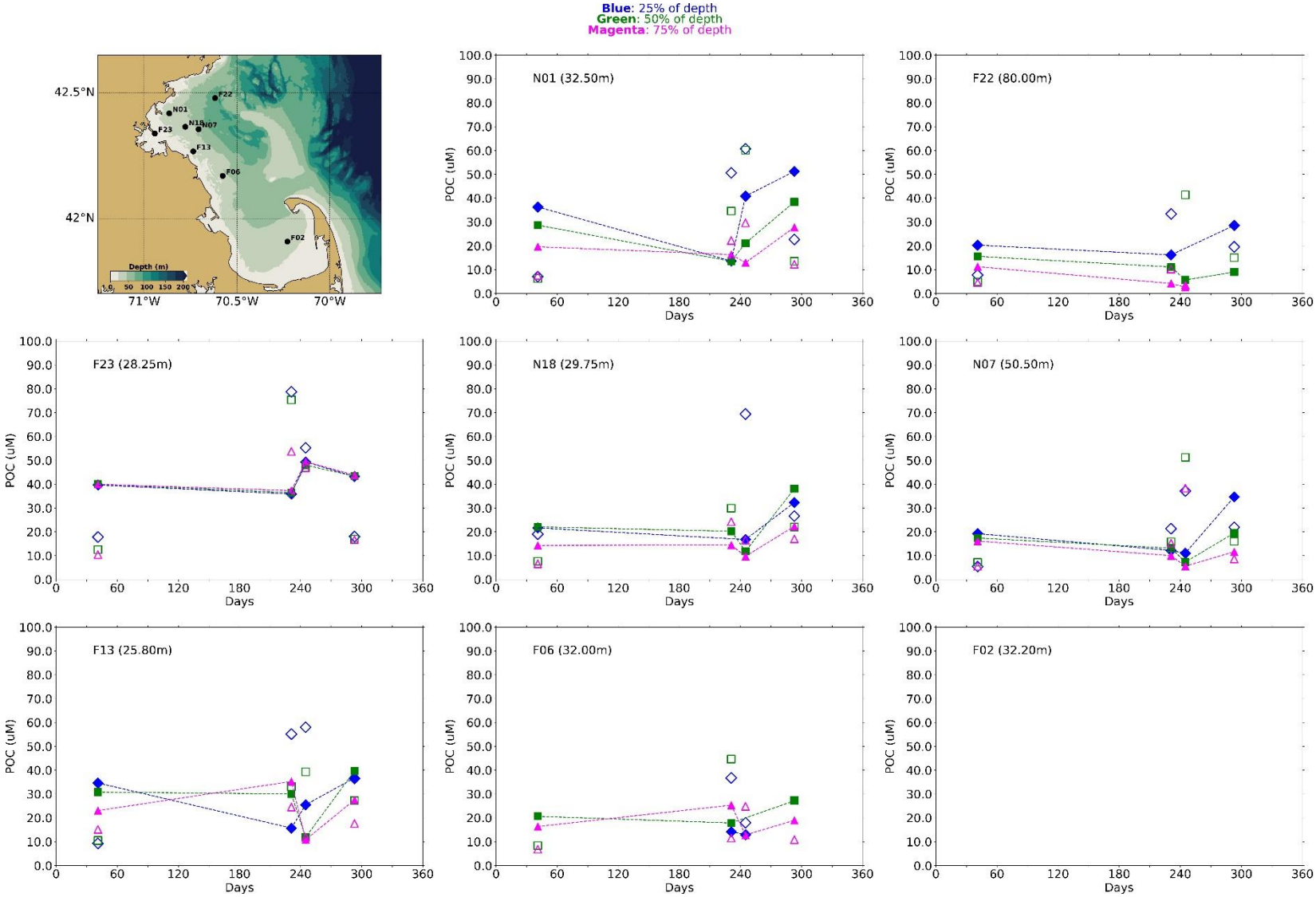

Figure 5-11: Particulate Organic Carbon time series, model-observation comparison within water column (between surface and seafloor). Model results: lines and full symbols. MWRA vessel-based survey observations: empty symbols.

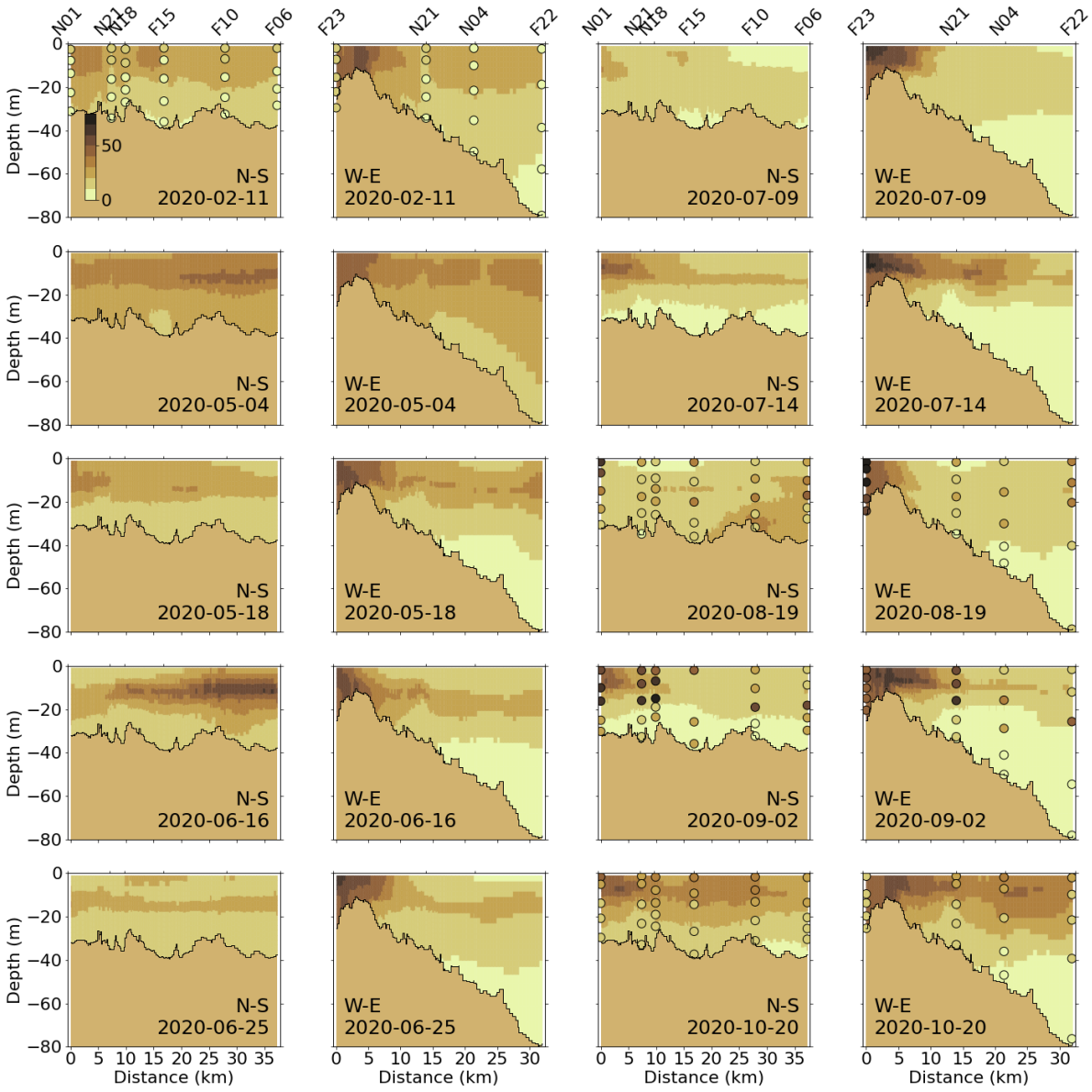

Figure 5-12: Particulate Organic Carbon (µM) for 2020 along North-South (N-S) and West-East (W-E) transects (Figure 2-4). MWRA measurements are plotted with round symbols. Model results are 5-day averages around the sampling date.

5.2.5 Dissolved oxygen

The 2020 seasonal variations of near-surface DO concentrations were well reproduced, with maximum concentrations observed at the end of winter or beginning of spring and decreasing until the end of summer before rising again (Figure 5-13). While winter concentrations at the surface and the bottom were comparable, bottom concentrations dropped lower at the end of the summer and beginning of fall. Differences between top and bottom concentrations reached about 2 mg L^{-1} at the end of October at several stations. Field measurements reported historic minima of dissolved oxygen at many stations in the summer. The field measurements included unusually low bottom DO concentrations in Cape Cod Bay at the end of August (about 3 mg L^{-1} lower than at the surface). The model does not capture these lowest concentrations at the plotted stations. The model-observation comparison at intermediate water depths showed similar behavior. However, in summer, the model slightly underestimated concentrations at smaller depths, and in fall, the decrease in DO throughout the water column was slightly underestimated (Figure 5-14).

At the A01 mooring station, the model reproduced the general seasonal pattern in the observed DO well, although it overestimated the end-of-fall minimum by about 1 mg L^{-1} (Figure 5-15).

As for previous years, the North-South and West-East cross-section plots show that DO generally had weak vertical gradients (Figure 5-16). Concentrations were higher at the end of winter and beginning of spring and decreased until fall. Slightly higher concentrations were observed and simulated in the subsurface, where phytoplankton biomass is located, at the end of spring or early summer. These vertical gradients were however less strong than during previous years. The modeled phytoplankton biomasses were also lower in that period compared to previous simulated years. The observed vertical gradients in DO concentrations were captured by the model.

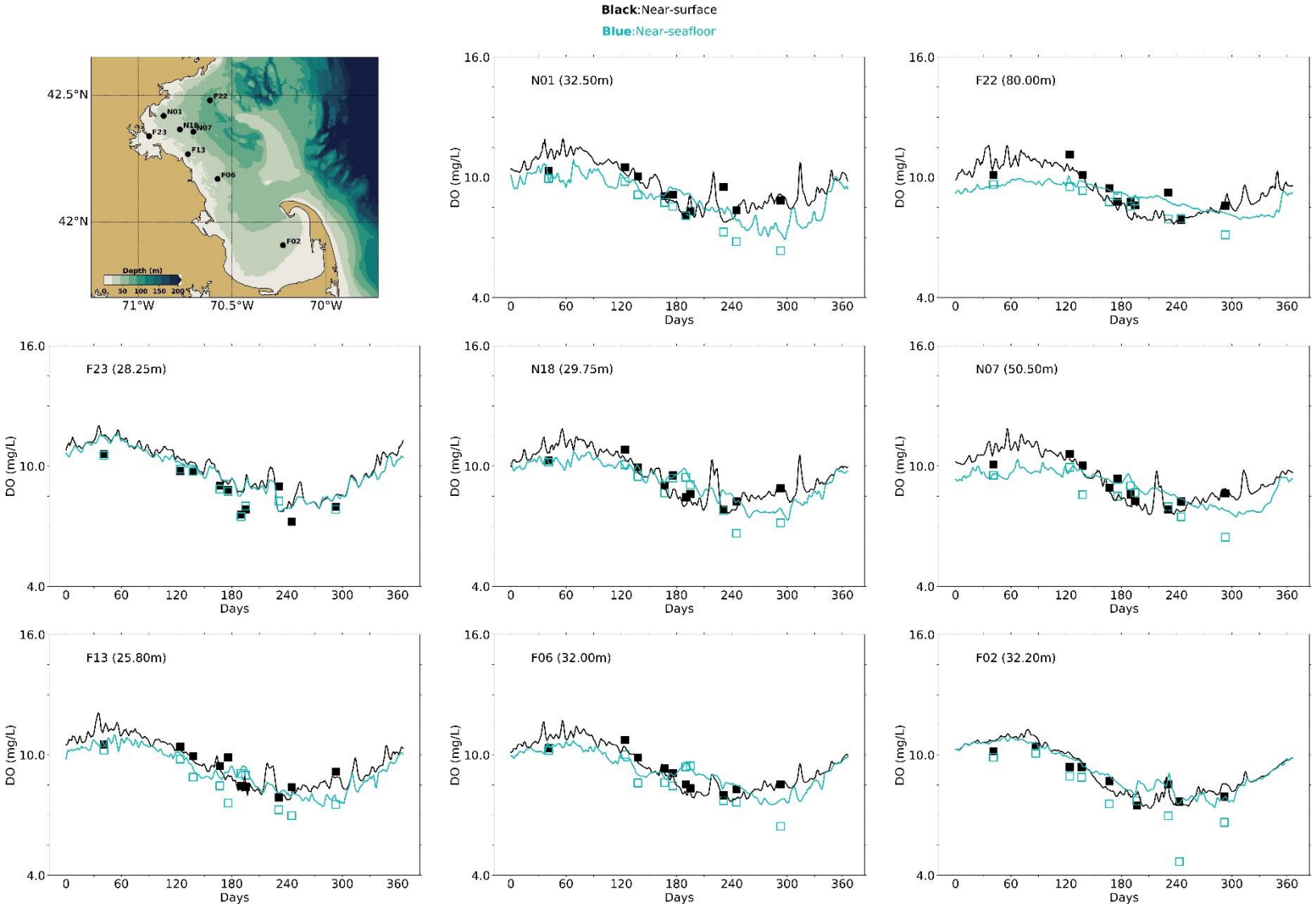

Figure 5-13: Dissolved Oxygen time series, model-observation comparison near surface and seafloor. Model results: lines. MWRA vessel-based survey observations: symbols.

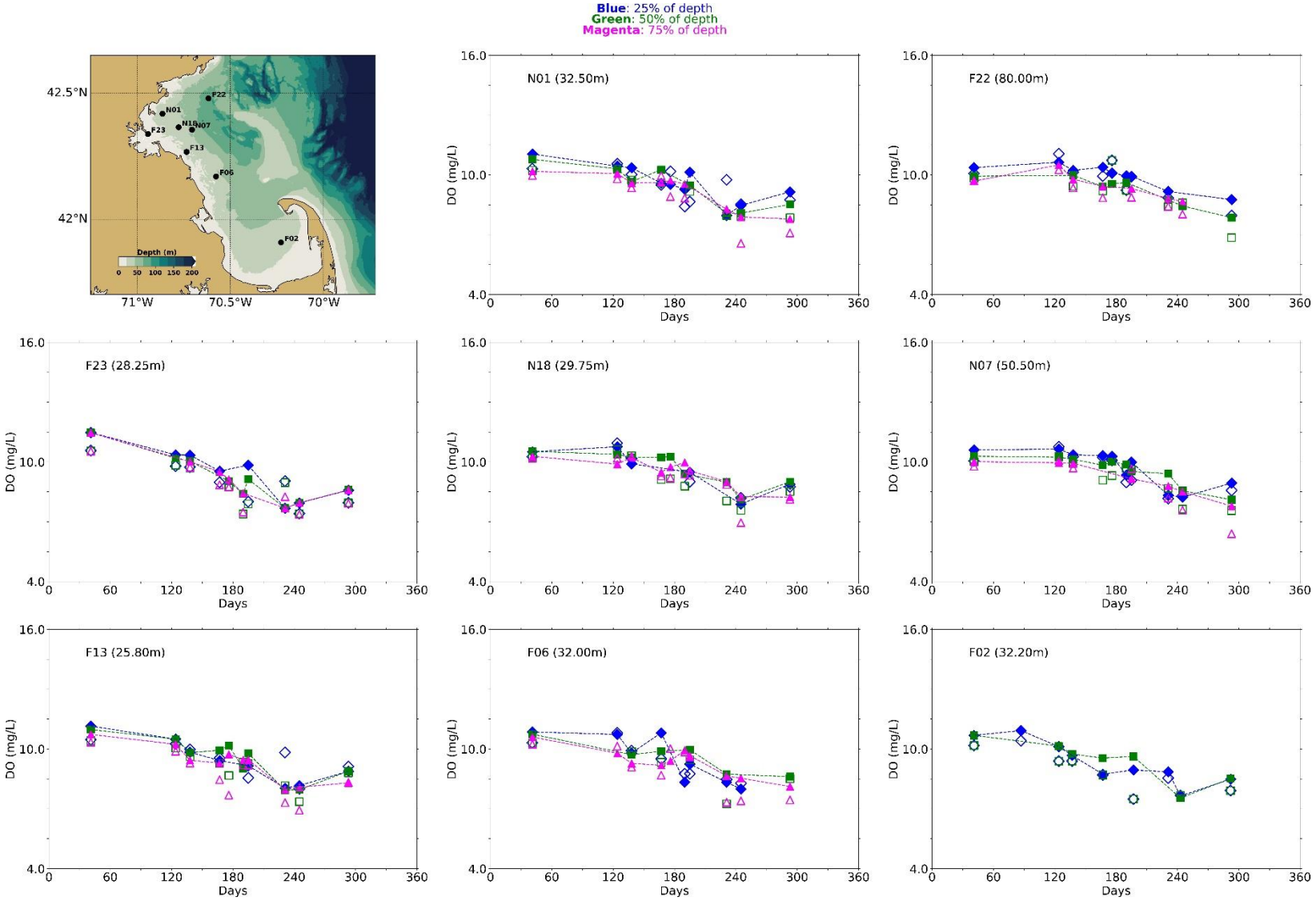

Figure 5-14: Dissolved Oxygen time series, model-observation comparison in water column. Model results: lines and full symbols. MWRA vessel-based survey observations: open symbols.

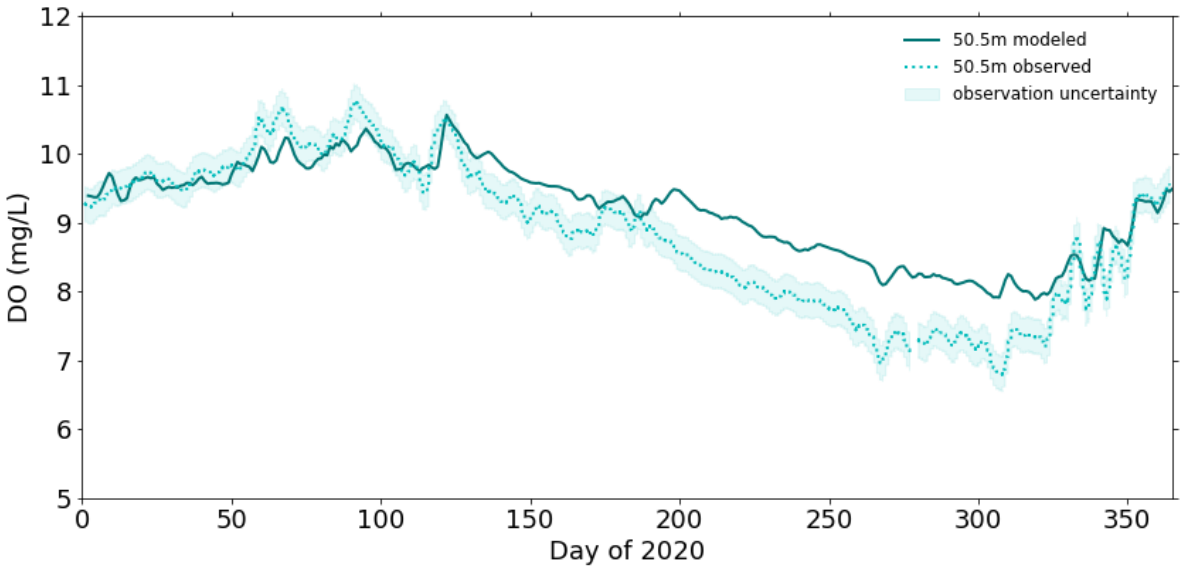

Figure 5-15: Dissolved Oxygen time series 50.5m deep at A01 mooring site, model-observation comparison for 2020.

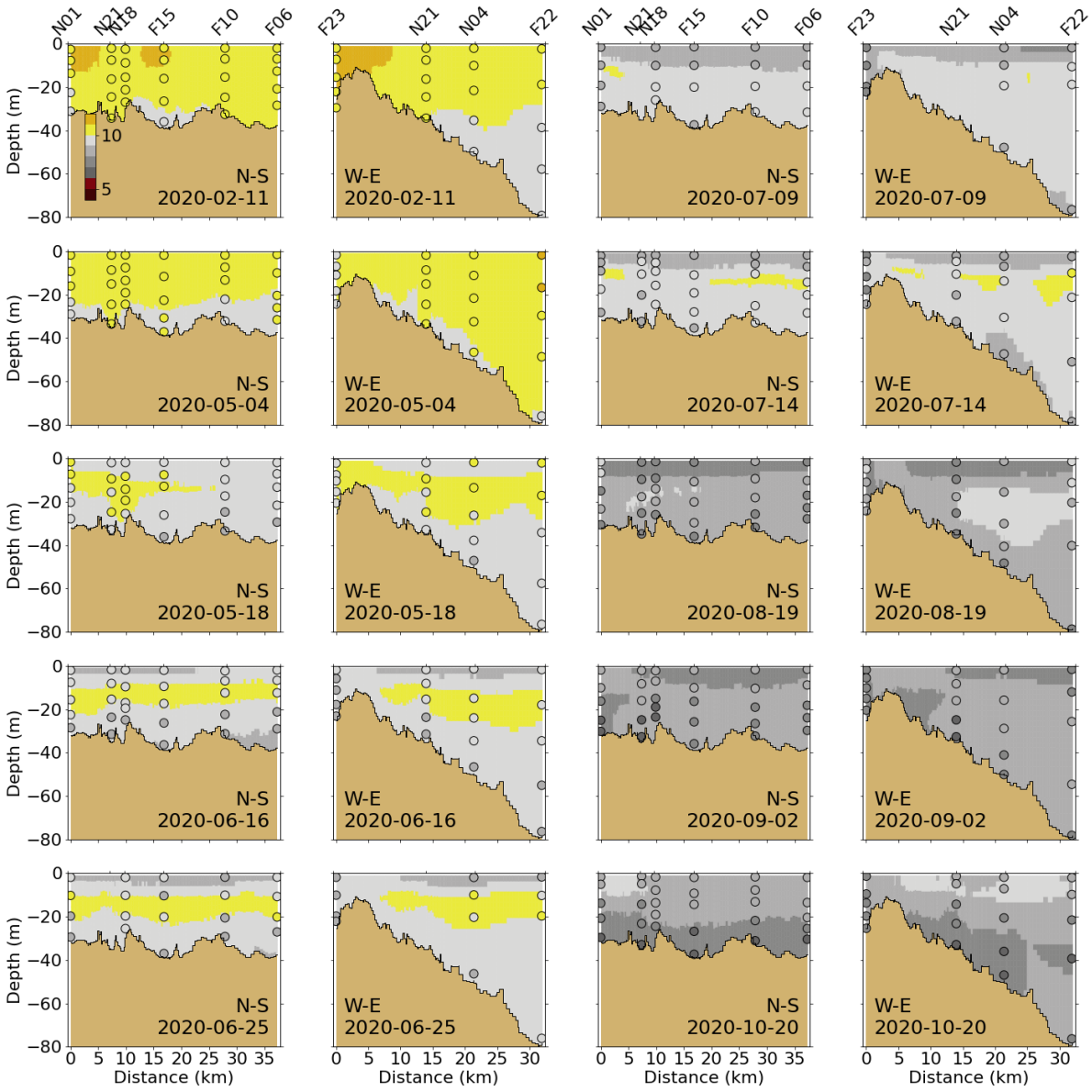

Figure 5-16: Dissolved Oxygen (mg/L) for 2020 along North-South (N-S) and West-East (W-E) transects (Figure 2-4). MWRA measurements are plotted with round symbols. Model results are 5-day averages around the sampling date.

5.2.6 Primary production

Simulated primary production was compared to historical measurements at three monitoring locations (Figure 5-17). Box whiskers represent the 9th, 25th, 50th, 75th and 91st percentiles of primary productions observations over the period 1995-2010 (Keay et al., 2012). Primary production was in the range of historical measurements for the entire year 2020 at stations N04 and N18. Highest simulated primary production at these stations, however, occurred slightly earlier than for 2012-2019. Simulated primary production closer to the harbor, at F23, is low in comparison to historical measurements and previous simulated years.

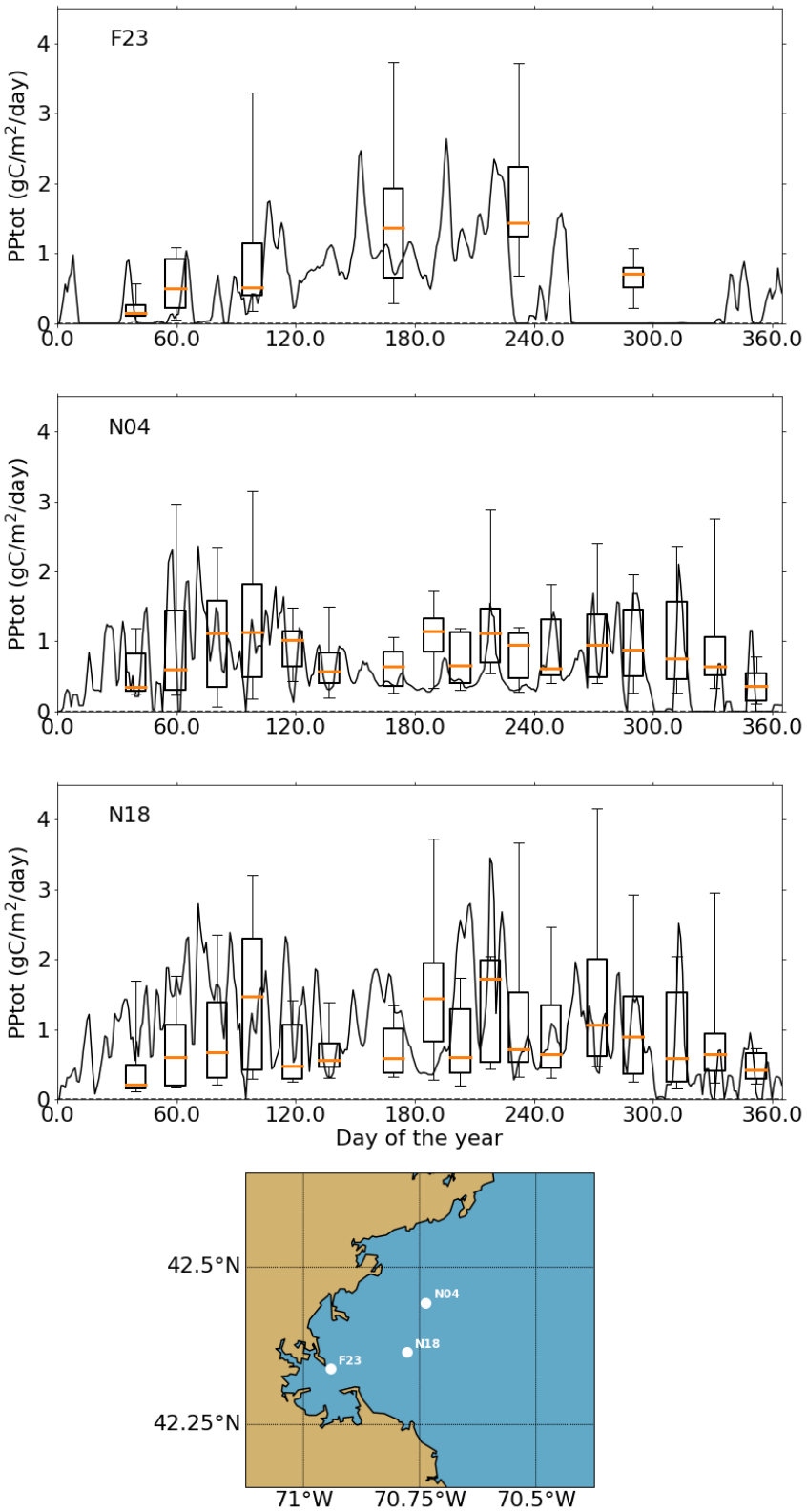

Figure 5-17: Simulated (lines; 2020) and observed (box-whiskers; 1995-2010) primary production.

5.2.7 Sediment fluxes

Sediment NH4 fluxes (Figure 5-18) and sediment oxygen demand (Figure 5-19) outputs from the model were compared to measurements from the 2001-2010 period from Tucker et al. (2010) at stations located in Boston Harbor and Massachusetts Bay using plots in the same format as Figure 5-17.

Simulated sediment fluxes were low in winter and peaked in the summer due to higher temperatures favorable to biogeochemical activity, which mineralizes organic matter in the sediment. Sediment fluxes were higher in the harbor area than in Massachusetts Bay, which was captured by the model. Results for the year 2020 were similar to those from the individual years 2012 to 2016. These were mostly in the range of historical measurements, except for NH_4 sediment fluxes at the Mass Bay stations (MB01, MB03 and MB05). This discrepancy is related to the simplified representation of sediment biogeochemical processes (see Deltares, 2021).

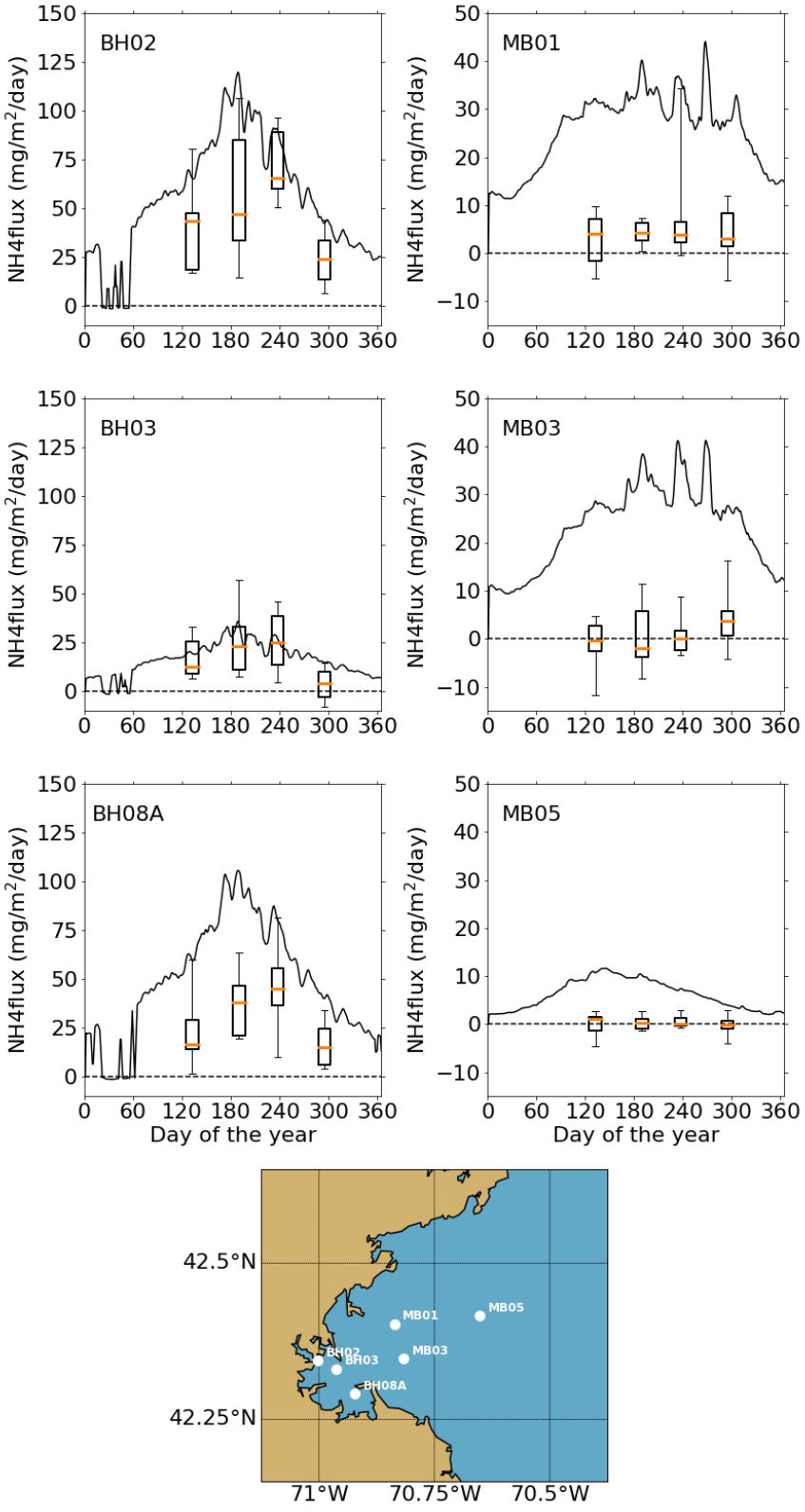

Figure 5-18: Simulated (line; 2020) and observed (box-whiskers; 2001-2010) sediment flux of ammonium. Note change of scale between the Boston Harbor stations (left) and Mass Bay stations (right).

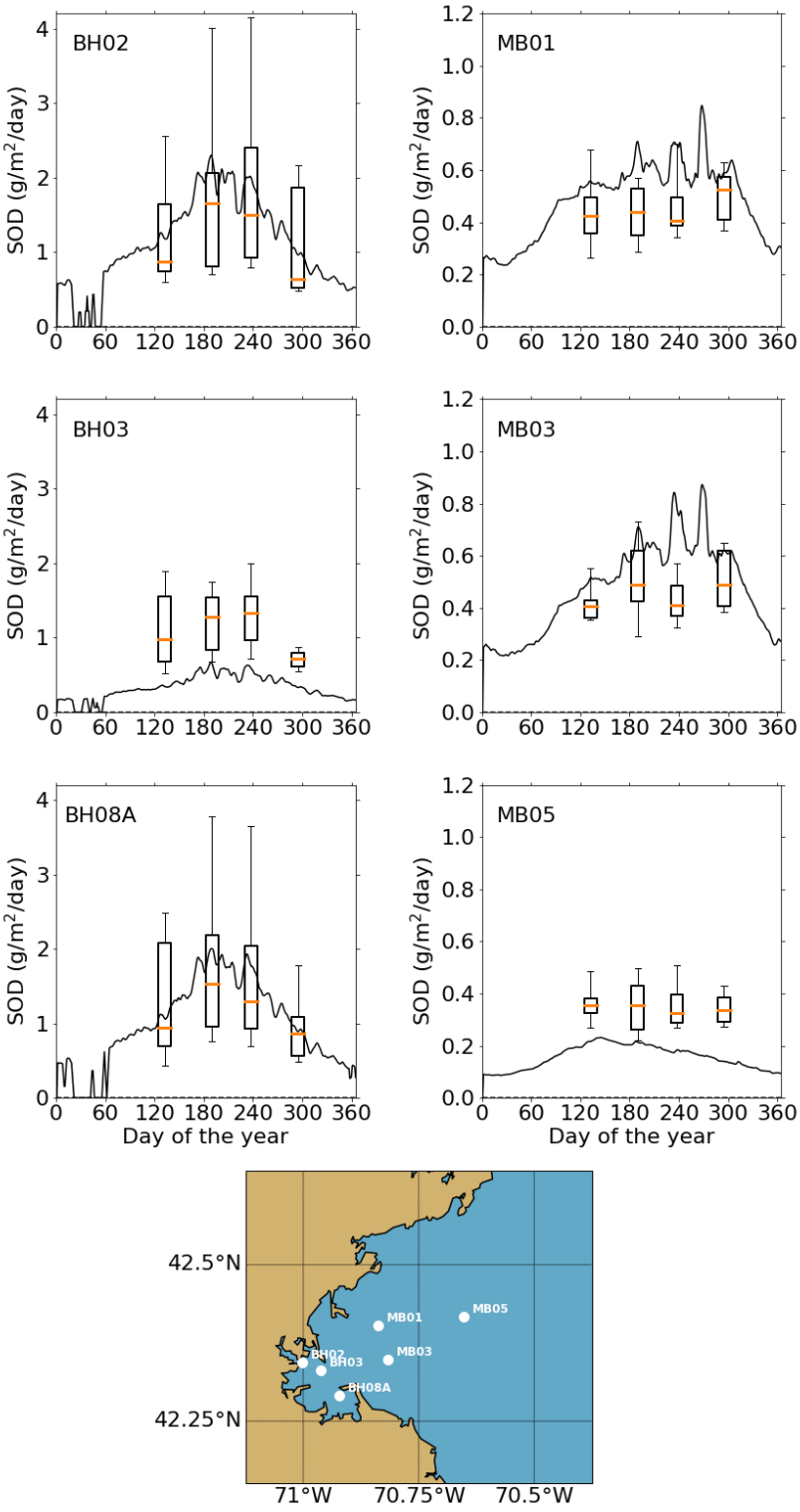

Figure 5-19: Simulated (line; 2020) and observed (box-whiskers; 2001-2010) sediment oxygen demand. Note change of scale between the Boston Harbor stations (left) and Mass Bay stations (right).

5.3 Phytoplankton community composition

Model phytoplankton community/species composition was not validated against field observations during model setup and calibration/validation. However, it is of interest to verify that its main characteristics in the model are not inconsistent with general patterns known to characterize the bays, based on monitoring observations.

The phytoplankton sub-module (BLOOM) simulated the dynamics of 4 functional groups and their adaptation to changing environmental conditions (i.e. light and nutrient limitation). BLOOM simulates the rapid shifts in phytoplankton communities due to these changes, using linear programming to optimize whole-community net primary production (Los, 2009). Simulated phytoplankton groups include: diatoms, dinoflagellates, other marine flagellates, and *Phaeocystis*. Their parameterization was initially based on that used in the North Sea eutrophication model (Blauw et al., 2009) and tuned during the BEM calibration process to better represent chlorophyll a as well as observed PON:POC ratios at MWRA monitoring locations (see Appendix B of Deltares, 2021).

Figure 5-20 shows the share of the different simulated phytoplankton groups in the total phytoplankton biomass near the water surface. Although total phytoplankton biomass temporal dynamics differed from station to station for the year 2020, phytoplankton composition showed similar temporal patterns. Marine diatoms dominated in the winter period and were succeeded in spring by marine flagellates. Dinoflagellates clearly dominated from June to October. This is similar to the simulated successions in communities for the previous years (2017-2019).

In 2020, during the May field survey, *Phaeocystis* was observed to be abundant. Simulated *Phaeocystis* biomass in the model showed noticeable levels during the spring flagellate bloom period (April-May), at all stations except for F23, near the harbor.

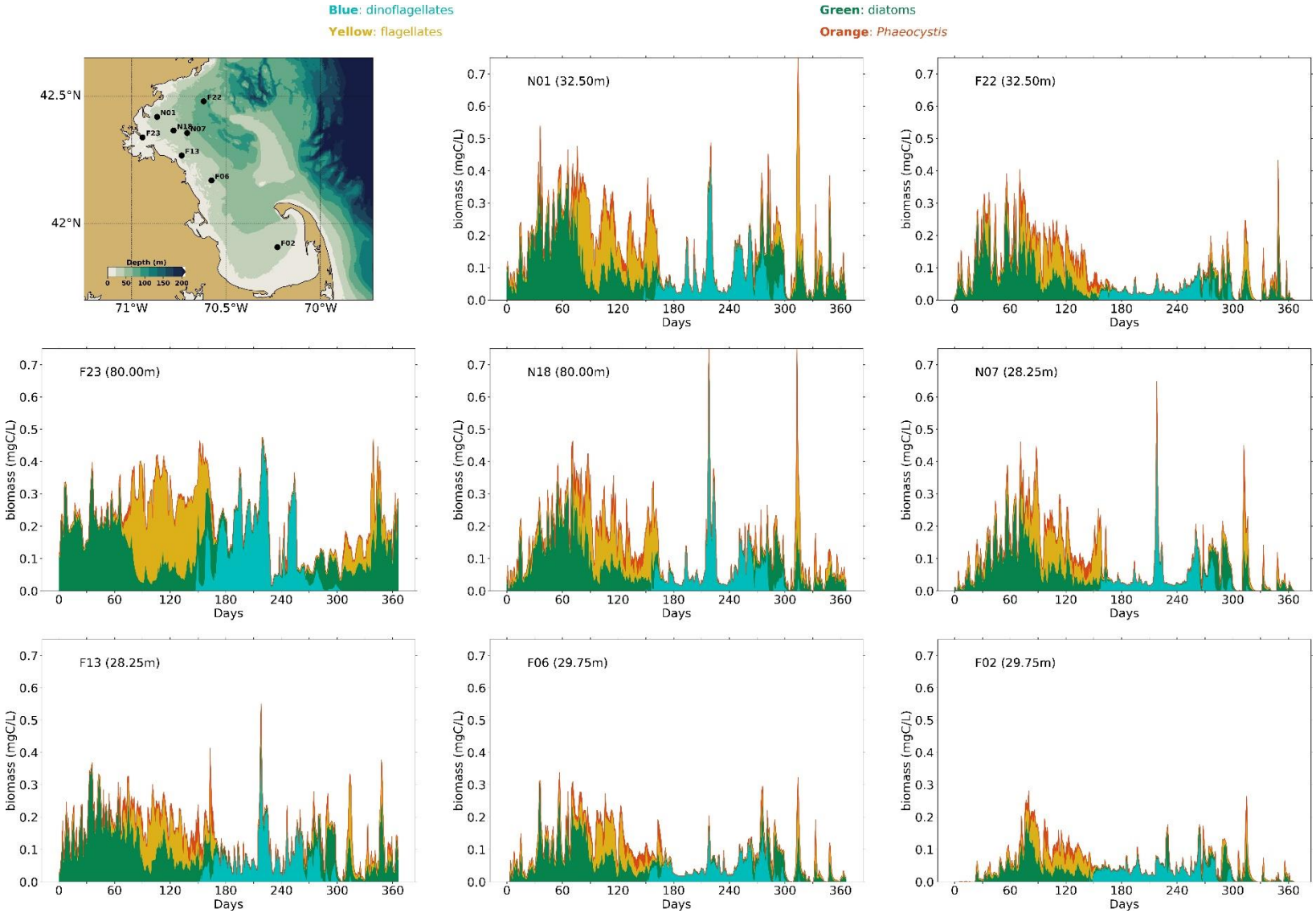

Figure 5-20: Simulated phytoplankton biomass time-series. Biomasses of the 4 simulated species groups (dinoflagellates, other flagellates, diatoms and Phaeocystis*) are stacked.*

5.4 Conditions on West-East transect through outfall

The signature of the outfall in terms of DIN concentrations was visible all year round, with increased concentrations up to a distance of about 10 km (Figure 5-21). The increased DIN was trapped in the lower layers of the water column in the period of stratification (April-October). During the other months, the effluent led to an increase in surface DIN concentrations. These temporal patterns were similar to those observed in previous years.

All year round, chlorophyll a concentrations were higher nearshore (Figure 5-22). This was most likely due to the nutrient inputs from rivers to the harbor area, promoting algal growth. Further offshore, highest chlorophyll a concentrations were simulated in late winter/early spring near the surface. In summer months, maximum chlorophyll a concentrations occurred at a depth of ~15 m. These patterns were mostly similar to those simulated for previous years, but highest concentrations occurred earlier in the year. Any effect of the outfall on chlorophyll a concentrations was difficult to detect.

The vertical cross-sections of DO concentrations for 2020 showed similar temporal and spatial patterns as for previous years, but slightly shifted in time (Figure 5-23). The highest concentrations occurred near the surface between January and April, while for previous years this was usually from February to May. The highest concentrations occurred slightly under the surface between May and July, which corresponded to the depths at which chlorophyll a was the highest. As for chlorophyll a, no effect of the outfall on DO concentrations was visible in the plotted cross sections.

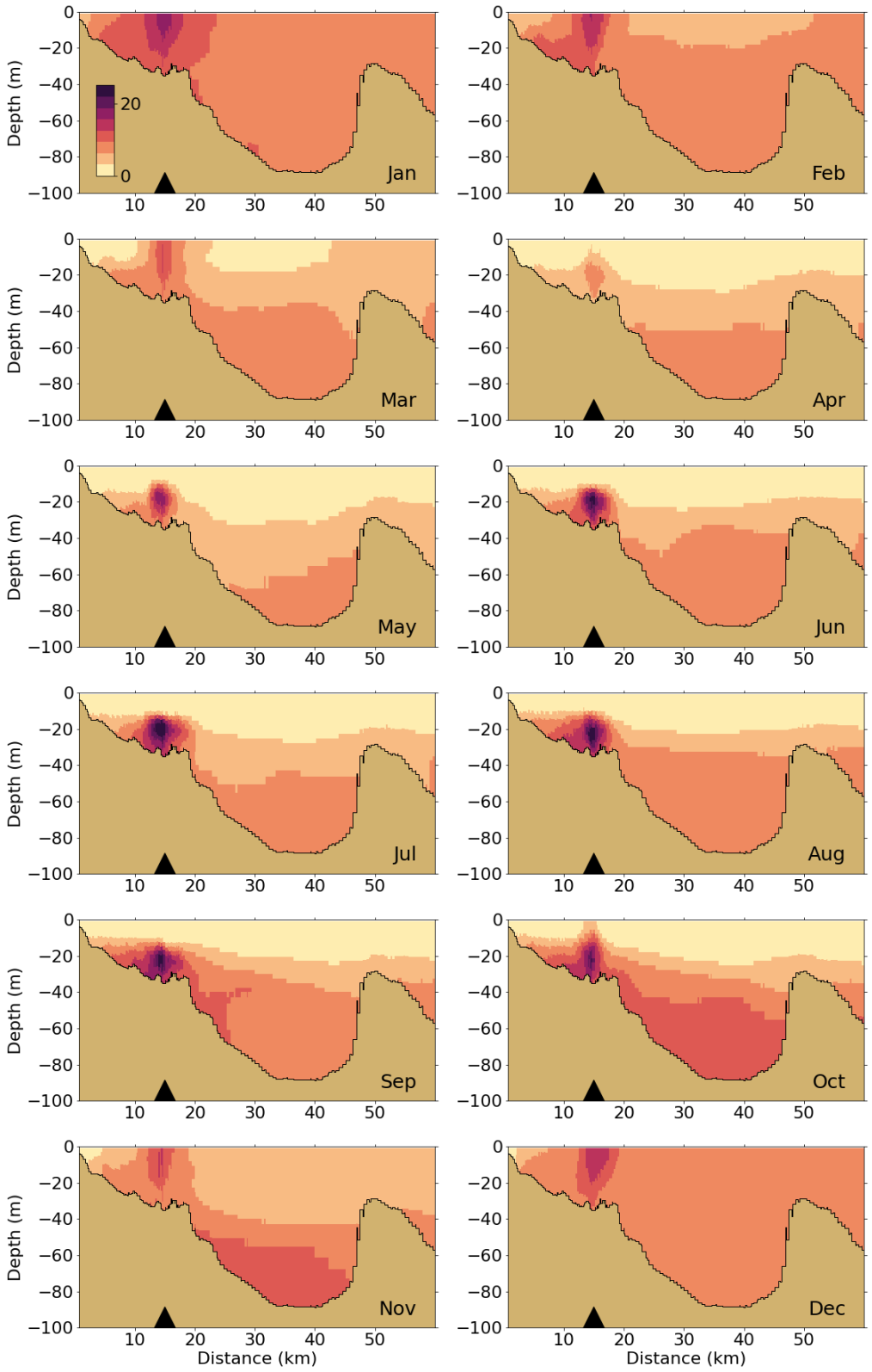

Figure 5-21: Dissolved Inorganic Nitrogen (µM) for 2020 along west-east transect (Figure 2-4). Horizontal axis is distance eastward from coast; black triangle indicates the location of the outfall on the seafloor.

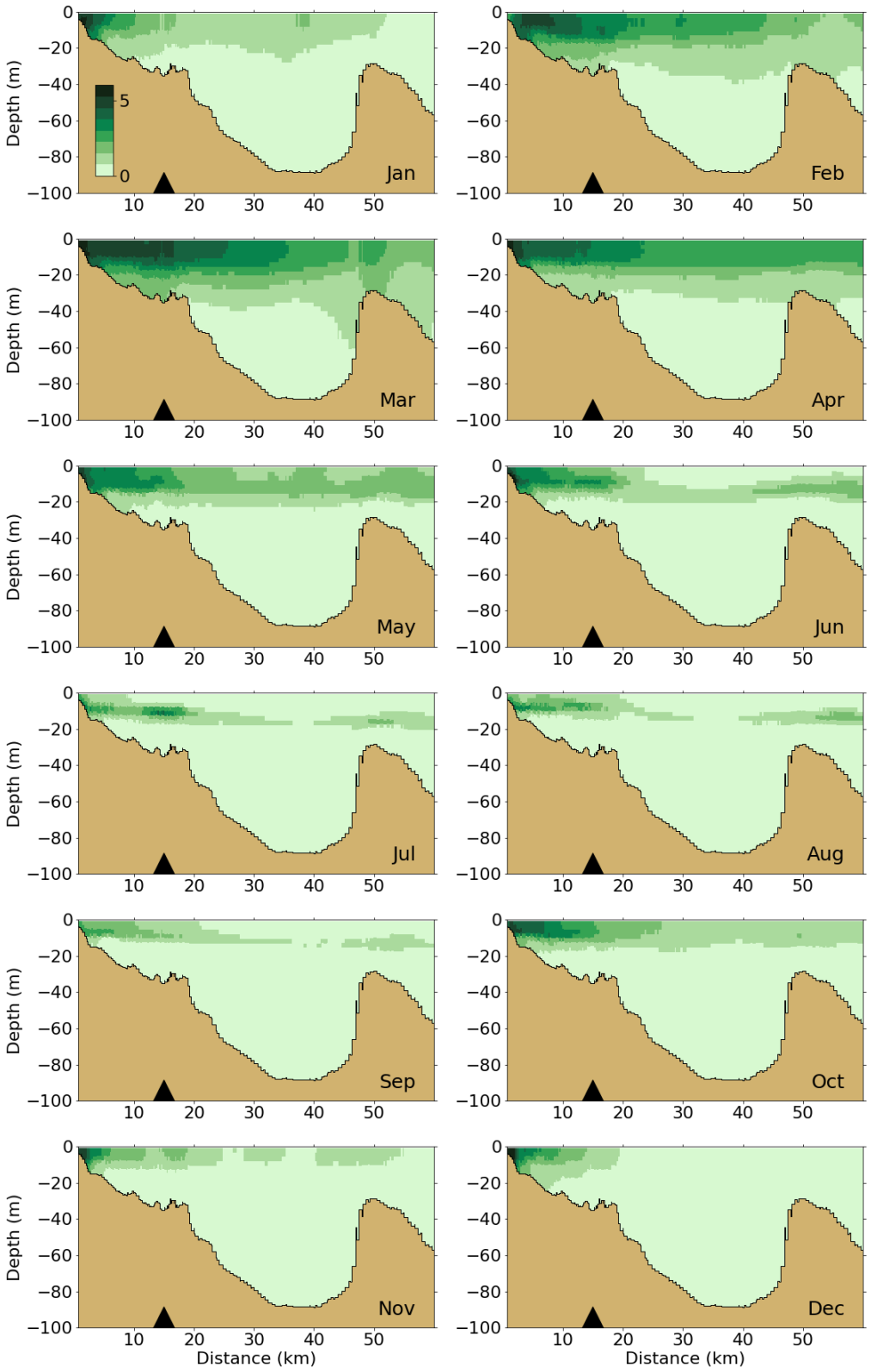

Figure 5-22: Chlorophyll a (µg/L) for 2020 along west-east transect (Figure 2-4). Horizontal axis is distance eastward from coast; black triangle indicates the location of the outfall on the seafloor

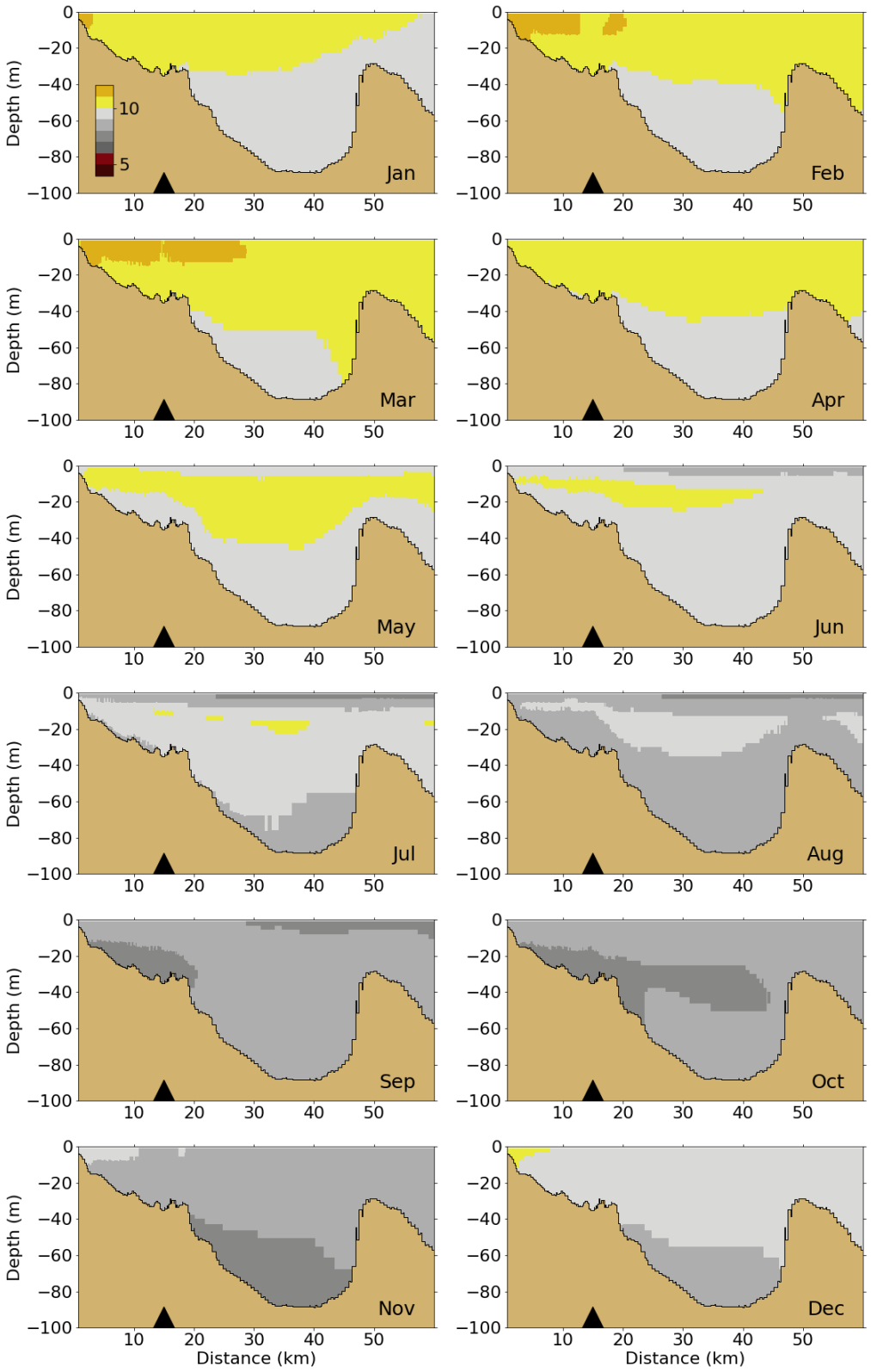

Figure 5-23: Dissolved Oxygen for 2020 along west-east transect (Figure 2-4). Horizontal axis is distance eastward from coast; black triangle indicates the location of the outfall on the seafloor.

6 Synthesis/Application

The synthesis/application simulation using 2020 conditions focuses on the potential ecosystem impacts of fictitious increased nutrient loads due to treated effluent released by MWRA through the outfall. Nutrient loads in this context refer to all nitrogen and phosphorus inputs delivered to the bay through the outfall, in their organic and inorganic forms. In the model, this includes ammonium, nitrate and nitrite, dissolved organic nitrogen, detrital particulate organic nitrogen, phosphate, dissolved organic phosphorous, and detrital particulate organic phosphorus. Details on how model input concentrations for these variables are derived from MWRA measurements in effluent samples can be found in Appendix A of Deltares (2021).

Two model runs were compared:

- Run 1X:
  the “maximal-realism simulation” (reported in the previous sections of this report) for 2020 conditions, using observed nutrient loads;
- Run 1.5X:
  using the same set-up as 1X, with nutrient concentrations in the effluent increased by 50%.

Run 1.5X was furthermore spun up for 2 years, using the conditions for 2018-2019, but with a 50% increase in nutrient loads from the MWRA outfall in the preceding years as well. During the development of the updated BEM, it was established that a 2-year spin-up period is required to achieve results representative for the applied forcings (Deltares, 2021).

The results presented here therefore characterize conditions for increased loading that has persisted for a number of years. In the context of similar scenario runs using earlier versions of the BEM (e.g. the 0.8X and 1.2X simulations of 2016 by Zhao et al, 2017), which may not have applied the increased loads for more than the one year simulated, our results can be expected to yield a larger influence of the load increase. For a simulation which applies the increased load over a one-year period only, the influence on the system will not extend as far from the outfall or show concentrations increase as high, compared to the case treated here.

In addition, the present scenario has scaled up all nutrient species, both inorganic and organic, in the effluent. This was done in order to explore the largest potential effect of scaling up effluent nutrients. In at least some similar past scenario runs (e.g. Zhao et al, 2017), only the inorganic species were scaled up. For this reason, in addition to the extended spin-up duration, the results here are expected to show a larger effect than seen in similar past model investigations.

It is further noted that the updated BEM reacts differently to these changes in loadings compared to the former BEM (Zhao et al, 2017), due to the different location of the boundary. In the former BEM, the offshore boundary conditions for the water quality component of the model were forced directly at the outer limit of the Massachusetts Bay. The former boundary was not far enough away to be independent of the MWRA outfall. Zhao et al. (2017) do not mention a change in the boundary conditions in the scenario runs. The use of the same conditions for these runs at the boundary, relatively close to the discharge point, would lead to simulation results forced to the prescribed 1X conditions at the boundary. The consequence would be an underestimation of the effects of changes

in the effluent concentrations. This also leads us to expect results here to show a larger effect than in prior similar scenario simulations.

Results for simulated near-surface and seafloor dissolved inorganic nitrogen (DIN; summed ammonium, nitrate, and nitrate), surface chlorophyll a, bottom DO concentrations, and bottom DO saturation from the 1X and 1.5X simulations were compared. This was done at seven stations in Massachusetts Bay, Cape Cod Bay and the mouth of Boston Harbor, including the outfall location (N21). The results from both simulations were also presented as maps and vertical cross-sections of monthly averaged differences of the ammonium concentrations. Finally, the relative differences between Run 1X and Run 1.5X were tabulated at three representative stations for the month of May, because that is when they were the largest, and for August, for comparison with results from the scenario runs carried out by Zhao et al. (2017). Timeseries results are shown with a 3-day running mean applied, to match the treatment in prior sections of this report.

Time series of surface DIN (Figure 6-1) show that concentrations are higher in the 1.5X run. The differences are noticeable at all stations and decrease with distance from the outfall. At station N21, the differences are in the 10 µM range except during the period of DIN depletion in summer. Away from the outfall, the differences decrease and are about 1 µM towards the Gulf of Maine (station F22) and Cape Cod Bay (station F02). Time series of bottom DIN concentrations presented in the same way (Figure 6-2) show highest differences exceeding 10 µM above the outfall (N21) throughout the year. Differences of a few µM are observed at other stations nearest the outfall. Far away from the outfall the differences drop to less than 1 µM.

The effect on surface chlorophyll a (Figure 6-3) is noticeable at all stations. Some peaks tend to be higher, although typically by less than 1 µg L^{-1}, while seasonal patterns are not affected. The effects on the bottom dissolved oxygen concentration (Figure 6-4) are very small. The surface oxygen saturation (Figure 6-5) shows higher peaks of oversaturation of typically a few percent that reflect the higher primary production peaks associated with the increases in chlorophyll a just noted.

Furthermore, model mass balances results indicate that the yearly primary production increases by 4.1% and 4.7% in Massachusetts Bay and in Cape Cod Bay, respectively (Table 6-1). This is equivalent to the increase in TN loads to the study area. The MWRA outfall represents 9.3% of the TN loads to the domain in 2020 (Figure 3-6), so an increase of TN in the effluent by a factor 1.5 causes an increase in TN loads (oceanic and non-oceanic) to the domain by 4.2%.

Table 6-1: Comparison of yearly primary production rates in Runs 1X and 1.5X, integrated over the entire water column of Mass Bay and Cape Cod Bay domains.

	Unit	Run 1X	Run 1.5X
Primary production in Mass Bay	[10^9 gO_2/year]	1,830	1,904
Primary production in Cape Cod Bay	[10^9 gO_2/year]	760	796

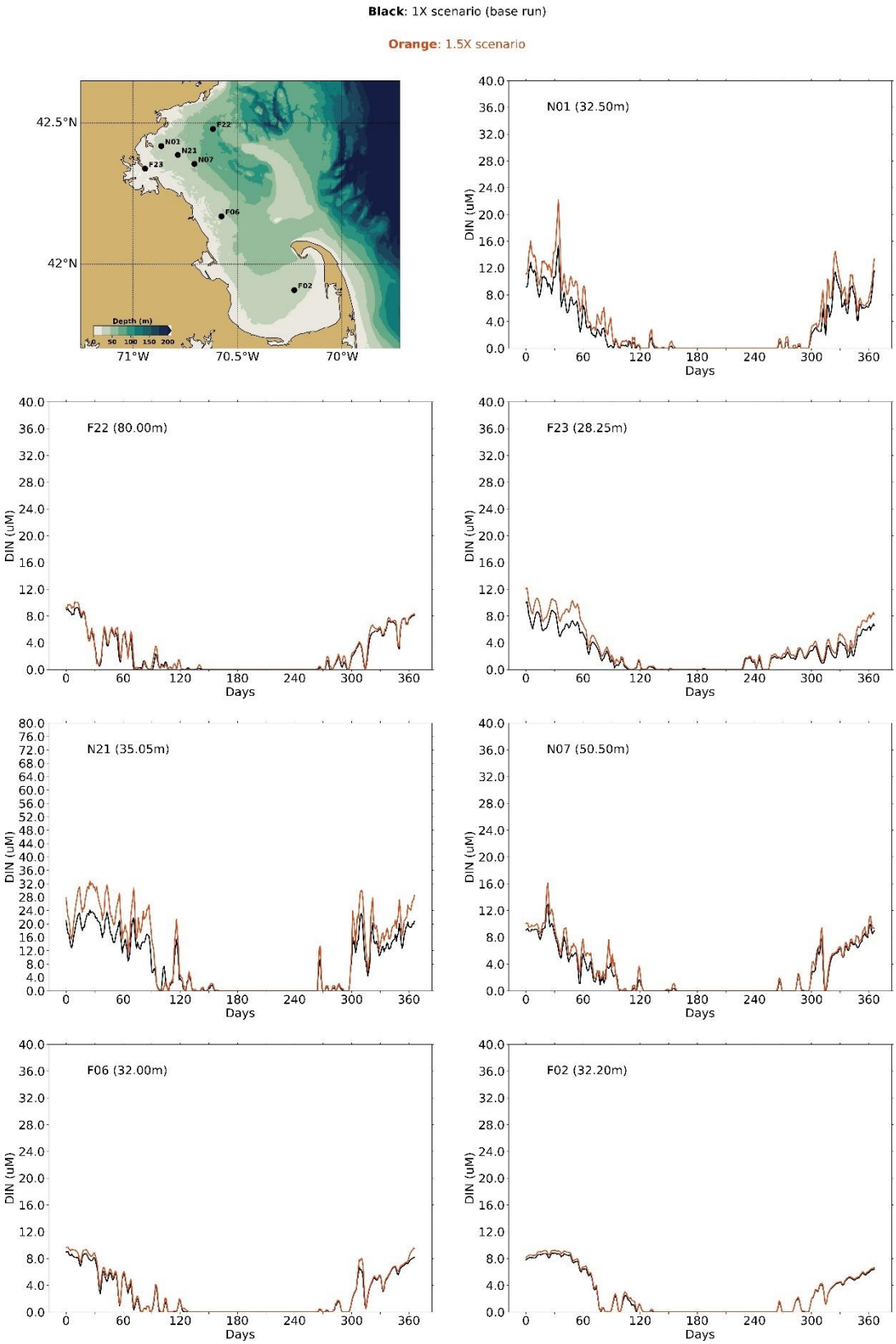

Figure 6-1: Surface DIN time-series for 1X (black) and 1.5X (orange) nutrient loads. Note that the y-axis range is doubled at station N21.

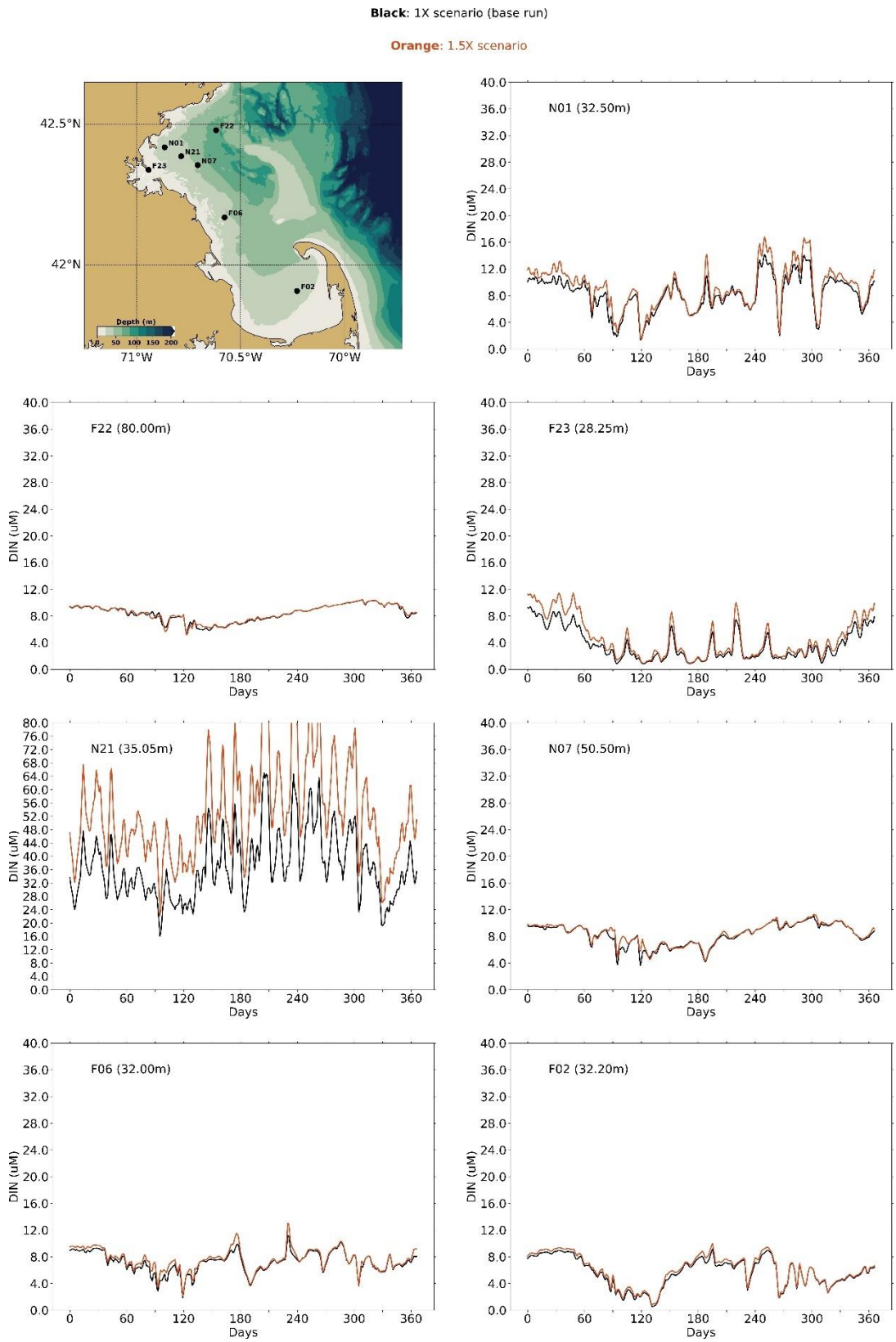

Figure 6-2: Seafloor DIN concentration time-series for 1X (black) and 1.5X (orange) nutrient loads. Note that y-axis range is doubled at station N21.

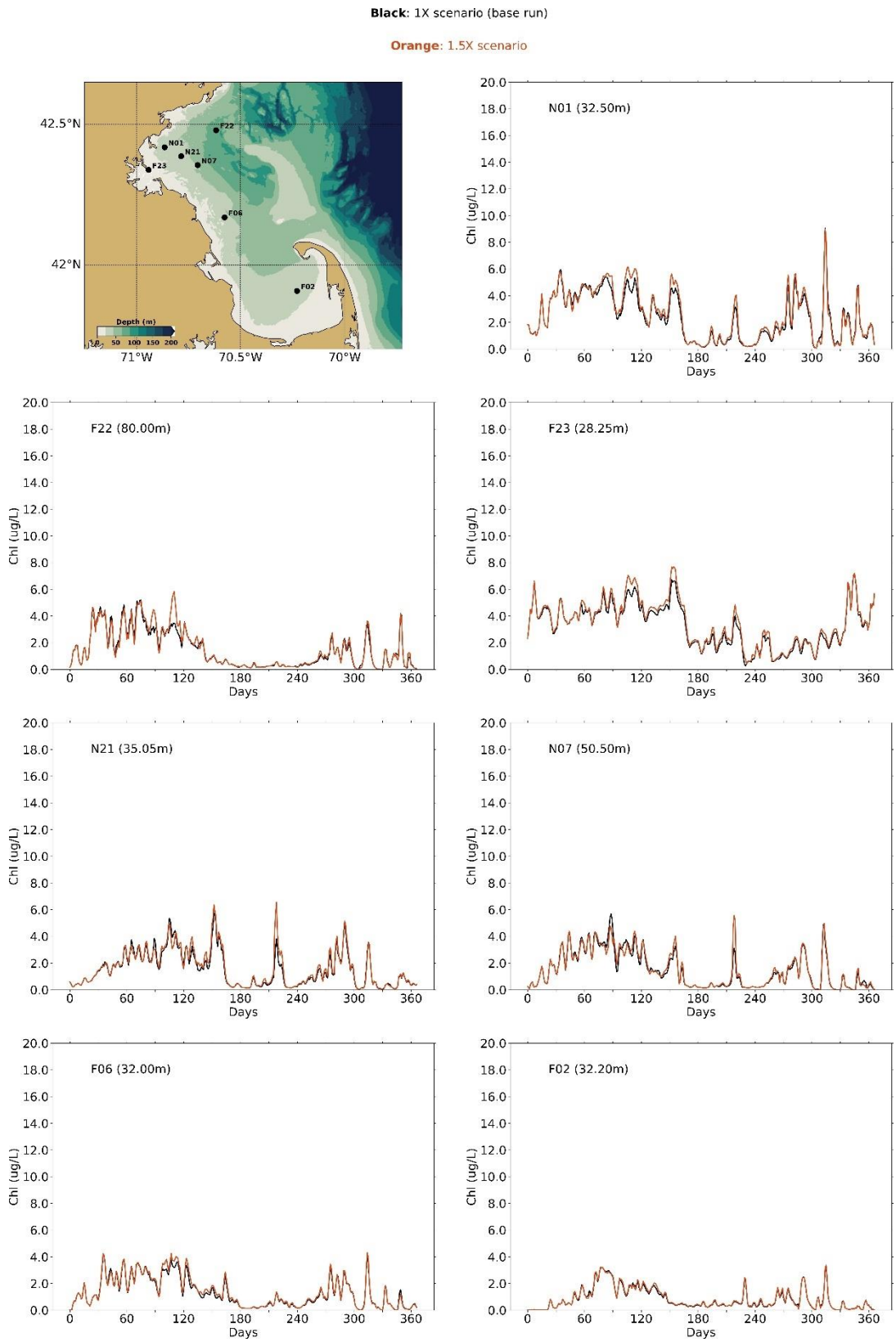

Figure 6-3: Surface chlorophyll a concentration time-series for 1X (black) and 1.5X (orange) nutrient loads.

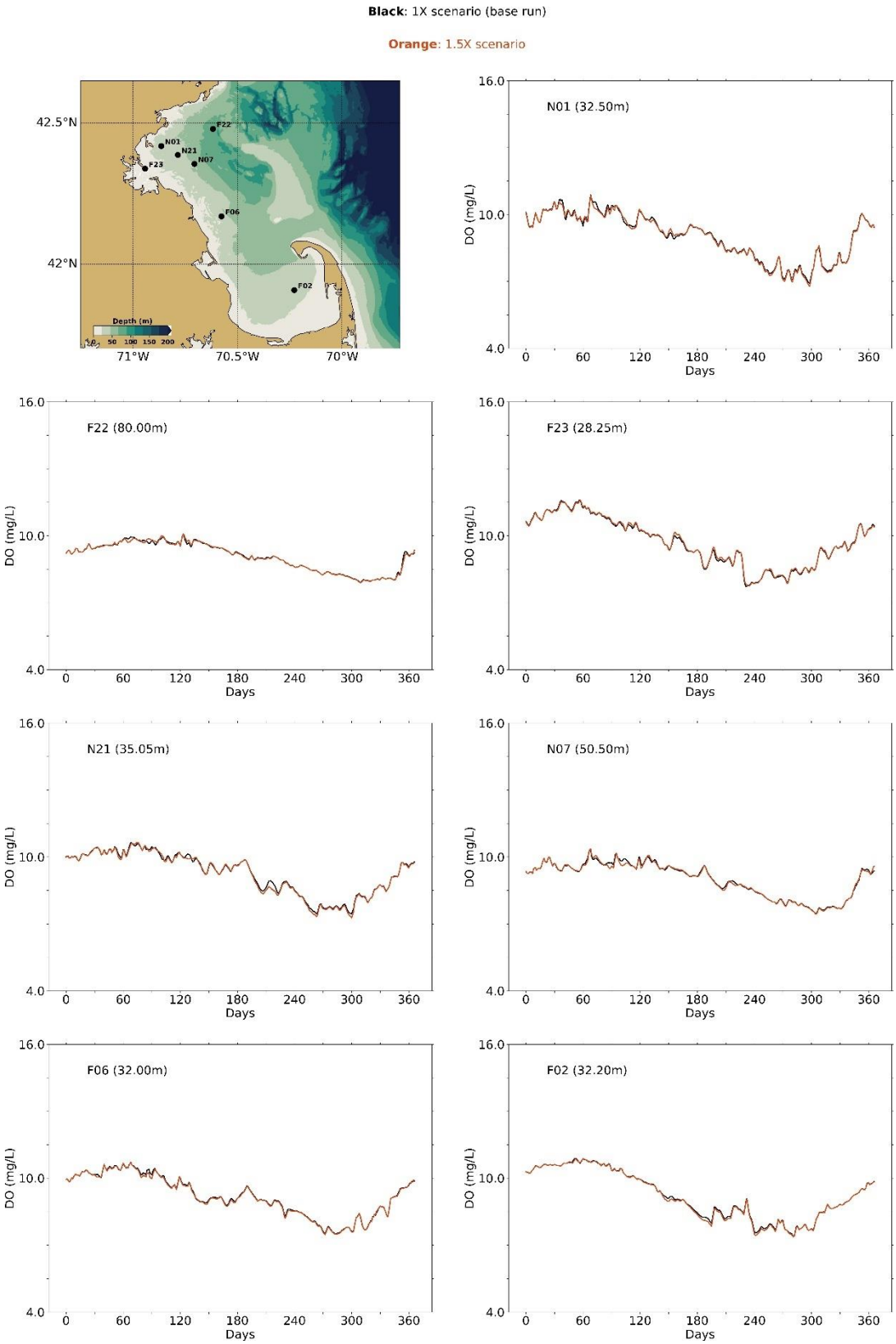

Figure 6-4: Seafloor DO concentration time-series for 1X (black) and 1.5X (orange) nutrient loads.

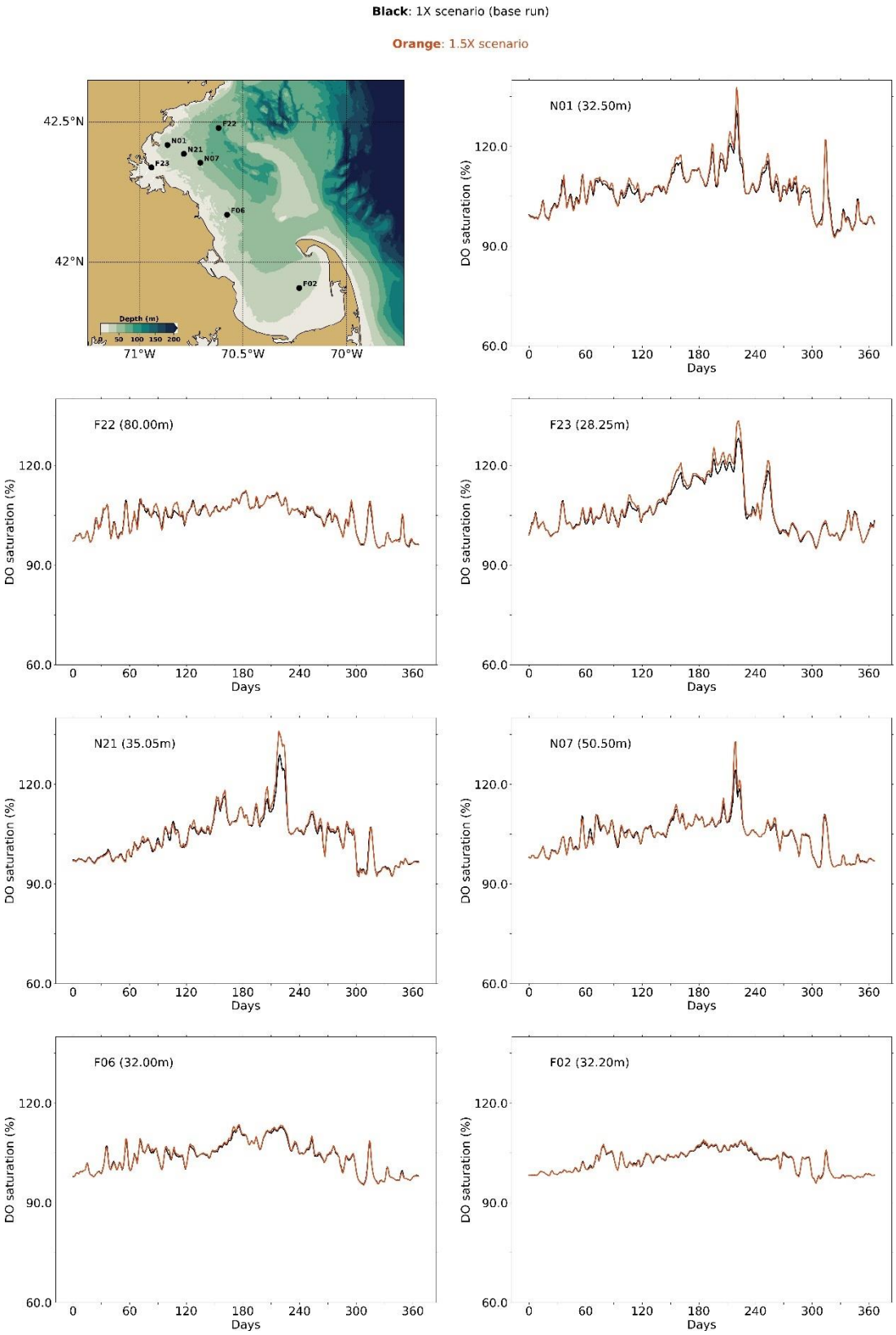

Figure 6-5: Surface DO percent saturation time-series for 1X (black) and 1.5X (orange) nutrient loads.

The ammonium concentration, which is the most sensitive parameter to outfall nutrient load increases (e.g., Zhao et al., 2017), was further examined. The differences between 1.5X run and the 1X run near the surface, at a 20m depth and near the seafloor (Figure 6-6), and along the west-east transect (see Figure 3-6) passing through the outfall (Figure 6-7), show that ammonium increases larger than 1 μM are in an area confined to within about 10 km of the outfall. The largest differences occur near the surface during the non-stratified periods (November-March) and beneath the pycnocline (at ~20m deep) during stratified periods (April-October). The differences can reach values of about 10 μM between the seafloor and the pycnocline, at the outfall location, and drop off with distance horizontally and vertically.

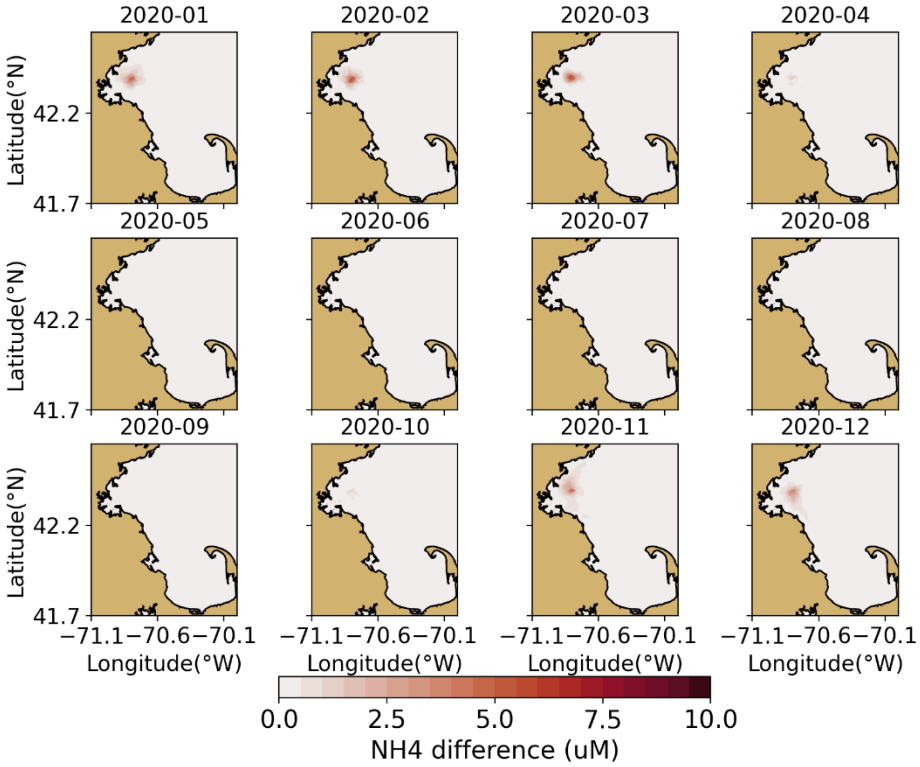

Figure 6-6: Monthly-mean difference in near-surface NH4 between 1.5X and 1X runs.

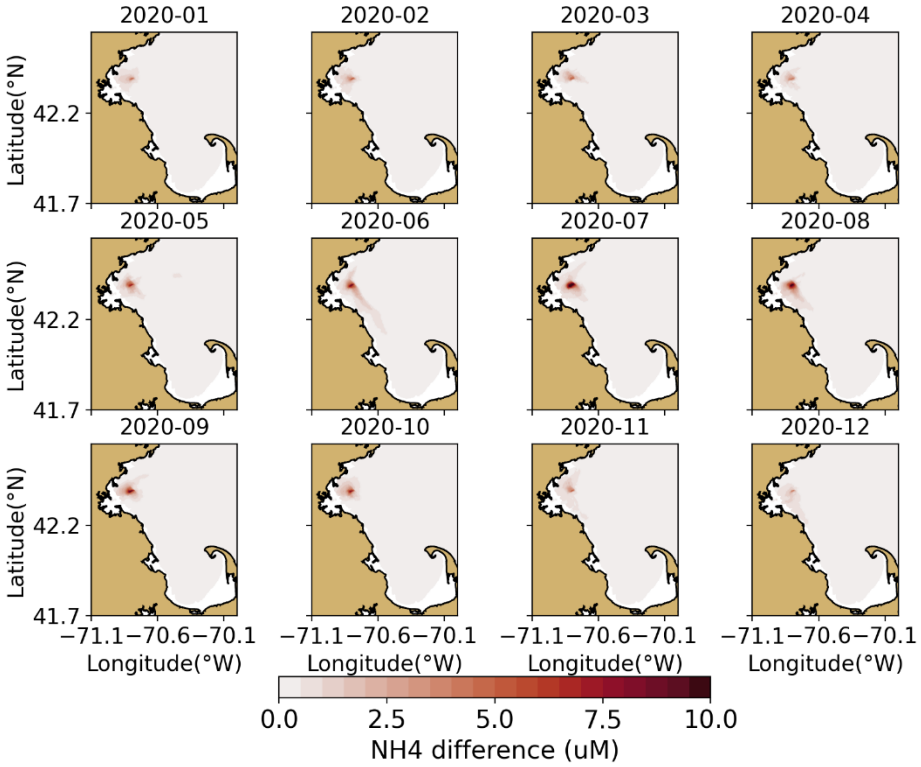

Figure 6-7: Monthly-mean difference in NH4 at a 20m depth between 1.5X and 1X runs.

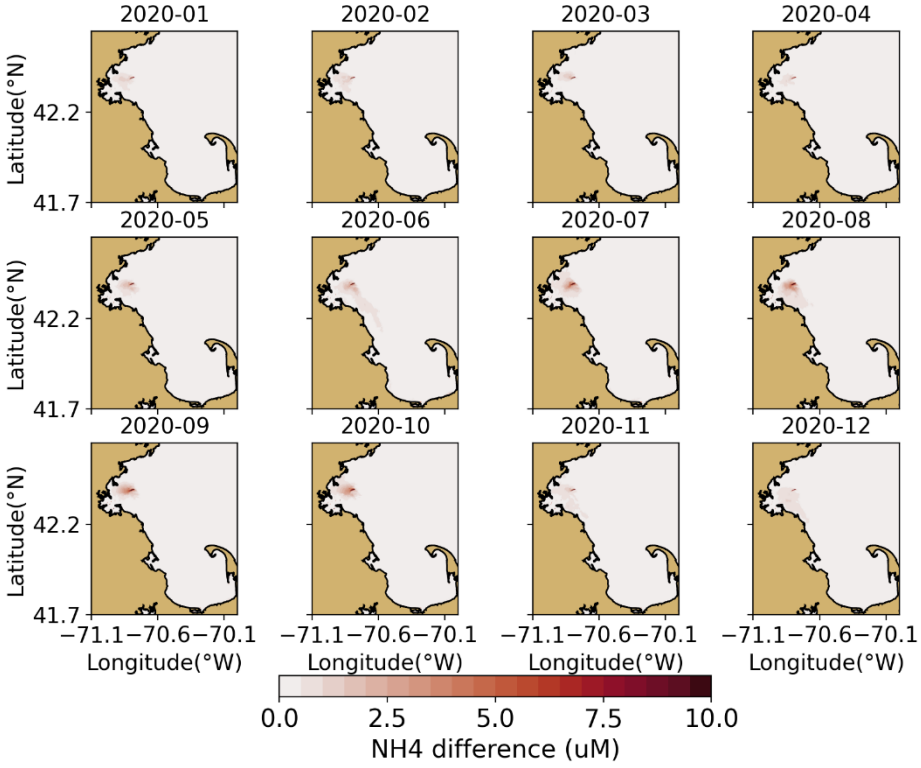

Figure 6-8: Monthly-mean difference near-seafloor NH4 between 1.5X and 1X runs.

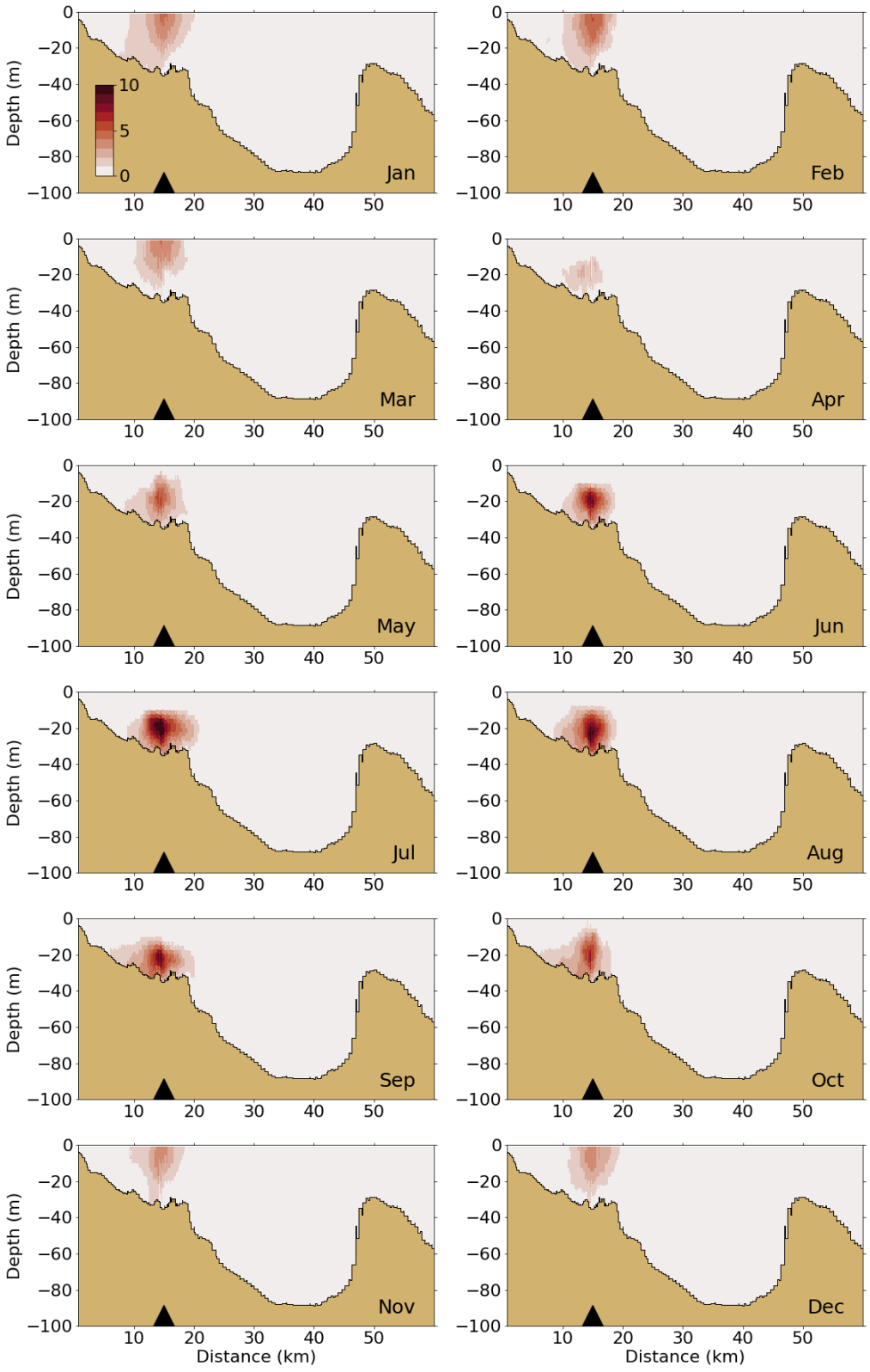

Figure 6-9: Monthly-mean difference in NH4 between 1.5X and 1X runs along west-east transect (Figure 2-4).

Table 6-2 shows monthly means in the 1.5X and 1X runs, as well as the relative difference between them, for the month of May 2020, when the relative differences were the largest. The table shows three representative stations (N18 near the outfall, F06 in west-central Massachusetts Bay, and F02 in Cape Cod Bay) and the same five parameters as examined above. Overall, differences of the 1.5X run compared to 1X are largest near the outfall site (N18). The absolute differences for surface DIN are small (less than 0.2 uM), but due to the low concentrations in the 1X simulation the relative differences (percent change Δ%) are large.

Table 6-2: May 2020 means and percentage differences to run 1X at three representative stations.

Station	Run	Surface chlorophyll a		Surface DIN		Bottom DIN		Bottom DO concentration		Surface DO saturation	
		[µg L^{-1}]	Δ%	[µM]	Δ%	[µM]	Δ%	[mg L^{-1}]	Δ%	[%]	Δ%
N18: near outfall	1X	2.11		0.09		6.11		9.76		106.28	
	1.5X	2.41	+14.12	0.26	+193.60	8.23	+34.67	9.70	-0.58	106.64	+0.34
F06: West-central MB	1X	1.69		0.03		6.23		9.30		104.92	
	1.5X	1.92	+13.54	0.11	+252.99	6.58	+5.68	9.26	-0.33	105.16	+0.23
F02: Cape Cod Bay	1X	1.31		0.04		2.56		9.53		103.57	
	1.5X	1.45	+10.63	0.06	+67.97	2.91	+13.61	9.49	-0.48	103.68	+0.11

Table 6-3 shows monthly means in the 1.5X and 1X runs, as well as the relative difference between them, for the month of August 2020, when a decrease in deep DO concentrations is likely. August results also enable direct comparison with Zhao et al. (2017). In August, near-surface DIN is depleted in both runs 1X and 1.5X. As expected, effects on bottom DO concentrations are higher than in May, with >1% difference near the outfall (N18).

Table 6-3: August 2020 means and percentage differences to run 1X at three representative stations for the 1.5X run. Differences between 1X and a hypothetical 1.2X scenario (20% increase in nutrient loads from the MWRA outfall) are also shown, as estimated by assuming a linear response to increased outfall nutrient loads.

Station	Run	Surface chlorophyll a		Surface DIN		Bottom DIN		Bottom DO concentration		Surface DO saturation	
		[µg L^{-1}]	Δ%	[µM]	Δ%	[µM]	Δ%	[mg L^{-1}]	Δ%	[%]	Δ%
N18: near outfall	1X	1.10		0.00		12.27		8.61		113.95	
	1.5X	1.77	+61.27	0.00	-	15.94	+29.90	8.51	-1.18	116.94	+2.62
	1.2X		*+24.51*		-		*+11.96*		*-0.47*		*+1.05*
F06: West-central MB	1X	0.49		0.00		7.96		8.70		108.95	
	1.5X	0.53	+8.80	0.00	-	8.47	+6.35	8.66	-0.43	109.34	+0.36
	1.2X		*+3.52*		-		*+2.54*		*-0.17*		*+0.14*
F02: Cape Cod Bay	1X	0.62		0.00		6.27		8.39		106.52	
	1.5X	0.67	+7.98	0.00	-	6.64	+5.85	8.34	-0.67	106.82	+0.29
	1.2X		*+3.19*		-		*+2.34*		*-0.44*		*+0.12*

For comparison with results from Zhao et al. (2017), in Table 6-3 the Δ% values for a hypothetical updated BEM 1.2X scenario (20% increase in nutrient loads from the MWRA outfall) were estimated assuming a linear response of the system to an increase in the nutrient loads from the outfall (factor 0.2/0.5 applied to the Δ% values for scenario 1.5X). Results of prior modeling of increased effluent nutrient loads show a linear response for increases of up to at least 2X (Zhao et al., 2015).

Such 1.2X results for chlorophyll a, bottom DIN and DO show a significantly higher sensitivity to the increase in nutrient loads than those from Zhao et al. (2017). The Δ% for surface chlorophyll a in the present runs reached about 24% at N18 and 3-4% at F06 and F02, but was well less than 1% in the run described by Zhao et al. The Δ% for bottom DIN in the present runs reached about 12% at N18, where it was about 8% in the run described by Zhao et al, and 2-3% at F06 and F02, where it was less than 1% in the run described by Zhao et al. The Δ% for bottom DO concentration in the present runs was less than 0.5%, but was 0.02% or less in the run described by Zhao et al. The Δ% for surface DO percent saturation in the present runs was about 1% or less, but was 0.01% or less in the run described by Zhao et al. These higher magnitudes of changes in the present run are most likely due, at least in part, to the factors noted above: longer spin-up time, possibly the scaling up of organic forms of nutrients from the outfall (neither done by Zhao et al., 2017), and the absence of a nearby offshore boundary constraining the model response.

To summarize, the model results for this scenario simulation, with effluent nutrient concentrations increased by 50% over observed, indicate that effects of the outfall on eutrophication-related conditions consist of localized increases in chlorophyll a and very minor decreases in oxygen by 0.1 mg L^{-1} or less. This is true even though the simulation included key attributes that led to a larger impact compared to similar scenario runs using the former BEM (Zhao et al., 2017). Results of the 1.5X scenario help put in context potential effects of effluent total nitrogen loads as high as the caution level and/or warning level thresholds for nitrogen load in the Contingency Plan (MWRA 2021). The 1.5X load investigated here is about 24% higher than the warning level threshold and did not lead to adverse effects, which implies that an exceedance of the Contingency Plan thresholds is not indicative of water quality or eutrophication issues.

7 Conclusion

The performance of the hydrodynamic model was comparable to the previous years. Temperatures were reproduced accurately, especially at the surface, even considering that the observed summer average water temperature was the warmest over the 29-year period of observations. Model salinity performed similarly to previous years at most stations, and less well as some stations. This was due to the lack of a strong spring freshet and thus weak seasonal variations, which meant skill measures were normalized with unusually low values; the un-normalized values were comparable to previous years.

At most stations, temperature stratification was present in the model from May until early November with its maximum in July and August, in agreement with the observation of a record-high temperature stratification in July. Salinity stratification in 2020 was very limited due to the low river flow. Sudden mixing events occurred in the model at the shallower stations in early August and late September. During the latter, the water column became fully mixed for a couple of days, after which stratification returned. These events occurred between field survey dates.

Modeled non-tidal current patterns were similar to observations, but the magnitudes near the surface, and the temporal variability, were slightly smaller. At the bays-wide scale, the expected circulation pattern driven by the Western Maine Coastal Current was visible in the model. In general, the agreement between the hydrodynamic model and the observations was sufficient to conclude that the representation of processes was adequate to support water quality modeling.

In the water quality model, light extinction for the year 2020 was similar to previous years and the model reproduced the extinction range and variability well at most stations. Seasonal variations of surface and bottom DIN concentrations in 2020 were similar to those observed and simulated for previous years. Surface and bottom were comparable in winter, when the water column was well mixed. Surface DIN concentrations declined at the end of winter and were depleted from April to October, before increasing again mid-fall. Bottom concentrations declined, to a much lesser degree than surface concentrations, in spring and summer. The model generally reproduced these observed seasonal variations and vertical differences throughout the water column.

Seasonal variations of chlorophyll a observations in 2020 showed higher values than typical during the end of summer and early fall. The model simulated the higher chlorophyll a peaks at the end of winter and early spring and in late fall, and some smaller peaks in the late summer. As for previous years, near surface simulated concentrations were in the same range as observations. Temporal variability was not always reproduced, owing mainly to the relatively low field sampling frequency and the high temporal variability. As in previous years, the model tended to underestimate bottom chlorophyll a at certain stations. Simulated chlorophyll a concentrations decreased eastward from the coast. Early spring increases occurred throughout the relatively well-mixed water column. During the more stratified months, simulated bottom chlorophyll a remained low and highest values occurred near the surface and in the subsurface. Because the model significantly underestimated the strong and spatially extensive observed bloom of dinoflagellates in the late summer, it did not capture the chlorophyll a peak during that period.

Particulate organic carbon (POC) concentrations at the observation stations were extremely variable and it was difficult to identify any clear seasonal pattern. Concentrations were however slightly lower in

winter and early spring than the rest of the year. Measured POC concentrations were highest closer to the harbor, likely due to the high river POC inputs. Concentrations were significantly lower near the bottom than at the surface. The model generally captured these POC concentration ranges, variability and vertical gradients. However, at stations closer to the harbor the model POC concentrations were higher than observed. As for chlorophyll a, simulated POC concentrations decreased from the coast eastward. High observed POC concentrations at the beginning of September were not fully captured by the model, which was most likely due to the underestimation of phytoplankton biomass (chlorophyll a) for that period.

The vertical cross-sections of DO concentrations for 2020 showed similar temporal and spatial patterns as for previous years, with the highest concentrations occurring near the surface between February and May. The 2020 seasonal variations of DO concentrations were well reproduced in the model, with maximum concentrations observed at the end of winter or early spring and decreasing until fall before rising again. While winter concentrations at the surface and the bottom were comparable, bottom concentrations dropped lower at the end of the summer and beginning of fall. As for previous years, the model reproduces minimum observed values at some stations, but not all. Some of this may be attributed to the fact that the field measurement campaign observed historic minima of DO at many stations in May and June, which is a very extreme situation for the model to capture. The model-observation comparison at intermediate water depths showed good agreement. In summer, the model slightly underestimated concentrations in the upper water column, and in fall, the decrease in DO throughout the water column was slightly underestimated. The North-South and West-East cross-section plots show that DO generally had weak vertical gradients. Concentrations were higher at the end of winter and early spring and decreased until fall. At the end of spring and early summer, slightly higher concentrations were both observed and simulated at the subsurface depths with relatively high phytoplankton biomass. These vertical gradients were however weaker than during previous years, with the phytoplankton biomasses being also lower in that period. The observed vertical gradients in DO concentrations were well captured by the model.

Although total phytoplankton biomass temporal dynamics differed from station to station, phytoplankton composition showed similar temporal patterns across stations. Diatoms dominated in the winter period and were succeeded in spring by flagellates. Dinoflagellates clearly dominated from June to the end of October. These were typical characteristics of community composition seen in monitoring observations. Simulated *Phaeocystis* biomass in the model showed noticeable levels during the spring flagellate bloom period (April-May), at all stations except for F23, near the harbor. This is similar to the timing of observed *Phaeocystis* abundances.

According to the model results, the MWRA outfall did not have visible effects on ecosystem functioning at the Massachusetts Bay scale. The signature of the outfall in terms of DIN concentrations was visible all year round, with increased concentrations up to a distance of about 10 km. The increased DIN concentrations were trapped in the lower layers of the water column during the period of stratification (April-October). During the other months, the effluent led to an increase in surface DIN concentrations as well. These temporal patterns were similar to those observed in previous years. All year round, chlorophyll a concentrations were higher nearshore. This was most likely due to the nutrient inputs from rivers to the harbor area, promoting algal growth. Any effect of the outfall on chlorophyll a concentrations could not be detected. As for chlorophyll a, no effect of the outfall on DO concentrations was apparent.

To investigate sensitivity to nutrient loads from the MWRA outfall, a synthesis/application simulation was carried out. It was configured identically to the maximal-realism case except that effluent nutrient concentrations (and therefore loads) were increased by 50%. The effect of the additional nutrients was

noticeable in the DIN concentrations throughout Massachusetts Bay and Cape Cod Bay, with concentration changes decreasing with increasing distance from the outfall. The additional nutrients led to a 4.1% and 4.7% annual primary production increase in Massachusetts Bay and in Cape Cod Bay (integrated over the whole domains and the entire water column), respectively. This was demonstrated by higher simulated chlorophyll a peaks and higher near surface DO saturation peaks. The added productivity did not lead to changes in near bottom DO anywhere in the bays. The percent increase to productivity was close to the percent increase of the total nitrogen loads.

References

Alessi, Carol A., Beardsley, Robert C., Limeburner, Richard, Rosenfeld, Leslie K., Lentz, Steven J., Send, Uwe, Winant, Clinton D., Allen, John S., Halliwell, George R., Brown, Wendell S., Irish, James D.,1985. "CODE-2: moored array and large-scale data report", Woods Hole Oceanographic Institution Technical Report 85-35, DOI:10.1575/1912/1641. (https://hdl.handle.net/1912/1641)

Blauw AN, HFJ Los, M Bokhorst and PLA Erftemeijer, 2009. GEM: a Generic Ecological Model for estuaries and coastal waters. Hydrobiologia 618: 175-198.

Deltares, 2019a. D-Flow Flexible Mesh, Technical Reference Manual. Released for: Delft3D FM Suite 2020. Version: 1.1.0 SVN Revision: 63652. December 4, 2019.

Deltares. 2019b. Delft3D Flexible Mesh Suite, D-Flow FM in Delta Shell, User Manual, Version 1.5.0, December 5, 2019 (https://content.oss.deltares.nl/delft3d/manuals/DFlow_FM_User_Manual.pdf)

Deltares, 2021. Demonstration of the updated Bays Eutrophication Model. Boston: Massachusetts Water Resources Authority. Report 2021-02. 138 p. plus appendices. (www.mwra.com/harbor/enquad/pdf/2021-02.pdf)

Deltares, 2022a. Simulations of 2017 Hydrodynamics and Water Quality in the Massachusetts Bay System using the Bays Eutrophication Model. Boston: Massachusetts Water Resources Authority. Report 2021-12. 107 p. https://www.mwra.com/harbor/enquad/pdf/2021-12.pdf

Deltares, 2022b. Simulations of 2019 Hydrodynamics and Water Quality in the Massachusetts Bay System using the Bays Eutrophication Model. Boston: Massachusetts Water Resources Authority. Report 2022-07. 86 p. https://www.mwra.com/harbor/enquad/pdf/2022-07.pdf

Hunt CD, RK Kropp, JJ Fitzpatrick, P Yodzis, and RE Ulanowicz, 1999. A Review of Issues Related to the Development of a Food Web Model for Important Prey of Endangered Species in Massachusetts and Cape Cod Bays. Boston: Massachusetts Water Resources Authority. Report ENQUAD 99-14. 62 p. (http://www.mwra.state.ma.us/harbor/enquad/pdf/1999-14.pdf)

Keay KE, WS Leo, and PS Libby, 2012. Comparisons of Model-Predicted and Measured Productivity in Massachusetts Bay. Boston: Massachusetts Water Resources Authority. Report 2012-03. 11 p. plus Appendix. (http://www.mwra.state.ma.us/harbor/enquad/pdf/2012-03.pdf)

Libby PS, Borkman DG, Geyer WR, Turner JT, Costa AS, Taylor DI, Wang J, Codiga DL. 2021. 2020 Water column monitoring results. Boston: Massachusetts Water Resources Authority. Report 2021-07. 57 p. http://www.mwra.com/harbor/enquad/pdf/2021-07.pdf

Los, FJ, 2009. Eco-hydrodynamic modeling of primary production in coastal waters and lakes using BLOOM. Ph.D. Thesis, Wageningen University, 2009.

MWRA. 2001. Massachusetts Water Resources Authority Contingency Plan Revision 1. Boston: Massachusetts Water Resources Authority. Report 2001-ms-71. 47 p. https://www.mwra.com/harbor/enquad/pdf/2001-ms-71.pdf

Scully, M. E., Geyer, W. R., Borkman, D., Pugh, T. L., Costa, A., and Nichols, O. C.: Unprecedented Summer Hypoxia in Southern Cape Cod Bay: An Ecological Response to Regional Climate Change?, Biogeosciences Discuss. [preprint], https://doi.org/10.5194/bg-2022-48, in review, 2022.

Tucker J, S Kelsey, and AE Giblin, 2010. 2009 benthic nutrient flux annual report. Boston: Massachusetts Water Resources Authority. Report 2010-10. 27 p. (http://www.mwra.state.ma.us/harbor/enquad/pdf/2010-10.pdf)

Xue, P, C Chen, J Qi, RC Beardsley, R Tian, L Zhao, and H Lin, 2014. Mechanism studies of seasonal variability of dissolved oxygen in Mass Bay: A multi-scale FVCOM/UG-RCA application. Journal of Marine Systems. 131, 102-119.

Zhao L, Beardsley RC, Chen C, Codiga DL, Wang L, 2017. Simulations of 2016 Hydrodynamics and Water Quality in the Massachusetts Bay System using the Bays Eutrophication Model. Boston: Massachusetts Water Resources Authority. Report 2017-13. 111p. (https://www.mwra.com/harbor/enquad/pdf/2017-13.pdf)

Zhao L, Chen C, Beardsley RC, Codiga DL, Leo WS, Mickelson MJ. 2015. Modeling 2013 in Massachusetts Bay Using the Unstructured-Grid Bays Eutrophication Model. Boston: Massachusetts Water Resources Authority. Report 2015-03. 102p. https://www.mwra.com/harbor/enquad/pdf/2015-03.pdf

Massachusetts Water Resources Authority
100 First Avenue • Boston, MA 02129
www.mwra.com
617-242-6000